AL-FARABI KAZAKH NATIONAL UNIVERSITY

UDC 66:546.661 On manuscript rights

SHALABAYEV ZHANDOS SMAGULOVICH

Solid-phase and liquid-phase preparation of sulfur nanoparticles and their composites: properties study and application fields

6D072000 – Chemical Technology of Inorganic Substances

Dissertation submitted in fulfillment of the requirements
for the degree of
Doctor of Philosophy (Ph.D.)

Scientific supervisors:
Doctor of chemical sciences, Professor
Mukhambetkali Burkitbayev

Doctor of chemical sciences Farit Urakaev
Sobolev Institute of Geology and Mineralogy
SB RAS, Russia

Ph.D. Matej Balaz
Institute of Geotechnics SAS, Slovakia

The Republic of Kazakhstan
Almaty, 2019

CONTENT

NORMATIVE REFERENCES 5
LIST OF ABBREVIATIONS 6
INTRODUCTION 8
1 LITERATURE REVIEW 13
1.1 Synthetic methods and properties of sulfur nanoparticles 13
1.1.1 Mechanochemical method 13
1.1.2 Electrochemical method 14
1.1.3 Microemulsion technique 16
1.1.4 Aqueous surfactant solutions method 18
1.1.5 Template method 19
1.1.6 Green synthesis method 20
1.1.7 Liquid-phase precipitation method 21
1.1.8 Dissolving sublimed sulfur in PEG-200 22
1.2. Application fields of sulfur nanoparticles and nanostructures 23
1.2.1 Antibacterial activity of sulfur nanoparticles 24
1.2.2. Antifungal activity of sulfur nanoparticles 25
1.2.3 Anticancer activity of sulfur nanoparticles 25
1.2.4 Possible mechanism of antimicrobial activity of sulfur nanoparticles 26
1.2.5 Possible anticancerous mechanism of sulfur nanoparticles 28
1.3 Preparation methods of semiconductor copper sulfide (CuS) nanoparticles and nanocrystals 29
1.3.1 Microwave-assisted synthesis 30
1.3.2 Facile room temperature synthesis 30
1.3.3 Solvothermal synthesis 31
1.3.4 Aqueous solution method 32
1.3.5 Facial grinding method 33
1.3.6 Wet chemical method 34
1.3.7 Sol-gel method 35
1.3.8 Hydrothermal method 35
1.3.9 Hydrogel method 36
1.3.10 Mechanochemical method 37
1.4 Application fields of copper sulfide (CuS) nanoparticles 38
1.4.1 Photocatalysis 38
1.4.2 Energy storage devices 39
1.4.3 Solar cells 39
1.4.4 Biomedical applications 39
1.4.5 Antibacterial applications 40
1.5 Preparation methods, properties and application fields of sulfur-containing nanocomposites 41
2 EXPERIMENTAL PART 44

2.1 Reagents and techniques....44
2.1.1 Chemical reagents and their descriptions....44
2.1.2 Equipment for the solid-phase synthesis....45
2.2 Liquid-phase preparation of sulfur and sulfur-containing S/$CaCO_3$ nanocomposites 46
2.3 Hydrothermal synthesis of CuS/S nanocomposites....47
2.4 Mechanochemical synthesis of CuS/S composite 48
2.5 Sulfur-mediated mechanochemical synthesis of spherical and needle-like copper sulfide nanoparticles....48
2.6 Preparation of sulfur nanoparticles in dimethyl sulfoxide (DMSO) 49
2.7 Characterization methods and techniques 50
2.7.1 XRD analysis 50
2.7.2 Raman spectroscopy analysis 50
2.7.3 TG-DSC analysis 51
2.7.4 Particle size analysis....51
2.7.5 Elemental analysis....51
2.7.6 XPS spectroscopy....51
2.7.7 AFM analysis 52
2.7.8 SEM and EDAX analysis 52
2.7.9 TEM and SAED analysis....52
2.7.10 UV-Vis spectroscopy 53
2.7.11 PL spectroscopy 53
2.8 Antibacterial activity analysis of as-synthesized S, CuS and nCuS nanocrystals ..53
2.9 Biological activities of S/$CaCO_3$ nanocomposites 54
2.10 Hydrophobic properties of S/$CaCO_3$ nanocomposites....54
2.11 Detection of iron wear in the mechanochemically synthesized CuS/S sample using magnetometry 55
3 RESULTS AND DISCUSSIONS....56
3.1 Liquid-phase synthesis of S/$CaCO_3$ nanocomposites....56
3.1.1 XRD analysis 56
3.1.2 Particle size analysis....56
3.1.3 AFM spectroscopy 57
3.1.4 Hydrophobic properties of S, $CaCO_3$ nanoparticles and S/$CaCO_3$ nanocomposites....58
3.1.5 Biological activity of S, $CaCO_3$ nanoparticles and S/$CaCO_3$ nanocomposites 59
3.2 Hydrothermal synthesis of CuS/S nanocomposites....60
3.2.1 XRD analysis 60
3.2.2 Raman spectroscopy analysis 61
3.2.3 TG-DSC analysis 62
3.2.4 SEM analysis....63
3.3 Mechanochemical synthesis of CuS/S composites....64

3.3.1 XRD analysis 64
3.3.2 Elemental analysis 65
3.3.3 Results of magnetometry measurements 66
3.4 Sulfur-mediated mechanochemical synthesis sulfur, spherical and needle-like copper sulfide (nCuS) nanoparticles 67
3.4.1 XRD analysis 67
3.4.2 Raman spectroscopy analysis 72
3.4.3 UV-Vis spectroscopy analysis 73
3.4.4 PL spectroscopy 74
3.4.5 XPS analysis 75
3.4.6 PCCS analysis 76
3.4.7 Microstructural and morphological analyses 77
3.4.8 SEM, EDS and elemental mapping analysis of not washed samples and dried filtrates 83
3.4.9 Results of antibacterial activity measurements 86
3.5 Preparation of sulfur nanoparticles in dimethyl sulfoxide (DMSO) 87
3.5.1 Results of DLS analysis 87
4 APPLIED ASPECTS OF THE DEVELOPED METHODS FOR PRODUCING SULFUR, COPPER SULFIDE NANOPARTICLES, AND SULFUR-CONTAINING NANOCOMPOSITES 89
CONCLUSION 93
REFERENCES 94

NORMATIVE REFERENCES

In this dissertation, references to the following standards are used:

GOST 6.38-90. Unified documentation systems. The system of organizational and administrative documentation. Requirements for documents.

GOST 7.1-2003. Bibliographic record. Bibliographic description. General requirements and compilation rules.

GOST 8.417-2002. State system for ensuring the uniformity of measurements. Units of physical quantities.

GOST 7.11. System of standards on information, librarianship, and publishing. Abbreviation of words and phrases in foreign European languages in bibliographic description.

GOST 7.9-95. System of standards on information, librarianship, and publishing. Thesis and abstract. General requirements.

GOST 24104-2001. Laboratory balance. General technical requirements.

LIST OF ABBREVIATIONS

%RIZD – percentage of relative inhibition zone diameter
AFM – atomic force microscopy
CA – citric acid
CL – chemiluminescence
CNT – carbon nanotube
CTAB – cetyltrimethylammonium bromide
DLS – dynamic light scattering
DNA – deoxyribonucleic acid
DSC – differential scanning calorimetry
EDAX - energy dispersive analysis using X-ray
EDS – energy-dispersive X-ray spectroscopy
EDX – energy dispersive X-ray
EG – ethylene glycol
ESEM – environmental scanning electron microscopy
ESI – electronic supplementary information
ESM – eggshell membrane
FFT – fast Fourier transform
FTIR – Fourier-transform infrared
GO – graphene oxide
GOD – graphene oxide dots
GPES – general purpose electrochemical system
GQD – graphene quantum dots
GSH – reduced glutathione
GSSB – oxidized glutathione
HRTEM – high resolution transmission electron microscopy
ICDD – international center for diffraction data
IZD – inhibition zone diameter
JCPDS – joint committee on powder diffraction standards
LLA – lauraylalanine
M – metal
MB – methylene blue
Me – metal
MES – ministry of education and science
MTT – cell proliferation assay
MWNT – multi-walled carbon nanotubes
nCuS – needle-like copper sulfide
NIR – near-infrared
NSCPs – nitrogen-sulfur co-doped particles
PAN – polyacrylonitrile

PCCS – photon cross-correlation spectroscopy
PEG – polyethylene glycol
PL – photoluminescence
RhB – rhodamine B
ROS – reactive oxygen species
RRS – Rayleigh scattering spectroscopy
RT – room temperature
SAD – selected area diffraction
SAED – selected area electron diffraction
SDBS – sodium dodecylbenzenesulfonate
SDS – sodium dodecyl sulfate
SEM – scanning electron microscopy
SFA – segmented flow analysis
SNPs – sulfur nanoparticles
STP – standard temperature and pressure
STS – sodium thiosulfate
STSPH – sodium thiosulfate pentahydrate
TAM – thioacetamide
TDAB – tetraoctylammonium bromide
TEM – transmission electron microscopy
TG – thermogravimetry
TGA – thermogravimetric analysis
UV – ultraviolet
XPS – X-ray photoelectron spectroscopy
XRD – X-ray diffraction
ZT – thermoelectric efficiency

INTRODUCTION

General description of work

The thesis is devoted to obtaining and studying properties of sulfur, copper sulfide (CuS) nanostructures (nanoparticles and nanocrystals), and sulfur-containing nanocomposites by the liquid-phase and solid-phase preparation methods. Since all nanomaterials in inorganic and/or organic chemistry are synthesized either in a liquid medium or in a solid medium, the abovementioned liquid-phase and solid-phase methods for the synthesis of nanomaterials include almost all methods of synthesis of the abovementioned nanoparticles and nanocomposites. In this regard, sulfur and CuS nanoparticles, as well as sulfur-containing nanocomposites were synthesized by methods that are fast, facile, energy-efficient, and low-cost. In a literature review, analyzing all types of methods for the synthesis of inorganic nanomaterials, mechanochemical and hydrothermal synthesis methods were selected for the synthesis of the abovementioned nanostructures.

In this work, the possibilities of using mechanochemical synthesis to obtain needle-like copper sulfide (nCuS) nanocrystals, liquid-phase production of sulfur-containing nanocomposites ($S/CaCO_3$, and CuS/S), as well as sulfur separation from the obtained nanocomposite are shown for the first time.

The relevance of the study

The use of functional materials based on semiconductor nanoparticles is actively expanding in advanced science-intensive fields. Recently, semiconductor copper sulfide nanoparticles have been the focus of the attention of researchers around the world. They are used for various purposes (e.g. in solar cells, cathode material in lithium batteries, optical filters, thermoelectric materials, biomedicine, and photocatalysis). In such materials, a quantum-size effect was discovered, consisting in the fact that the bandgap of nanoparticles and the energy of electronic transitions can vary significantly with a slight change in the size of the same nanoparticles.

Sulfur nanoparticles are suitable for similar applications like semiconductor CuS nanoparticles, namely their use in lithium battery and pharmaceutical technologies are of importance. This comes from its anti-cancer, antibacterial and antifungal activities.

Nowadays, in addition to the synthesis of sulfur and semiconductor copper sulfide nanoparticles, which are used for various abovementioned purposes, the synthesis of binary, ternary, and quaternary nanocomposites based on them is intensively studied. This is explained by the fact that nanocomposites, unlike nanoparticles, have a wider range of application fields and improved properties.

The traditional methods for producing sulfur and copper sulfide nanoparticles, as well as sulfur-containing nanocomposites are characterized by a number of disadvantages, among which the need to use expensive and toxic precursors, the duration of the process, the difficulty of isolating nanoparticles in free form, and also

obtaining them in relatively large quantities should be noted. All of these are factors that limit the scope of the practical application of the abovementioned nanoparticles and nanocomposites.

Thus, the research topic aimed at developing a method for producing sulfur, copper sulfide nanoparticles, and composites based on them, providing the possibility of its scaling, not involving the use of expensive and toxic precursors, with the possibility of isolating the nanoparticles in free form, is very relevant.

The purposes of the thesis are the synthesis of sulfur, CuS nanostructures, and sulfur-containing nanocomposites using simple, quick, environmentally friendly and cost-effective methods, and investigation of their physicochemical, and anti-biological properties against bacteria and fungi.

The tasks of the thesis:

- determination of conditions for the liquid-phase and solid-phase synthesis of target sulfur, semiconductor CuS, and sulfur-containing nanocomposites;
- characterization of as-obtained sulfur, CuS nanoparticles, and sulfur-containing nanocomposites with modern physicochemical methods and techniques;
- determination of physicochemical, biological, and anti-biological properties of as-obtained sulfur, CuS nanoparticles, and sulfur-containing nanocomposites;
- development of a principal scheme of preparation sulfur, CuS nanostructures, and sulfur-containing nanocomposites;
- preliminary assessment of the economic efficiency of using the developed method for producing sulfur, CuS nanostructures, and sulfur-containing nanocomposites in comparison with known methods.

The object of the thesis is sulfur, CuS nanostructures (nanoparticles and nanocrystals), and sulfur-containing nanocomposites.

The subject of the research is the composition, structure, morphology, and physicochemical, anti-biological (antibacterial and anti-fungicidal) properties of sulfur, CuS nanostructures, and sulfur-containing nanocomposites.

The methodological framework of the research

Solid-phase (mechanochemical) and liquid-phase synthesis methods; separation of solids from liquid in a centrifuge and by filtration; precipitation; agar well plate method; physicochemical and analytical methods.

The scientific novelty of the thesis

1. For the first time, the chemical reaction with the formation of sulfur nanoparticles and calcium carbonate under the action of carbon dioxide on alkaline earth

metal polysulfide was established. It was found that sulfur particles are first synthesized from the corresponding carbonate with sizes of about 20–25 nm, which are subsequently enlarged (aggregated) with the deposition of a composite ($S/CaCO_3$) consisting of hydrophobic particles of sulfur and carbonate.

2. For the first time, sulfur-containing nanocomposite CuS/S have been synthesized via liquid-phase (hydrothermal) synthesis method reacting step-by-step copper acetate, copper chloride, and thiourea in an aqua media at 80 ºC. Results of SEM analysis revealed that CuS nanoparticles had an elongated parallelepipedal shape.

3. For the first time, sulfur-containing composite CuS/S has been synthesized via the mechanochemical method from elemental precursors. After 12.5 min of milling, elemental copper was not identified in the sample, forming pure CuS and S phases. Also, the possibility of detecting iron wear which comes from stainless steel chamber using magnetometry is shown.

4. For the first time, elongated needle-like copper sulfide (nCuS) nanocrystals with a thickness in the range between 6 and 8 nm and lengths up to 60 nm (aspect ratio up to 1:10) have been synthesized via the mechanochemical method. The synthesis is completed in just 5 min. It was found that nCuS is a less selective antibacterial agent, as it possessed activity against both *E. coli* and *S. aureus* bacteria, whereas the spherical CuS sample showed activity only against *E. coli*.

The scientific and practical significance of the study

The results obtained in the framework of the thesis can form the basis of the technology for the production of sulfur nanopowders, semiconductor needle-like CuS nanocrystals, and sulfur-containing nanocomposites in large quantities. The new knowledge gained in the field of solid-phase (mechanochemical) and liquid-phase synthesis of sulfur nanoparticles, semiconductor copper sulfides nanocrystals, and sulfur-containing nanocomposites will find application in the nanotechnology industry. The developed "Methods for producing sulfur nanoparticles, semiconductor needle-like copper sulfide nanocrystals, and sulfur-containing nanocomposites" can be used by enterprises producing sulfur, needle-like copper sulfide (nCuS), and sulfur-containing nanostructures due to its simplicity and cost-effectiveness.

The main provisions for the defense of the thesis

1. Among the sulfur, calcium carbonates nanoparticles, and sulfur-containing $S/CaCO_3$ nanocomposites, $S/CaCO_3$ nanocomposite has the strongest effect on wheat-seed germination by accelerating the growth of shoots and roots by 55 and 45%, respectively.

2. In the mechanochemical synthesis of CuS/S composites from elemental precursors in stoichiometric amount, after 12.5 min of milling elemental copper completely reacts with elemental sulfur. By the increasing time of milling, the trace amount of iron wear released from the steel chamber also increases.

3. Introducing *in situ* prepared sulfur nanoparticles to the reaction media of acetate route synthesis of copper sulfide (CuS) nanoparticles promote the formation of needle-like copper sulfide (nCuS) nanocrystals. Elongated needle-like copper sulfide (nCuS) nanocrystals are less-selective antibacterial agents in comparison with spherical ones.

Experimental and theoretical methods

The composition, structure, and morphology of as-prepared sulfur, needle-like copper sulfide (nCuS) nanostructures, and sulfur-containing nanocomposites ($S/CaCO_3$ and CuS/S) were studied by XRD, Raman spectroscopy, TG-DSC, PCCS, FTIR, XPS, AFM, SEM and EDAX, TEM and SAED, UV-Vis, PL spectroscopy, and elemental analysis.

The personal contribution of the author

The author has reviewed and analyzed the literature on the topic under study, studied the methods of experiments on the solid-phase (mechanochemical) and liquid-phase synthesis of nanoparticles and nanocrystals, their isolation in free form, as well as the characterization of the isolated nanoparticles and nanocrystals. In addition, the contribution of the doctoral candidate is to process and interpret the results, as well as approbation at conferences and registration in the form of scientific papers.

Approbation of work

The results of the thesis were reported and discussed at international symposia and scientific conferences such as:

- INESS-2017. The 5th International Conference on nanomaterials and advanced energy storage systems (Astana, Kazakhstan, 9-11 of August 2017);
- INCOME-2017. The 9th International Conference on mechanochemistry and mechanical alloying (Kosice, Slovakia, 3-7 of September 2017);
- CSMAG-2019. The 17th Czech and Slovak Conference on magnetism (Kosice, Slovakia, 3-7 of June 2019);

Publications

Based on the results of the thesis 9 scientific papers were published, including:

- in two articles (ACS Sustainable Chemistry and Engineering (IF ≈ 7) and Colloid Journal (IF ≈ 1)) published in international scientific journals having, according to the information base of the company Clarivate Analytics (ISI Web of Knowledge, Clarivate Analytics) a non-zero impact factor;
- in one article published in scientific journals recommended by the Committee for the Control in Education and Science of the Ministry of Education and Science of the Republic of Kazakhstan;
- in four abstracts at international and national conferences and symposia.

In addition, a conclusion was received on the issuance of two patents for the invention “Method for obtaining of sulfur nanoparticles”, application №2017/0532.1 dated 20.06.2017 of RSE “National institute of intellectual property” (Republic of Kazakhstan) and “Method for producing sulfur nanoparticles from solutions in dimethyl sulfoxide” application №201700540 dated 2017.11.29 of “Eurasian patent organization” (Russian Federation). All of these publications were made during the Ph.D. program.

Relation of the thesis with research and government programs

The dissertation work was performed within the framework of the program of targeted financing for 0130/PCF-14 “Development of new methods for obtaining sulfur nanoparticles to create technologies for the production of drugs for various functional purposes” (2015-2017 yy.) and BR 05234566 “Development and approbation of technologies for obtaining new sulfur-containing nanocomposites and drugs” (2018-2020 yy.). Also, this dissertation work was performed and supported within the framework of the grant funding project of MES of Republic of Kazakhstan AP 05133115 “Mechanochemical and solution synthesis of metal sulfide and sulfur nanocomposites (MeS@S; Me = Cd, Cu, Pb, Zn): properties and application prospects” (2018-2020 yy.).

Also, the thesis work was carried out as part of international cooperation between Al-Farabi Kazakh National University and the Institute of Geotechnics of the Slovak Academy of Sciences, (Kosice, Slovakia) under the supervision of the leading researcher at the Department of Mechanochemistry Ph.D. Matej Balaz.

Volume and structure of the thesis

The thesis consists of an introduction, four sections, a conclusion, and a list of references. The work is presented on 106 pages, contains 40 figures, 8 tables, and 159 bibliographical references.

1 LITERATURE REVIEW

1.1 Synthetic methods and properties of sulfur nanoparticles

Recently, in the chemical technology uses lots of methods of synthesis inorganic nanoparticles and nanomaterials. The type of synthetic methods depends on various characteristics of the target product. In chemical technology, the correct choice of the method that is used to obtain the target products is of particular importance. Morphology and functionality depend on this, and they, in turn, directly affect the efficiency and functionality of nanoparticles and nanocrystals.

There are many preparation methods of sulfur nanoparticles such as mechanochemical, electrochemical, microemulsion technique, ultrasonic treatment, acid hydrolysis of sodium thiosulfate, aqueous surfactant solutions, template method, from H_2S gas, green synthesis, liquid-phase method, reverse microemulsion, solvent-free and facile syntheses, and membrane-assisted precipitation methods, etc. Consider the above methods that are used to produce sulfur nanoparticles, and a detailed comparison of these methods with each other and the possibility of their application in production are further discussed in the conclusion.

Since there are many methods for the synthesis of sulfur nanoparticles, we consider those that are often found in scientific publications in recent years. Below is a detailed description of each approach with examples are presented.

1.1.1 Mechanochemical method

A mechanochemical method based on the mechanochemical reaction which is induced by the direct adsorption of mechanical energy. Mechanical energy can be transferred to the system by various methods of mechanical action, i.e. impact, compression, shear, tensile, grinding, etc. This mechanical action can lead to a reduction in particle size, the creation of active sites for chemical reactivity or the formation of fresh active surfaces for contact, fusion, and reaction of other particles [1].

Sulfur nanoparticles have been successfully prepared using the mechanochemical method by Urakaev et al. [2]. In their work, according to authors for the first time, they could synthesize dispersed nano sulfur with the dilution method by the side final product. As a sulfur source, they used sodium thiosulfate pentahydrate and it is activated by the solid succinic acid according to the following reaction:

$$Na_2S_2O_3 \times 5H_2O + yC_4H_6O_4 + zNa_2SO_3 = (z+1)Na_2SO_3 + yC_4H_6O_4 + 5H_2O + S_n^0. \quad (1)$$

There, succinic acid $C_4H_6O_4$ and Na_2SO_3 played the roles of a catalyst and a diluent agent, respectively.

Mechanochemical synthesis of sulfur nanoparticles was performed in a Pulverisette (Fritsch GmbH, Germany) ball mill in the range of rotation speed between 100-600 rpm

equipped with stainless steel chamber (V = 500 mL). As a milling body also used stainless steel balls with a diameter of 10 mm. The stoichiometric coefficients which are calculated with the special formula on the basis molar mass and density of reactants in mechanochemical reaction (1) for the catalyst and diluent were y = 1 and z = 19.6, respectively.

In order to avoid overheating the steel chambers, mechanochemical synthesis was performed at rotations rates of 140, 210, 280, and 350 rpm (14 min at each rate, 56 min in all). And then, the stainless steel chamber was opened, inspected, and restacked. After that, the mechanochemical synthesis was performed at 420, 490, 560, and 600 rpm (8,4, 2, and 1 min, respectively, 15 min in all).

After mechanochemical synthesis, the powder mixture analyzed with XRD analysis and there they could not confirm the presence of sulfur in the product sample. It can be explained with the amorphous phase of sulfur and produce many side products. After that, authors carefully washed as-obtained powders with distilled water and made XRD analysis again. From the XRD pattern definitely could be seen sulfur peaks and they confirmed with standard sulfur peaks (PDF-2 83-2285).

For the characterization morphology of obtained sulfur nanoparticles, TEM analysis was performed by the authors. Results of TEM analysis showed that the size of not washed mechanochemically synthesized sulfur nanoparticles was between the range 20-80 nm. It was found that size (as large as 300 nm) and morphology of washed sulfur sample differ from not washed.

Thus, the authors could successfully synthesize sulfur nanoparticles with the mechanochemical approach.

1.1.2 Electrochemical method

In this methodology, authors could synthesize sulfur nanoparticles from the sodium thiosulfate solution via the novel electrochemical approach [3]. They could control the size of synthesized sulfur nanoparticles adjusting the operating parameters including the initial sodium thiosulfate concentration.

The synthetic method performed as follows: in order to synthesize sulfur nanoparticles from the sodium thiosulfate solution, as a reactor, a single component cell was used. It should be noted that the presence of hydrogen ions formed on the anode during the oxidation of water was necessary to create soft acidic media for the oxidation of sulfide ions to elemental sulfur, as well as to prevent sulfide from further oxidation to sulfate ions.

Then authors studied the effect of thiosulfate concentration on the particle size of the prepared sulfur nanoparticles, performing electrical synthesis at three different concentrations of sodium thiosulfate, maintaining all other conditions constant.

The chemicals used, including sulfur powder, sodium thiosulfate, acetone, carbon disulfide, and ethanol, were provided by Merck™ for use in the form in which they were obtained. All reagents used were of analytical purity. Electrochemical experiments were

carried out on the modular electrochemical system μ-Autolab type W with computer control (Eco Chemie Ultecht, the Netherlands), controlled by the software GPES. The electrical synthesis was carried out using a programmable power supply system (psp-603/405/2010) by electrolysis at room temperature in a single cell.

As a comparison, the method of solvent/non-solvent precipitation was also used for the synthesis of sulfur nanoparticles. A saturated sulfur solution was obtained by dissolving the pure sulfur powder in 50 mL of each solvent (i.e., carbon disulfide and hot-ethanol). In order to obtain a saturated sulfur solution, pure sulfur powder was dissolved in 50 mL of each solvent (that is, carbon disulfide and hot ethanol). For the separation a possible insoluble sulfur powder, a membrane filter with pore size of 0.45 μm was used to the filtration prepared sulfur-containing solution. The deposition process was performed at room temperature (22±1 °C) for the CS_2/acetone system.

The effect of sodium thiosulfate concentration on the particle size of electrochemically synthesized sulfur nanoparticles is shown as a table form in Table 1.

Table 1 – Size of electrochemically synthesized sulfur nanoparticles in the different concentration of sodium thiosulfate [3, p. 448]

№	$C(Na_2S_2O_3)$, M	Average particle size, nm	SD, nm
1	0.5	35	± 5
2	0.1	44	± 5
3	0.01	65	± 16

Table 2 shows the effect of nature of solvent/non-solvent system and commixing rate on the average particle size of sulfur nanoparticles.

Table 2 – The average size of sulfur nanoparticles synthesized by the solvent/non-solvent method [3, p. 450]

№	Solvent	Non-solvent	The flow rate of commixing (mL/min)	Average size (μm)	SD (μm)
1	Hot ethanol	Cold water	100	0.25	± 0.04
2	Hot ethanol	Cold water	2.5	11	± 5
3	Carbon disulfide	Acetone	100	15	± 10
4	Carbon disulfide	Acetone	2.5	22	± 11

According to the obtained results, the authors noted that the particle size and shape of sulfur nanoparticles prepared by electrochemically and solvent/non-solvent

precipitation methods are quite different. A comparison of the main results of the two synthetic methods definitely shows that electro synthesized sulfur nanoparticles have significantly smaller particle sizes and much more uniform spherical shapes than those obtained by the solvent/non-solvent procedure. In addition, the method of electrosynthesis is a very clean method that avoids both the use of large amounts of organic solvents and the formation of residues. However, the electrochemical synthesis of sulfur nanoparticles from the thiosulfate solution has a lower yield compared to the solvent/non-solvent precipitation method.

1.1.3 Microemulsion technique

Monoclinic sulfur nanoparticles have been successfully synthesized via the reverse water-in-oil microemulsion technique by Guo et al [4]. Authors prepared sulfur nanoparticles reacting sodium polysulfide with hydrochloric acid in a reverse microemulsion system using theolin, butanol and mixture of Span-80 and Tween-80 (weight ratio 8:1) as the oil phase, co-surfactant and surfactant, respectively. The composition of the microemulsion system is presented in Table 3.

Table 3 – Composition of microemulsion systems [4, p. 84]

	Microemulsions I	Microemulsions II
Aqueous phase	2 mol/L Na_2Sx:25 mL	2 mol/L HCl:25 mL
Surfactant	S and T:60 g	S and T:60 g
Co-surfactant	Butanol: 10 mL	Butanol: 10 mL
Oil phase	Theolin: 450 mL	Theolin: 450 mL

In order to prepare sodium polysulfide solution, in a typical procedure, 12.8 g of sulfur powder was transferred to the flask and then 100 mL of sodium sulfide solution with concentration 2 mol/L was added. The chemical reaction was carried out at the room temperature under stirring for 30 min. The color of the solution was changed to orange-yellow indicating the preparation of sodium polysulfide solution according to the chemical reaction (2).

$$(x-1)S + Na_2S \rightarrow Na_2S_x \quad (2)$$

For the preparation reverse microemulsion systems, as mentioned above, theolin, a mixture of Span-80 and Tween-80, butanol and water was used as oil phase, surfactant and co-surfactant and aqueous phase, respectively.

After preparation all chemicals, by the typical procedure, monoclinic sulfur nanoparticles were synthesized according to the following chemical reaction:

$$Na_2S_x + 2HCl \rightarrow 2NaCl + H_2S + (x-1)S \quad (3)$$

Results of XRD analysis showed that the pattern has a broad of peaks. The intensity and positions of peaks closely matched with the literature values of the standard monoclinic sulfur phase (JCPDS N34-0941). According to the Debye-Sheerer formula, crystallite size of as-synthesized monoclinic sulfur nanoparticles was about 20 nm.

In order to determine the size and shape of sulfur nanoparticles, TEM analysis was performed by the authors. Results of TEM analysis showed that sulfur nanoparticles had a spherical shape with a particle size of around 20 nm.

Therefore, by the author's novel method of preparation sulfur nanoparticles with reverse water-in-oil microemulsion technique using surfactants and surfactants were developed. According to the authors, the microemulsion method is promising method for the synthesis of sulfur nanoparticles.

Using the above-mentioned approach [4], Choudhury et al. [5] have successfully synthesized monoclinic sulfur nanoparticles (β-SNPs) at room temperature after suitable modifications of the surface. In this work, they could prepare rod-shaped monoclinic sulfur nanoparticles with size c.a. 50 nm in diameter. For the characterization of the obtained sulfur nanoparticles, various characterization methods such as XRD, TEM, TGA, DLS, and surface topology, etc. are used. Also, the antimicrobial properties of as-synthesized monoclinic sulfur nanoparticles are estimated.

Diffraction peaks of XRD analysis showed that the sample contains only monoclinic sulfur and no other peaks were not detected indicating high purity of the sample. All peak positions were confirmed with the standard monoclinic sulfur peaks JCPDS (77-0227).

The TEM image of the sulfur sample distinctly presents that sulfur nanoparticles (β-SNPs) were rod-like in shape an average diameter of c.a. 50 nm and length of c.a. 550 nm.

Results of FE-SEM analysis showed that the surface of fungi which is treated with β-SNPs was unevenly crumpled and significantly deformed. On the other hand, the treated bacterial cells were found to shrink heavily at many sites of their bodies.

In order to confirm the presence of sulfur nanoparticles on the surface of the bacteria body, TEM coupled with EDS analysis is performed by the authors. β-SNPs have been found to form precipitation, nonspecific, in many places of bacterial cells and fungal gifs.

According to all obtained results, it can be concluded by the authors as follows: In this study, β-SNPs were obtained by water-in-oil microemulsion technique, which is considered as one of the best methods to save size nanoparticles in the non-aggregated configuration under the stable thermodynamic state. Authors also found that

encapsulation with the conjugate Span 80-Tween-80 not only stabilizes the monoclinic form of sulfur nanoparticles at room temperature but also increases their biocompatibility with mammalian cells.

In 2012, Choudhury et al. [6] continued working on the synthesis of sulfur nanoparticles with water-in-oil microemulsion technique. And at that time authors could prepare using this method sulfur nanoparticles with different shapes. In this work, they could synthesize orthorhombic (spherical; c.a.10 nm) and monoclinic (cylindrical; c.a. 50 nm) sulfur nanoparticles and that sulfur nanoparticles were examined for their effects on the total lipid content and desaturase enzymes of *Aspergillus Niger*. The as-synthesized sulfur nanoparticles were characterized for size with TEM, elemental composition with energy-dispersive X-ray spectroscopy and allotropic nature with X-ray diffraction pattern.

Orthorhombic sulfur nanoparticles which are encapsulated with polyethylene glycol-400 (PEG-400) were prepared through liquid-phase precipitation method [7].

Results of XRD analysis confirmed the presence of sulfur in each sample and the main peaks of each sulfur phase were compared with standard JCPDS peaks and both sulfur phases matched with orthorhombic (JCPDS file no. 83-2284) and monoclinic (JCPDS file no. 77-0227) sulfur phases, respectively.

According to literary data, authors found that both the SNP-allotropes significantly change the form of fungal conidiophores. It was found that orthorhombic sulfur nanoparticles convert the spherical conidiophores into concave hemispheres. A graphical representation has been included by the authors to this study to clarify and corroborate the ESEM data after treatment with and without the orthorhombic sulfur nanoparticles at different stages of the fungal development.

Authors also found that both allotropes of sulfur nanoparticles decreased total lipid content considerably among the treated isolates. In addition, a disproportionate 16:0 (palmitic acid) increase was found among SFA, which is considered a major enzyme of the unsaturation of membrane glycolipids. Subsequent desaturation of glycolipids with membrane-bound desaturase enzymes is typical of the biosynthetic pathway of fungal/plant lipids. In contrast, elemental sulfur had no lipogenic effects at equivalent concentrations of sulfur nanoparticles.

1.1.4 Aqueous surfactant solutions method

Sodium thiosulfate is one of the most abundant sources of sulfur. Because one molecule of this compound contains two atoms of sulfur and one of them can emit from the molecule during catalyzing in acid media. As above mentioned before [2], Urakaev et al. have synthesized colloidal sulfur nanoparticles via the solid-phase synthesize, i.e. with the mechanochemical method. In this method, authors synthesized sulfur nanoparticles with similar approach, but in aqua media [8]. In this work authors reported a surfactant-assisted method for the synthesis of sulfur nanoparticles by acid-catalyzed precipitation of sodium thiosulfate. As a catalytic agent, authors used both the inorganic

and organic acids and found that organic acid gives lower size of sulfur particles. They set that the size of the particles also depends on the reactant concentration and acid to reactant ratio. Also, it was found that the effect of different surfactants (TX-100, CTAB, SDBS, and SDS) on particle size shows that the surfactant can significantly reduce the particle size without changing the shape. According to results, authors found that size reducing ability was not same for all the surfactants, depending on the type of surfactant. The anionic surfactant SDBS is more effective for obtaining a uniform size in both the acid media.

In a typical procedure, the solution of sodium thiosulfate was reacted with hydrochloric, sulfuric and organic acetic acids. The chemical reaction was as follows:

$$Na_2S_2O_3 + 2HCl \rightarrow NaCl + SO_2 + S\downarrow + H_2O \quad (4)$$

$$SO_2 + H_2O \rightarrow H_2SO_3 \quad (5)$$

For the full completion of the chemical reaction, after mixing reactants, 30 and 40 min equilibrium time was given in the case of inorganic and organic acid, respectively. In order to measure the particle size of obtained sulfur nanoparticles, after equilibrium, the sample was sonicated in a bath for 2 min and analyzed with DLS analyzer.

Results of XRD analysis of sulfur samples which are prepared in the different acidic media and with the different types of surfactants are obtained. The positions and intensities of sulfur peaks were definitely confirmed by the standard orthorhombic standard sulfur peaks JCPDS (74-1465). The obtained phase of sulfur nanoparticles is also independent of acid media. Since, samples, after synthesis was washed successfully with freshwater, in XRD patterns were observed only sulfur peaks, indicating high purity of the sample.

TEM images showed that sulfur nanoparticles formed at a concentration of thiosulfate 5 mM as a result of the reaction catalyzed by inorganic acid in the medium of CTAB, and the size of the obtained particles was close to 50-55 nm. This phenomenon once again confirmed the formation of smaller particles in the CTAB medium.

Thus, the results of experiments showed that mostly orthorhombic sulfur nanoparticles with spherical shape produced by acid catalyze thiosulfate reaction. It was found that inorganic acids can synthesize larger size particles than the organic acid. Also, the authors mentioned that all anionic, cationic and nonionic surfactants play a major role in reducing particle size. Finally, authors are set that sulfur nanoparticles with a particle size of approximately 30 nm can be synthesized by organic acid-catalyzed thiosulfate deposition in the presence of an aqueous medium of CTAB.

1.1.5 Template method

Chinese scientists in 2011 had been published an article about the synthesis of sulfur nanoparticles using eggshell membrane as a template material [9]. Since, eggshell

membrane (ESM) is a natural biomaterial with high surface area, microporous, and water-insoluble fibers, the use of ESM as a template material was reported in a vast of publications [10]. In this work, authors successfully synthesized sulfur nanoparticles with an average diameter of 5-35 nm using ESM as a template material in the presence of Tween-80 surfactant.

First of all, the authors prepared a sulfur-containing precursor solution. For this, 1 g of sublimed sulfur was transferred to the beaker with volume 250 mL. After that, 5 mL of ethanol and 30 mL of $NH_3 \times H_2O$ (1+1) solutions were added. The chemical reaction was carried out at room temperature under stirring. The color of the solution was changed to the orange-yellow indicating dissolution of sulfur in the as-prepared solution.

XRD pattern contained 5 distinguishable peaks of sulfur. The peak intensity and positions were confirmed with standard monoclinic sulfur peaks (JCPDS 34-0941). Crystallite size of sulfur nanoparticles calculated using the Debye-Scherer equation and according to half-width of the diffraction peaks it was around 16 nm.

SEM image of sulfur nanoparticles showed that aggregations of sulfur nanoparticles with an average size of around 30 nm exhibit a small nanocrystal. Authors also mentioned that during using ESM as a template, distributed long hydrophobic carbon chains could also influence the growth of sulfur nanocrystals. When authors added to the system surfactant Tween-80 with different concentrations (0.1-0.5%), the size of obtained sulfur particles was different. After that authors had selected 0.3% of Tween-80 as a suitable concentration for the synthesis of sulfur nanoparticles. It was also found that the acid medium was played significant role in the synthesis of sulfur nanoparticles. In order to obtain sulfur nanoparticles with average diameter less than 30 nm, 6 mol/L of acetic acid solution was used in this synthesis. 10 h of reaction time was also optimal for the synthesis process.

According to results, it can be concluded by the authors as follow: biotemplate ESM plays important roles as a physical substrate and functional macromolecule template to achieve the synthesis of sulfur nanoparticles. They also found that the concentration of surfactant Tween-80 can also affect the size of the target product. Thus, according to authors, this novel method can be recommended to the synthesis of other interesting superstructure inorganic materials.

1.1.6 Green synthesis method

Recently, the context “green synthesis, green method, etc.” is becoming popular among scientists because of the increasing number of articles about this topic. One of the main reasons for this phenomenon can be harmless influence of this method to the environment. According to literary data, it was found that sulfur nanoparticles also can be synthesized using this green synthetic method. Salem et al. [11] have successfully prepared sulfur nanoparticles from sodium thiosulfate in the presence of *Punica granatum* peels aqueous extract at room temperature. As-synthesized spherical sulfur

nanoparticles with average particle size of 50 nm were tested in different concentrations for plant growth.

In order to prepare an aqueous extract of *Punica granatum* peels, 20 g of dried *Punica granatum* peels powder was well mixed with 500 mL of distilled water and boiled for 20 min. After cooling, mixture was filtered with an eye to removing solid particles. For separating heavy biomaterials, extract was centrifuged at 1200 rpm for 5 min. Finally filtrate was stored at room temperature condition for further experimental work.

For the preparation of sulfur nanoparticles, 24.8 g of sodium thiosulfate pentahydrate (STSPH) was dissolved in the as-prepared *Punica granatum* peels extract under vigorously stirring for 10 min, and then was diluted with 500 mL of deionized water. After that, a 10% solution of HCl was added to the STSPH solution drop by drop to precipitate sulfur particles under stirring. Precipitated sulfur particles separated from extract via centrifuging at 5000 rpm for 10 min. The chemical reaction of this procedure was as follow:

$$Na_2S_2O_3 \times 5H_2O + 2HCl \rightarrow 2NaCl + S\downarrow + SO_2 + 6H_2O \quad (6)$$

Results XRD analysis confirmed the presence of the sulfur compound in the sample. The peak location and intensity were definitely matched with standard monoclinic sulfur peak data (JCPDS 34-0941). The average crystallite size was calculated by the Debye-Scherrer formula and it was found around 20 nm.

To determine the morphology of the obtained sulfur nanoparticles, the authors performed SEM-EDS analysis for sulfur-containing tomato leaves and tomato fruits. SEM images portray sulfur crystals of various shapes, the leaves are incorporated into the leaves and spherical crystals in the fruits.

The effect of sulfur nanoparticles on tomato leaves and fruits is also investigated. It was found that sulfur-containing solution with a concentration of 200 ppm significantly increased weight percent of sulfur content in the leaves and fruits of tomato. In this work, authors also observed that tomato leaves with sprayed 200 ppm solution of sulfur nanoparticles, were healthier and greener than those of control leaves.

Thus, according to the abovementioned results, the authors concluded that foliar spraying tomato leaves plant with sulfur nanoparticles were very beneficial to plant growth. Also, authors are set that solution of sulfur nanoparticles with concentration 200 ppm can produce healthy and high quality of tomato fruits.

1.1.7 Liquid-phase precipitation method

Surface-modified sulfur nanoparticles have been successfully synthesized by Choudhury et al. [12] via modified liquid-phase precipitation method [4] using sodium polysulfide and ammonium polysulfide as starting material and polyethylene glycol 400 (PEG-400) as the surface stabilizing agent. As-synthesized sulfur nanoparticles were

characterized using vast physical-chemical methods such as AFM, ESEM, HR-TEM, and DLS, etc. Obtained sulfur nanoparticles were tested for antibacterial activity against *Aspergillus Niger* and *Fusarium oxysporum.*

Sulfur nanoparticles were prepared via a modified liquid-phase precipitation method as mentioned before [4]. In a typical procedure, the thoroughly homogenized sulfur powder was mixed with sodium sulfide and ammonium sulfide solution (2 mol/L) and kept under continuous stirring until these two reactants formed sodium/ammonium polysulfide solution. Then, 5 mL of as-prepared polysulfide solution was added to alkalinized solution of PEG-400 solution and precipitated with aqueous solution of formic acid.

Results of DLS analysis showed that size distributions in hydrodynamic diameters in the range of 20-70 nm and 10-100 nm of sulfur nanoparticles synthesized using sodium polysulfide (SNP-1) and ammonium polysulfide (SNP-2), respectively. HR-TEM images showed an average particle size c.a. 20 and 50 for SNP-2, respectively.

Results of ESEM analysis had been presented for the lowest effective and the highest applied the dose-dependent effect of as-prepared sulfur nanoparticles on ultrastructural modifications of hyphae and conidiophores. For *Aspergillus Niger* strains, ESEM micrographs showed signs of hyphae morphology weakening when treated with SNP-1 concentrations of 125 ppm. When authors use SNP-1 with concentration 2,000 ppm the trunks of conidiophores were greatly distorted and destroyed from their usual structure.

Therefore, in this study, authors have been synthesized sulfur nanoparticles with two different inorganic alkaline metal sulfides as starting materials, formic acid as a precipitating reagent, and PEG-400 as a surface stabilizer surfactant. Formic acid was chosen by the authors to keep the sulfur nanoparticles in a small size. Authors also are set that results of a modified poisoned food method using micron-sized sulfur and two types of sulfur nanoparticles confirmed that inhibition of fungal growth is directly proportional to the increase in concentration and inversely proportional to the increase in particle size.

1.1.8 Dissolving sublimed sulfur in PEG-200

Sulfur nanoparticles with the rod-like structure were synthesized in this work by Xie et al. [13]. As in this method obtained self-assembled sulfur nanoparticles with rod-like shape, the method also can be named as shape-controlled synthesis of sulfur nanoparticles. Dissolving sublimed sulfur in a green PEG-200, in this facile synthesis authors synthesized homogeneous rod-like structure of sulfur with a typical diameter of about 80 nm and an average aspect ratio of 6-8. Also, authors investigated spectral properties of as-synthesized sulfur nanorods by ultraviolet-visible (UV–vis) absorption and resonance Rayleigh scattering spectroscopy (RRS).

Synthetic method of rod-like sulfur nanostructures took place as follows: in a facile typical procedure, 20 ml of PEG-200 and 0.4 g of sublimed sulfur were transferred into

a 50 mL flask and then the flask was attached to a reflux condenser. After that, the content of flask was heated up to 125 ºC under stirring and kept for a 1 h at a set temperature for complete dissolution. Finally, a clear and light yellow saturated solution of sulfur PEG-200 was obtained. Then, obtained solution quickly transferred into an ice-water bath and vigorously stirred for 10 min producing yellow suspended solution. Using centrifuge formed precipitate separated from the yellow solution. Obtained nano sulfur-PEG sol stored at 30 ºC for further characterization.

XRD analysis was performed to characterize the chemical composition of sample. The sharp and strong diffraction peaks of sulfur showed that the sample was well crystallized. Standard XRD pattern of orthorhombic sulfur (JCPDS 83-2285) confirmed the sample contained S_8 structured sulfur.

In order to reveal the morphology of as-synthesized sulfur nanoparticles, HR-TEM with SAED analysis was performed. The particles in the sol nano sulfur–PEG were spherical. The particle size was inhomogeneous in the range of 20 to 100 nm, and explicit aggregation was also observed. After 15 days authors noticed that the size and aspect ratio of the particles increased, indicating that the spherical sulfur particles began to combine to form a rod-like structure. After 30 days the aspect ratio of the nanorods has increased further. The nano sulfur–PEG sol was a monodisperse and homogeneous rod-shaped structure with a width of about 80 nm in diameter and an average aspect ratio of about 6-8. HRTEM image recorded from the middle part of the individual nanorods, clearly shows that the distance between any two adjacent lattice bands was 3.2 A, which corresponds to the distance (206) of the planes of the rhombic S_8 phase, and the direction of growth was revealed.

1.2. Application fields of sulfur nanoparticles and nanostructures

Sulfur is the most universal in use element in the various areas of biomedicine. Its versatility can be attributed to its unique physicochemical properties. Sulfur has gained a reputation as one of the most beneficial drugs known to humans. In particular, sulfur is most important to humans because it is part of various amino acids such as methionine, cysteine, cystine, homocysteine, homocysteine, and taurine, which are an absolute dietary element. Sulfur has a long history of use in various dermatological disorders such as scabies, as an ingredient in acne ointments, anti-dandruff shampoos and as an antidote for acute exposure to radioactive material [14]. It has been found that when sulfur is absorbed into the skin, it is converted into inorganic sulfide or into some organic sulfur compounds. Sulfur can also be used to treat vitiligo. A two-year study conducted at the Regional Research Institute (homeopathy) showed significant improvement in patients with white spots after treatment with sulfur [15].

When using elemental sulfur in nanoform, there are many important applications and uses. Recently, sulfur nanoparticles are useful in the manufacture of nanocomposite for lithium batteries [16] and modification of carbon nanotubes [17]. Also, other biomedical applications of sulfur nanoparticles have been provided in Figure 1.

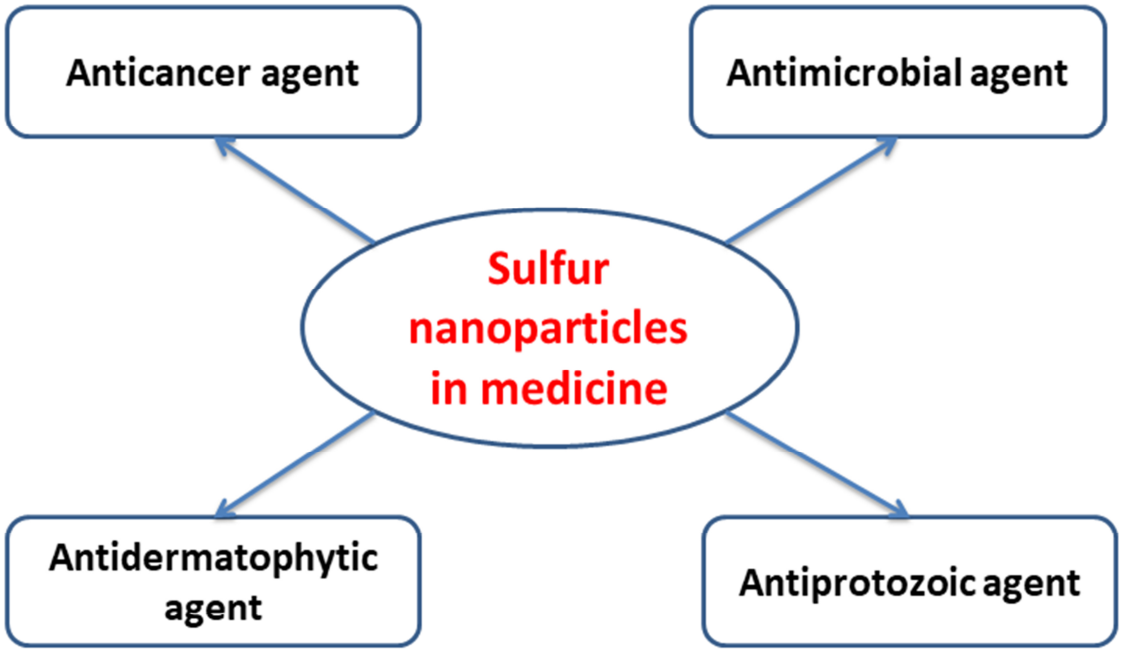


Figure 1 – Biomedical application fields of sulfur nanoparticles [31, p. 23]

Sulfur helps in healing wounds with keratin and has a popular use as a remedy for skin rashes. The keratolytic activity of sulfur is caused by H_2S, which is formed by the direct interaction of sulfur with keratinocytes [18]. Sulfur can cause a variety of histological changes, including hyperkeratosis, acanthus, and dilation of skin vessels. Sulfur is no longer used on its own in medical treatment, but sulfur in combination with modern medicines, now called sulfamide, are used to treat diseases in humans. In addition, sulfur also exhibits antitumor activity. Studies of sulfur antitumor activity have shown that sulfur compounds, such as hydrogen sulfide donors, exhibit new anti-cancer properties without affecting normal cells of the body [19]. A recent study showed that sulfur significantly inhibits the growth of prostate cancer [20]. In addition to drugs, sulfur is used in various industries: sulfuric acid, pulp, and paper industry, refining gasoline, etc. the most important component in these dyes; manufacture of fungicides and agrochemicals [21, 22].

1.2.1 Antibacterial activity of sulfur nanoparticles

Like other nanoparticles, sulfur nanoparticles also have antibacterial activity. Until now, much work has not been done on the assessment of the antibacterial potential of sulfur nanoparticles. Recently, Suleiman et al. [23] showed the antibacterial activity of sulfur nanoparticles against *Staphylococcus aureus*, Escherichia *coli,* and *Pseudomonas aeruginosa* bacteria. The authors found that sulfur nanoparticles demonstrated significant antibacterial activity against *S. aureus*. Although, these nanoparticles did not

present any activity against *E. coli* and *P. aeruginosa* even at high concentration i.e. up to 800µg/mL. Similar tests have been done by Roy Choudhury et al. [24]. In their work, sulfur nanoparticles failed to demonstrate antibacterial activity against multidrug-resistant gram-negative bacteria such as *E. coli*, *Klebsiella pneumoniae*, *Acinetobacter baumannii*, *Stenotrophomonas maltophilia,* and *Enterobacter aerogenes.* However, unlike the above study, Roy Choudhury et al. [5] have been synthesized β-sulfur nanoparticles and they evaluated for antibacterial activity with *S. aureus*, *E. coli,* and *K. pneumoniae*. The authors found that β-sulfur nanoparticles inhibited the growth of *S. aureus* at 576 µg/mL and the growth of *E. coli* and *K. pneumoniae* at 2,304 ug/mL. From these studies it can be concluded that with increase in the concentration of sulfur nanoparticles the growth of bacteria slows down. Also, Roy Choudhury et al. [25] reported that sulfur nanoparticles were to be able to exhibit antibacterial activity, while elemental sulfur did not show any inhibition of bacterial growth against the gram-positive and gram-negative bacteria tested.

1.2.2. Antifungal activity of sulfur nanoparticles

As mentioned above, sulfur is used as a fungicide to prevent diseases caused by plant pathogens for a long time. Various powdery mildew, black spot of roses, roses and other plant disease fungi are reduced by the formation of hydrogen sulfide in sulfuric fungal cell and increases the toxicity of hydrogen sulfide, the result of which leads to the death of fungal cells [26]. The antifungal activity of sulfur nanoparticles was evaluated by Deshpande et al. [27] in comparison with colloidal sulfur by plate analysis method. Sulfur nanoparticles are reported to inhibit normal growth of fungal cells at higher concentrations (1500-3000 µg/mL) in the case of *Aspergillus Niger* and *A. flavus*, while they do not exhibit fungicidal activity at lower concentrations (30-150 µg/mL). The efficiency of sulfur nanoparticles is directly proportional to the particle size reduction. Colloidal sulfur did not show antifungal activity against the tested fungi.

Gogoi et al. [28] studied *in vitro* the activity of sulfur nanoparticles and the traditional sulfur composition available on the market at a concentration of 1000 ppm against *Erysiphe cichoracearum*, powdery mildew causing okra disease. The authors found that commercial sulfur products and nano sulfur are inhibiting the germination of conidia, but the nanospheres inhibit both conidial germination and non-germinated conidia. Thus, this investigation proved that reducing particle size increases the efficiency of sulfur nanoparticles as an antifungal agent.

1.2.3 Anticancer activity of sulfur nanoparticles

It is known that sulfur-containing amino acids such as cysteine, methionine, play a significant role in anticancer chemotherapy because they have a high propensity for platinum compounds. Lee et al. [29] reported apoptosis and the effect of inhibition of purified sulfur growth on human oral keratinocytes and oral cancer cells through MTT analysis, nucleus staining, cell cycle analysis, and western blotting. The results showed

that sulfur inhibits the proliferation of cancer cells over time and dose-dependent. The study conducted by Ali [30] showed that sulfur nanoparticles stabilized with TOAB (tetraoctylammonium bromide) exhibit high antitumor activity against the kidney cancer cell line, followed by leukemia and colon cancer cell lines. Whereas TOAB stabilized nanoparticles of sulfur had any influence on the weak cell line.

1.2.4 Possible mechanism of antimicrobial activity of sulfur nanoparticles

All possible mechanisms of antimicrobial activity of sulfur nanoparticles and nanostructures well described in the review of Rai et al. [31]. In general, it has been suggested that when the nanoparticles come in contact with the bacterial surface, the electrostatic interaction of the nanoparticles with the bacterial cell promotes their penetration into the cell membrane, resulting in membrane rupture and reduced viability. Similarly, it has also been suggested that the attachment of nanoparticles to the bacterial cell wall and membrane causes a change in membrane integrity, membrane potential, and depolarization, which in turn leads to improper transport, disruption in energy transfer, which ultimately leads to cell lysis or cell death [32]. Another mechanism claimed for nanoparticles as an antimicrobial agent involves the destruction of DNA during replication and the release of toxic metal ions and volatile compounds that are responsible for cell lysis [33].

In the context of the review of Rai et al. [31], authors had focused on the mechanism of the action of sulfur nanoparticles on microbes, including bacteria and fungi. It is well known that elemental sulfur has been used for medicinal purposes since ancient times [34]. It has also been reported that optimal amounts of sulfur are beneficial for protein synthesis, whereas high concentrations of sulfur, however, are considered toxic to microbes due to the formation of a number of volatile compounds such as H_2S, after inclusion or adsorption of microbial cells [35, 36]. There are more theories available about how elemental sulfur works. According to them, elemental sulfur is absorbed by pathogens and then oxidized to form pentathionic acid or reduced to form hydrogen sulfide (H_2S). In addition, H_2S promotes obstruction or oxidation of free-SH groups of many important enzymes in the cell and disrupts important intermediate metabolism in mitochondria.

The exact mechanism for sulfur nanoparticles remains to be determined. On the basis of the above-mentioned theories, certain mechanisms of action of sulfur nanoparticles on bacteria and fungi have been proposed, which should be more or less similar to each other. In the case of bacteria, possible mechanisms may include: (i) the strong interaction of sulfur nanoparticles (negatively charged) with biological target molecules, such enzymes, and proteins that are present on the cell surface, pits and leaks cell components [37]; (ii) it is assumed that nanoparticles like silver nanoparticles of sulfur ions also generate sulfur that subsequently forms toxic H_2S, interact with groups -SH and generate ROS-stress, which denatures proteins and lipids [29]; (iii) another possibility of H_2S formation is the reduction of sulfur nanoparticles due to some

unknown molecules such as NADH; (iv) there are also chances of sulfur nanoparticles interacting with DNA, leading to its destruction and cell death. The schematic overview of the mechanism of sulfur nanoparticles on the bacteria body is presented in the Figure 2.

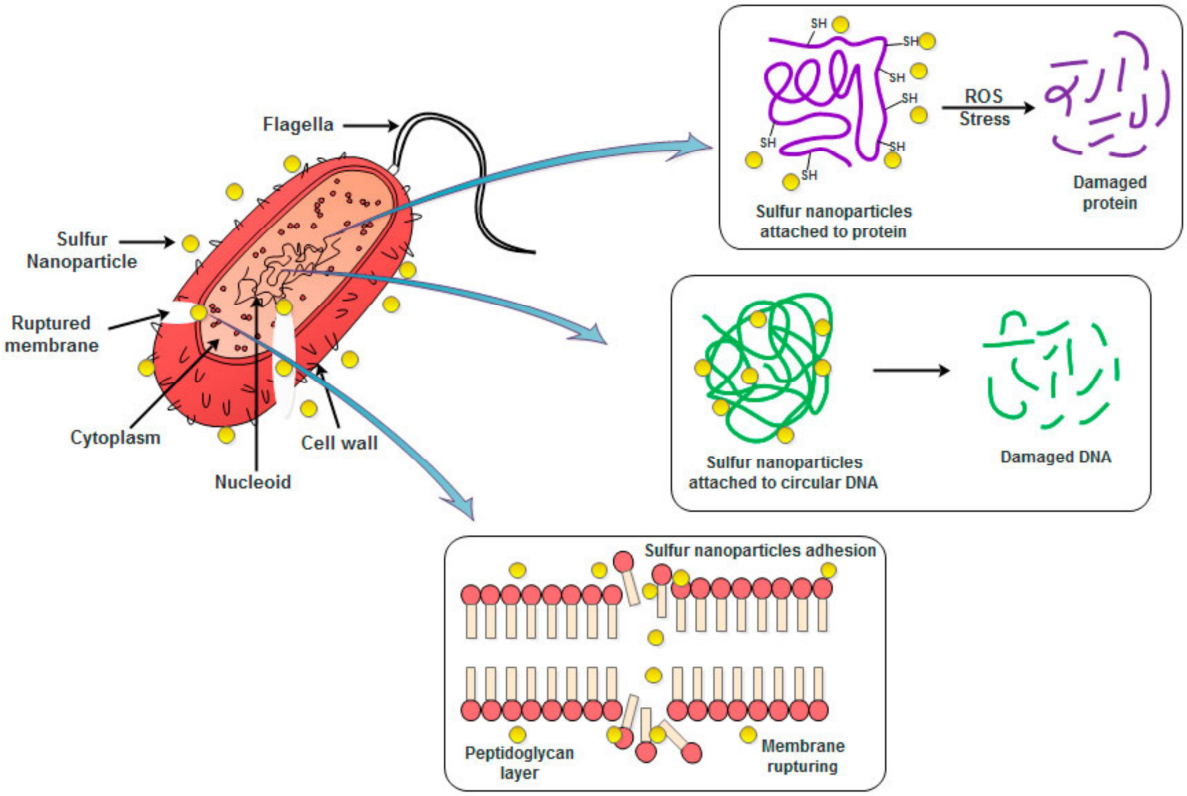


Figure 2 – Schematic overview of the action mechanism of sulfur nanoparticles on bacteria [31, p. 24]

In addition to all the above possibilities, in the case of fungi, some additional explanations have been proposed that interact with the cellular lipids of sulfur nanoparticles and reduce the total lipid content, as well as change its structure, resulting in the destruction of fungi [6]. According to another view, the ingress of sulfur nanoparticles into the mitochondrial matrix inhibits oxidative phosphorylation and disrupts cellular metabolism. Possible mechanisms of action of sulfur nanoparticles on fungi are shown in Figure 3.

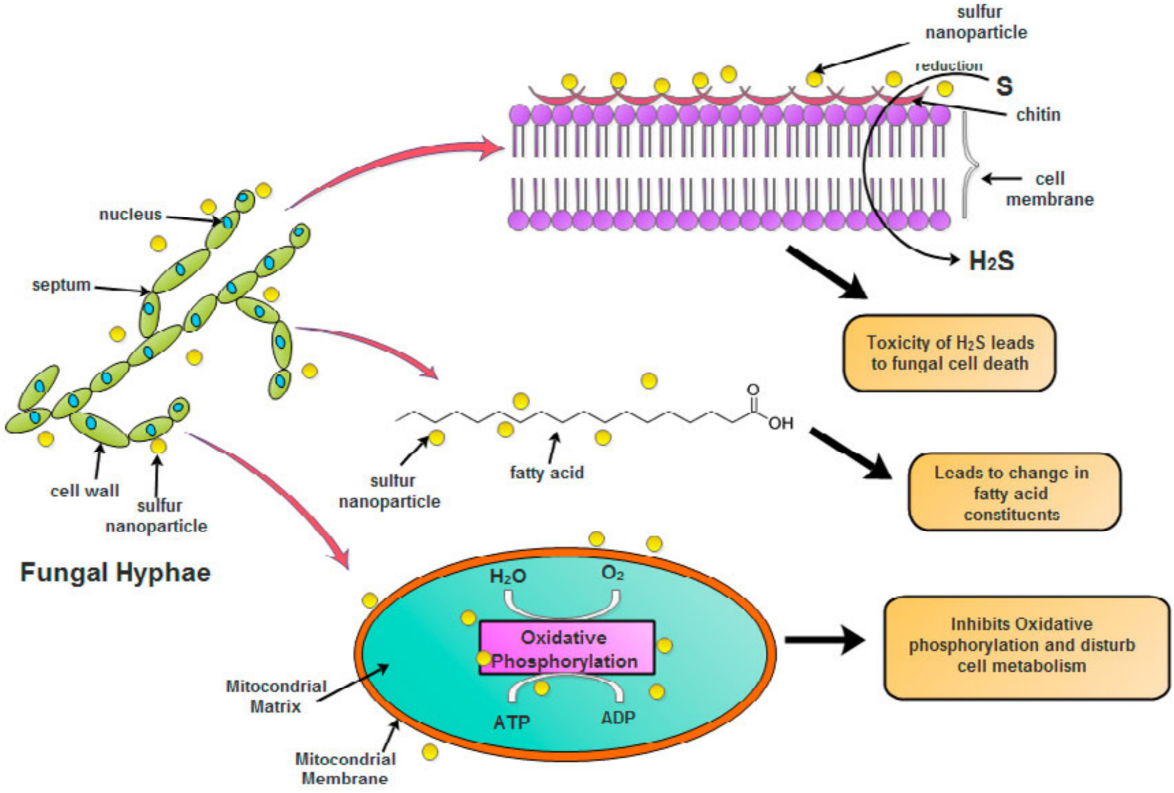


Figure 3 – Schematic overview of mechanism for mode of action of sulfur nanoparticles on fungi [31, p. 25]

1.2.5 Possible anticancerous mechanism of sulfur nanoparticles

Recently, the use of nanoparticles against cancer is becoming the most growing area of research. Many works confirm their anti-cancer properties through various mechanisms [38].

According to the authors, a possible mechanism of anti-cancer activity of various nanoparticles involves the leakage of cancer cells, which leads to an increase in the permeability of nanoparticles, which leads to the accumulation of nanoparticles and the death of cancer cells [39]. Sulfur nanoparticles with an average size of 80 nm have been reported to induce apoptosis in C6 glioma cells depending on concentration, thereby significantly inhibiting its growth. In addition, it has also been found to enhance Bax regulation and reduce Bcl-2 expression to cause apoptosis in the cancer cell [40]. All such a sequence of mechanisms eventually leads to a decrease in cell viability in the presence of nanoparticles. Considering the anticancerous mechanisms of various nanoparticles, the authors proposed a hypothetical mechanism of action of sulfur nanoparticles on cancer cells (see Figure 4).

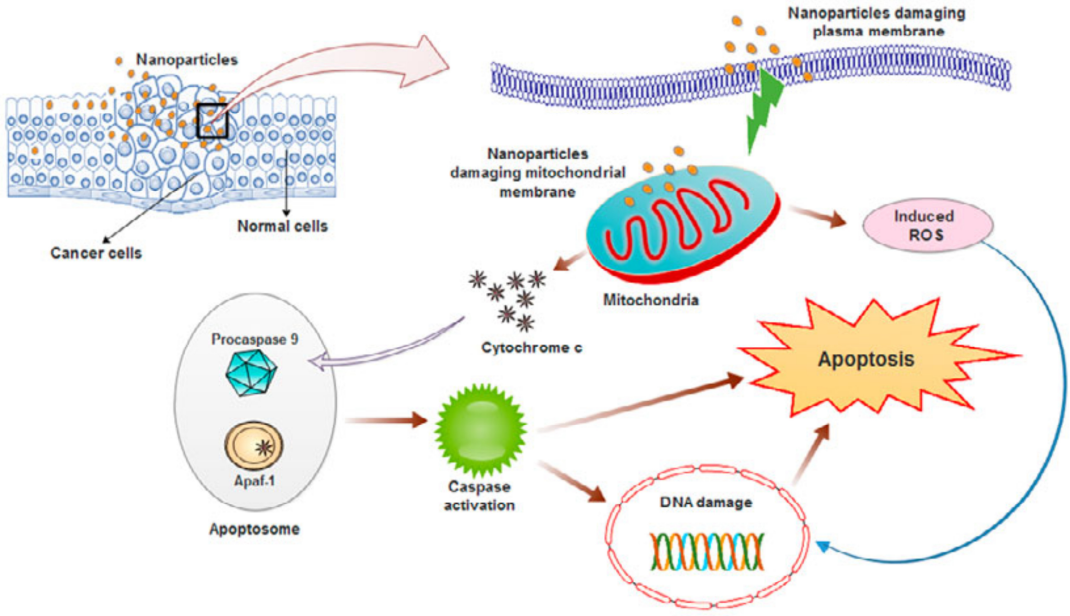


Figure 4 – Schematic representation of the hypothetical anticancer mechanism of sulfur nanoparticles [31, p. 26]

1.3 Preparation methods of semiconductor copper sulfide (CuS) nanoparticles and nanocrystals

When a substance moves from macro-size to size, it is only one or two orders of magnitude larger than molecular, its properties change dramatically - with an increase in surface energy, its surface tension, melting temperature and structural transitions change, the structure itself, electronic and optical characteristics can change - that is, the whole range of physical-chemical properties. Striking examples of such objects are semiconductor nanocrystals or quantum dots. A size effect is observed in them, which are expressed in the dependence of electronic and optical properties, more precisely, the bandgap and the shape of the energy spectrum, on the linear dimensions of the nanoparticles.

Semiconductors are materials that have an intermediate conductivity between conductors and dielectrics and differ from conductors in the strong dependence of the conductivity on the concentration of impurities, temperature, and exposure to various types of radiation. Semiconductors include substances such as germanium (Ge), silicon (Si), gallium (Ga), arsenic (As), indium (In), as well as some oxides, sulfides, and metal alloys. The main property of semiconductors is an increase in electrical conductivity with increasing temperature [41].

Semiconductor nanoparticles have caused many studies of their unique properties, such as charge transfer, light emission, mechanics and thermal diffusion, etc.,

characteristic of size scaling effects at nanometer sizes. Moreover, they are actively researched in the biomedical sciences, which are a dynamic field of research in molecular and translational medicine. Their increasing importance in the detection and treatment of cancer and other diseases, drug delivery and applications biosensitive in vitro may in part explain their favorable and easily adjustable physical, chemical, magnetic and optical properties [42].

Among the vast types of semiconductor nanoparticles, we have selected copper sulfide (CuS, covellite) nanoparticles as copper sulfide, a p-type semiconductor with excellent optical and electrical properties which has been extensively studied for a variety of uses [43].

Below, methods of preparation of copper sulfide nanoparticles with applications are given.

1.3.1 Microwave-assisted synthesis

Semiconductor copper sulfide (CuS) mesoporous nanosheet structures have been successfully synthesized using an instant microwave-assisted system by Naveed et al. [44]. As-synthesized material consists of mesoporous structures with a pore diameter less than 25 nm and a large surface area (~169m^2g^{-1}).

In order to synthesis CuS nanosheets, at room temperature 100 mL of ethylene glycol and 10 mL of deionized water were mixed and in this solution, 6 mmol of thioacetamide (TAA) and 6 mmoles copper nitrate tetrahydrate were dissolved. And then the prepared solution was stirred without stopping for 20 min. After that, obtained homogenous solution was heated in a microwave oven at 140 ºC for 8 min. Finally, as-prepared CuS was directly used for the electrochemical tests without any other processing.

XRD pattern demonstrated that sharp peaks of the covellite phase definitely matched with the standard hexagonal sulfur peaks indicating the pure crystallinity of obtained sample. This covellite type CuS hexagonal structure did not have any characteristic peak associated with impurities.

Thus, the authors successfully synthesized mesoporous CuS nanosheets with the low frequency and the instantaneous microwave synthesis method.

1.3.2 Facile room temperature synthesis

The synthetic protocol of aqueous soluble copper sulfide (CuS) nanocrystals has been set in this report by Chen et al. [45]. In this paper, the authors report on a general simple technique for the direct synthesis of water-soluble CuS nanocrystals with well-defined NIR absorption of plasmon under ambient conditions at room temperature (RT) requiring neither high temperature nor inert atmosphere, in the presence of various copper, sulfur precursors and various ligands such as 3-mercaptopropionic acid (MPA), TGA, reduced L-glutathione (GSH) and oxidized l-glutathione (GSSG).

All synthesis procedures were carried out in the open-air atmosphere at room temperature. With the aim to prepare aqueous soluble CuS nanocrystals, copper chloride with sodium sulfide was reacted in the presence of MPA. The solutions of all precursors were separately prepared using deionized water under the vigorously magnetic stirring. A clear dispersed solution called the S-MPA precursor was then obtained by adding 1 mL of MPA to the above Na_2S solution. The resulting sample solution was then added to the copper chloride precursor with stirring, and the reaction was held for another 2 hours at room temperature. After that, dark-green dispersion obtained and it was precipitated adding 5 mL of ethanol. Then, precipitated copper sulfides separated from the unnecessary solution by centrifugation at 4000 rpm for 5 min.

After testing all types of ligands with each precursor, the authors found that the introduction of ligand L-glutathione, GSSG, and GSH enables a unique morphology while saving the phase of covellite and well-defined NIR plasmon absorption. In addition, TEM and HRTEM images of nanocrystals formed in the presence of GSSG or GSH showed a spiral feature. The lattice interval of 0.31 nm can be attributed to the plane (102) of the covellite phase (CuS). Definitely, X-ray patterns confirmed the formation of the covellite phase.

Thus, the authors can conclude that in this paper a method of synthesis at room temperature was developed to obtain CuS nanocrystals with well-defined NIR-plasmon absorption in the presence of various copper and sulfur precursors and various ligands.

1.3.3 Solvothermal synthesis

In this synthesis method, photocatalytic 3D flower-like copper sulfide (CuS) nanoparticles have been successfully synthesized by Wang et al. [46]. As-synthesized flower-shaped CuS nanoparticles have shown good photocatalytic properties for the decomposition of organic dyes (methylene blue) in water. Authors are set that the rate of photodegradation in the photothermal system increased by ~ 212.7%.

The experimental procedure was performed on the basis template-free solvothermal method of synthesis CuS nanoparticles [47]. In a typical procedure, 0.5 mmol of $CuCl_2$ was dissolved in 10 mL of EG solution and magnetically stirred at 170 °C for 30 minutes to prepare a homogeneous green solution. At the same time, another 5 mmol of sulfur powder was dissolved in 5 ml EG and heated at 170 °C for 30 min with constant magnetic stirring. The color of the sulfur-containing solution turned yellow during the heating and mixing process. The yellow solution was then rapidly added to the green $CuCl_2$ solution at 170 °C at normal pressure and the resulting mixture was stirred for another 5 minutes, after which it turned black. CuS particles were collected by centrifugation and washed several times with CS_2, ethanol and distilled deionized water. Finally, the pure CuS particles were dried in a drying oven at 70 °C for 12 hours to form powders.

In the XRD results, the peak intensity and locations were compared with standard copper sulfide data and they definitely confirmed hexagonal phase structure of CuS

compound indicating pure phase and crystallinity of the prepared product. The strong peaks located at 27.92°, 29.37°, 31.99°, 48.06°, 58.74° are attributed to the (102), (103), (006), (110) and (116) planes of hexagonal CuS.

SEM images of the obtained three-dimensional color-like CuS nanoparticles showed that the resulting CuS particles exhibit good homogeneity and dispersion as well as regular morphologies. The structure of the flower-like CuS particle is clearly demonstrated in the high-magnification SEM image. It is noteworthy that these CuS nanoparticles consist of numerous CuS nanoplates. The diameters of newly synthesized CuS nanoparticles range from 1.4 to 3.1 microns, and the average diameter is 2.3 microns.

Thus, in this work, three-dimensional flower-like CuS nanosheet structures have been synthesized by a simple and template-free solvothermal method at 170 °C. This study provides a large-scale, economical and convenient method of obtaining catalyst CuS with broadband optical absorption properties.

1.3.4 Aqueous solution method

In this paper, plate-like copper sulfide (CuS) nanoparticles have been synthesized by a facile aqueous solution method using Radix *Puerariae* extract [48].

With the aim to synthesis CuS nanoparticles, 2 mL of 50 mmol copper sulfate solutions and 1 mL of Radix *Puerariae* root extract were mixed together in a vessel. The mixture was then stirred with a magnet for 5 minutes at room temperature. Ammonia sulfide solution (50 ml, 20 wt.%) transferred to a vessel and mixed thoroughly. Then the pH of the solution was increased to 9 by adding a 100 mL sodium hydroxide solution. The reaction was maintained at 60 °C with magnetic stirring for 10 hours.

In order to prepare plate-like CuS thin films, 2mL of deionized water and 1 mg of additive BYK 2000 were mixed in a glass vessel and mixed with a magnetic stirrer for 5 min. After that, several portions of CuS nanoparticles with different amounts (10, 20, 30 and 40 mg) were added to the prepared solution. Then, it is sonicated for 10 min and mixed with a magnetic stirrer for 20 min. The solutions were used as coatings with a thickness of 0.5, 1.0, 1.5 and 2 wt.% on slides ($76\times26\times1$ mm^3). The glass panes were washed several times with distilled water, then with acetone and left to dry. Copper sulfide was coated on the slides with a coating device and after application, the glass slides were placed in an oven for 10 minutes at 60 °C.

CuS/PVA thin films have been synthesized similarly by adding PVA. In a glass vessel, the required amount of distilled water was heated to 80 °C for 30 minutes, then 5 wt.% PVA was added, and the mixture was then stirred for 3 hours at the same temperature. In order to prepare thin films, 10, 20, 30, and 40 mg of CuS was added to 2 mL of water.

The crystallinity of as-prepared CuS samples was investigated by XRD, which revealed the diffraction pattern of CuS nanostructures corresponding to the hexagonal structure of covellite (JCPDS 06-0464). No additional diffraction peaks from other

phases or impurities were observed, indicating the high purity of the resulting CuS nanoplate structures.

TEM and SEM images of the CuS sample after 10 hours of synthesis are demonstrated irregular lamellar structures ranging in size from 10 to 250 nm. The SEM image shows that the lamellar structures are assembled and intertwined with each other.

1.3.5 Facial grinding method

Nanosheets of CuS particles happily prepared at room temperature via a fast, facile and efficient grinding method by using copper chloride, thiourea, and NaOH as precursors [49]. The specific surface area of freshly prepared CuS nano-sheets was obtained from isotherm N_2 adsorption/desorption, and its value was 23.18 m^2 g^{-1}, which is higher than the CuS synthesized by others in the traditional way.

With the aim to prepare CuS nanosheets, 2 mmol of copper chloride and 4 mmol of thiourea were exactly mixed by grinding in an agate mortar for 5 min. After 5 min, the color of mixture is changed to light green. Then 4 mmol NaOH was transferred into the mortar and another grinding process was performed for 5 min. Subsequently, obtained black precipitate was collected and washed by distilled water, and then washed by ethyl alcohol several times by centrifuging. After that, it is dried at 60 ºC and finally dark-green powder was obtained. All grinding synthesis procedure was performed at room temperature and ambient conditions.

In order to reveal the structure of as-prepared CuS, XRD analysis was performed. JCPDS 06-0464 card of standard hexagonal copper sulfide exactly confirmed the orthorhombic crystalline structure of as-synthesized copper sulfide nanoparticles. No pronounced impurity peaks can be discovered in XRD patterns, showing that the CuS samples synthesized under their experimental conditions were of high purity.

Microstructural SEM with EDS analyses was carried out by the authors in order to reveal the morphology and elemental composition of as-prepared CuS samples. SEM images of CuS with EDS results evidently displayed the uniform sheet-like morphology of the prepared CuS samples. EDS analysis showed that the atomic ratio of the element Cu to S is about 50.54/49.76 for CuS-0 and 52.19/47.81 for CuS-batch, both consistent with the standard CuS composition within the allowable error range.

The optical properties of CuS-0 and CuS-batch were investigated by authors using diffuse reflection spectroscopy in the UV-visible region of the spectrum. The transmission spectra obtained from spectroscopy were replaced by absorption spectra by means of the equation expressed as:

$$A = -\lg(T) \tag{7}$$

where A stands for optical density and T for transmittance. On each spectrum of freshly prepared CuS samples, a wide absorption peak appears a broad absorption peak located in the visible region and closed in the near-infrared region. These wavelength-dependent

absorption curves were further analyzed using the Tauc graph method, and curves $(Ahν)^2$ as a function of hν were obtained. The bandgaps of the CuS-0 and CuS-batch were assumed (from $(Ahν)^2$ vs. hν curves) to be 1.81 and 1.83 eV, respectively, which are in agreement with the board absorption peaks. Skimpy bandgap points out those as-synthesized CuS nanosheets can be excited by low-energy light. In the interim, a broad absorption range in the visible area may lead to high applying and conversion efficiency of natural light. Consequently, the resulting CuS nanosheets may have excellent photocatalytic properties, and relevant studies are under consideration.

Therefore, in this work, the authors reported a rapid, simple and effective approach to grinding for the synthesis of CuS nanosheets at room temperature, which allowed producing 10 grams high yield in their own laboratory. The authors investigated the crystal structure, morphology, surface structure and optical properties of the freshly prepared CuS nanosheets.

1.3.6 Wet chemical method

In this paper, Islam et al. [50] have synthesized copper sulfide (CuS) nanodisks using a tetraaza (N_4) macrocyclic complex precursor by a wet chemical method.

Copper sulfide (CuS) nanoparticles (nanodisks) prepared in a three-neck flask, dissolving copper complex (see preparation procedure here [50]) and $CuCl_2$ (cyclic N_4-L) (0.003 mol) in a 50 mL deionized distilled water stirring for 30 min. After that, 0.003 mol of thiourea was added in order to maintain the final molar ratio 1:1. Subsequently, a few drops of 5% aqueous NaOH were added to maintain a neutral pH of 7. The yellow precipitate was obtained a few minutes later, indicating the formation of a Cu-thiourea complex. The reaction mixture is boiled under reflux for 2 hours until a dark-brown precipitate is obtained. After the synthesis procedure, the resulting suspension of nanocrystals was centrifuged, and the precipitate was washed three times and centrifuged in distilled water and ethyl alcohol.

XRD pattern of CuS sample definitely indexed to the covellite-type hexagonal phase of CuS with space group P63/mmc, which also can be confirmed by the standard JCPDS 06-0464 card of CuS. The obtained XRD patterns of nanodisks also verify the formation of CuS with Cu/S = 1:1 stoichiometry. As shown in the XRD pattern, no other diffraction peaks rising from impurities are observed.

The catalytic activity of CuS nanodisks toward MB degradation with the light displays the higher MB degradation rate than under dark in the presence of H_2O_2. The C_t/C_0 plot as a function of time displays the higher MB degradation activity of CuS nanoparticles with H_2O_2. The recycle stability of CuS nanoparticles was even found to be >80 % after five cycles studied by repeating the MB degradation with same CuS nanoparticles sample.

Thus, authors successfully synthesized CuS nanodiscs from macrocyclic complex tetraaza through wet chemical methods using thiourea as a sulfur source. CuS pure phase

nanodiscs are polydisperse in morphology with an average lateral size of 15-20 nm and a thickness of 5 nm.

1.3.7 Sol-gel method

Semiconductor copper sulfide (CuS) nanocrystals (NCs) have been successfully synthesized via a simple sol-gel method by Li et al. [51]. The average diameter of the samples was about 3 nm with a narrow size distribution.

With an aim to synthesize and purification of CuS nanoparticles, 5 mmol of copper acetate was dissolved in the solution which consists of deionized water and pyridine with volumetric ratio 1:3, respectively, and heated to 80 ºC. In another parallel, in the 20 mL of deionized water also 5 mmol of sodium sulfide crystallohydrate was dissolved. With intensive magnetic stirring, a solution of sodium sulfide was added dropwise to the solution of copper acetate for 20 minutes. The mixture reacted for 2 hours at 80 °C.

In the XRD pattern of as-prepared CuS nanocrystals, standard CuS peaks (JCPDS 06-0464) distinctly confirmed the hexagonal CuS crystal structure of obtained sample. No other diffraction peaks of other copper sulfides were observed indicating the high purity of the sample.

The authors mentioned that CuS nanocrystals sample coated with pyridine surface ligands has a suitable dispersion, and most CuS nanocrystals are irregularly shaped with sizes ranging from 2 to 5 nm. Also, HR-TEM results confirmed that the CuS sample particle was single crystal with clear interplanar distances of 0.28 nm, which corresponded to the hexagonal phase of covellite. EDX analysis also confirmed presence of only CuS in the sample showing atomic ratio of elements close to 1:1.

In conclusion, the authors presented a facile solution method for the synthesis of colloidal CuS nanocrystals.

1.3.8 Hydrothermal method

Recently, copper sulfide nanoparticles with spherical shapes have been prepared via the hydrothermal synthesis method by Darouie et al [52]. As a precursor, authors used copper acetate monohydrate and thioacetamide. The synthetic process was performed in the presence and without CTAB and SDS surfactants. Results of XRD analysis confirmed that the size of obtained copper sulfide crystallites was in the range 16-23 nm.

With aim of prepare CuS nanoparticles in the absence of surfactants, 3 mmol of thioacetamide (TAM) solution with a volume of 35 mL was slowly transferred to the copper acetate solution with the same concentration at 80 ºC. After that, the color of the solution turned into green and then even dark green. After this, the obtained solution stored for 24 h in the autoclave at 80 ºC. Finally, temperature of system is decreased to room temperature and solution was centrifuged and washed with distilled deionized water and ethanol. Hydrothermal synthesis of copper sulfide in the presence of surfactants took place as follows: 1.5 mmol of copper acetate solution was added to the

2.1 mmol of surfactant solution and kept at reflux for 1 h. After that, under vigorous stirring, 3 mmol of TAM solution was added to the mixture. Continuous processes repeated the previous procedure.

In bots of approaches, obtained products were added to the 25 mL of ethanol. Black precipitates were separated by centrifuging and was washed by distilled-deionized water several times. Finally, dried under vacuum at 60 ºC for 12 h.

All reflections in the XRD pattern showed that the products crystallize well and all peaks can be well indexed to pure hexagonal copper phase sulfide in the form of covellite, which is in good agreement with the data given in the literature (JCPDS 06-0464). Reflections, such as chalcocite or sulfur, were not reflected, indicating phase purity in the synthesized samples.

TEM images revealed that without the use of surfactants, particles agglomerate in such a way that a heterogeneous platelet-like morphology is created. However, in the presence of SDS particles become smaller in size, somewhat spherical, but still heterogeneous. In the presence of CTAB a homogeneous spherical morphology with an average size of 16 nm was obtained, which is in good agreement with the results of X-ray diffraction analysis.

Thus, in this work, authors synthesized copper sulfide nanoparticles in the presence and absence of surfactants. Authors found that CTAB is more appropriate than SDS and is an effective surfactant for the synthesis of homogeneous and spherical CuS nanoparticles. It was also concluded by authors that if the reaction method is changed, the size and phase of the products will not change.

1.3.9 Hydrogel method

In this method, Tan et al. [53] discovered a novel approach of preparation copper sulfide nanotubes using hydrogel-based on *N*-lauroylalanine as a template under mild condition. The authors also found that the intermolecular hydrogen bonds play an important role in the formation of the hydrogel and the Cu^{2+} coordination gel.

The synthetic procedure of *N*-lauroylalanine (LAA) proceeds as follows: in a typical procedure, 200 mL of the well-mixed aqueous solution of sodium salt of alanine was in the 800 mL beaker and there 0.2 moles of lauryl chloride solution was added by dropwise. In order to keep pH of as-obtained solution at pH=9-12, 10% of sodium hydroxide solution was added. Then, after 2 h they acidified solution with sulfuric acid to pH=4.5. After that, white precipitate is obtained and it was filtered and recrystallized.

For the preparation copper sulfide (CuS) nanotubes, as-obtained LLA was dissolved in acetic acid, ethanol, and water (v/v = 1:5:19), then stoichiometric proportion of copper (II) acetate was added at 70 ºC under stirring and addition ethanol was added to dissolve the precipitate. After cooling to room temperature, a translucent gel (Cu-LAO gel) was formed, and then a double thioacetamide (TAA) was added to the gel, which dissolved in 0.5 mL of water. After 2 days, CuS precipitate was obtained. It was found that in the XRD pattern, the CuS sample is poorly crystallized. The results of

SAED analysis also confirmed this phenomenon. According to authors, the intensity and 2-theta location of peaks can be confirmed by standard data (JCPDS 36-379) as a hexagonal phase of covellite (CuS).

The TEM image of the LAA gel displayed a number of tubular aggregations with a diameter of ca. 70–150 nm, lengths of 1–20 nm. The TEM image of the CuS nanocrystals revealed that CuS nanotubes are found in the hydrogel system based on LAA. [54].

Thus, in this work authors could synthesize CuS nanotubes using hydrogel as a matrix from TAA and copper (II) acetate under soft conditions. Accordingly, other inorganic chalcogenide nanotubes with the desired diameter can be readily obtained by selecting a suitable hydrogel as the matrix.

1.3.10 Mechanochemical method

Acetate route mechanochemical synthesis of metal sulfides has been proposed by Balaz et al. [55]. Later, using this approach Godocikova et al. synthesized copper sulfide nanoparticles in an industrial mill [56]. In this work, authors aimed to synthesize semiconducting nanoparticles of MS (M: Pb, Zn, Cd, and Cu) by high-energy milling in an industrial mill and therefore to illustrate the potential of this approach for the large-scale production of nanopowders. Synthesis procedure took place at following conditions: time of milling in an air atmosphere 6 min, loading of the mill with steel balls of 30 mm diameter in a total amount of 17 kg, rotation speed of the milling chamber 960 rpm. MS nanoparticles were prepared by high-energy milling of corresponding acetate and sodium sulfide according to the equation:

$$(CH_3COO)_2M \times xH_2O + Na_2S \rightarrow \mathrm{MS} + 2CH_3COONa + xH_2O \quad (8)$$

where *x*=3, 2, 2 and 4 for Pb, Zn, Cd, and Cu acetate, respectively.

In the XRD pattern, except the covellite phase of copper sulfide (JCPDS 06-0464), with small amounts of chalcanthite $CuSO_4 \cdot 5H_2O$ (JCPDS 11-0646) and bonattite $CuSO_4 \cdot 3H_2O$ (JCPDS 22-0249) have been detected.

Lately, M. Balaz et al. have been synthesized CuS and Cu_2S nanoparticles using the mechanochemical approach within a few seconds from the elemental precursors [57]. It was found that the morphology of the copper used, related to the method of its production, is a key factor for the ultrafast reaction. The explosive nature of the mechanochemical reaction was controlled by changes in the gas pressure in the milling chamber, and the course of the reaction was monitored by the X-ray diffraction and Soxhlet's extraction analysis. The mechanochemical synthesis was performed at the Pulverisette 7 Premium line planetary ball mill (Fritsch, Germany) in a special 80 mL tungsten carbide milling chamber equipped with a sensor for monitoring gas and temperature changes during milling - the EASY GTM system (Fritsch, Germany). In a typical procedure, mixtures of Cu and S in stoichiometric ratios of 1:1 and 2:1 were

milled to synthesize CuS and Cu_2S, respectively. In the synthesis of CuS from elemental precursors, electrolytic copper (Cu(M)) was reacted with different types of sulfur. From this, the authors found that type of sulfur influences the reaction pathway. According to XRD results of 1:1 ratio, it can be concluded that the desired copper sulfide covellite (CuS) (ICDD-PDF2 65-3561) has been synthesized as a major phase. In addition to covellite, as a minor phase, also cubic digenite (ICDD-PDF2 076-6653) was identified. When atomized powdered copper was used, even after 5 minutes of milling, a significant amount of unreacted copper is contained, and the main peaks of sulfur could be observed in the XRD pattern.

Thus, in this work, authors could successfully mechanochemically synthesize copper sulfides (CuS, Cu_2S) from elemental precursors within a few seconds. The authors also concluded that the reaction pathway is strongly influenced by the morphology of copper, in particular, the electrolytically obtained method contributes to the development of an ultrafast reaction pathway.

1.4 Application fields of copper sulfide (CuS) nanoparticles

Chalcogenides, as advanced promising materials, have a wide variety of properties that continuously present opportunities for application in materials science [43]. Among them, the applications of copper sulfides, in general, is quite interdisciplinary, as can be seen in recent literature [58]. For instance, naturally occurred covellite phase (CuS) of copper sulfides demonstrates unusual superconductivity at 1.63 K [59]. Due to the wide variety of optical and electrical properties, copper sulfides are finding promising applications in optoelectronic devices [60], photocatalysis [61], photovoltaic cells [62], sensors [63], battery electrodes [64], and biomedical [65] fields.

1.4.1 Photocatalysis

Due to the fact that strong absorption in the visible range and stability in a wide pH range, copper sulfide nanoparticles are widely used in the photocatalytic decomposition of various organic pollutants [43, 66]. Lately, the productivity of the photocatalytic activity of various copper sulfide nanoparticles in the attendance of different dyes, e.g., methylene blue (MB), Rhodamin B (RhB), etc. has widely been studied [67, 68]. Photocatalytic activity of various CuS nanostructures (nanoflowers, dough-nut-shaped nanospheres, and dense nanospheres, mixtures of nanoneedles, nanoparticles, and nanoplates) with bandgap distributed between the 1.61 and 2.01 eV in Rhodamine B was studied by Zhang et al. [69]. In the work [68], monodisperse CuS micro flowers also showed excellent photocatalytic activity against MB degradation. Srivastava et al. found that CuS nanoparticles decompose MB to ~90% in 90 min and also indicated magnificent reusability [70]. A very high rate of Rhodamine B decomposition, reaching 98% decomposition in 15 min, was observed for a mixture of CuS and Cu_7S_4 with flake-like nanostructures compared to pure CuS and Cu_9S_5 [67].

1.4.2 Energy storage devices

Recently, cathode materials on the basis of transition metal chalcogenides are becoming versus lithium-ion battery technology [71]. Nanostructures on the basis copper sulfide (CuS) compounds are considered as an efficient cathode material in lithium-ion batteries according to high lithium activity, high abundant and low cost [64]. According to authors [72], the reactivity of Li/CuS system can be expressed as follows:

$$2CuS + 2e + 2Li^{+} \Leftrightarrow Cu_2S + Li_2S \quad (9)$$

$$Cu_2S + 2e + 2Li^{+} \Leftrightarrow 2Cu + Li_2S \quad (10)$$

Lai et al. could synthesize array-like Cu_2S nanowires on the surface of conductive copper-substrate and it has been used as a cathode material in LIB [64]. The obtained electrode exhibited a good capacitive performance of 230 $mAh \cdot g^{-1}$. Also, similar experiments on capacitive performance of flake-like CuS nanostructures have been performed by Guery et al. [73]. So, in their work electrode initially demonstrated discharge capacity value of 350 $mAh \cdot g^{-1}$.

1.4.3 Solar cells

Bera et al. [74] investigated the current tunneling effect as well as state density spectra (DOS) in individual nanorods designed as Cu_2S/CdS (p-n) or Cu_2S/CdS/Cu_2S (p-n-p) heterojunctions to determine strip edges across the intersection. It is also reported that the Cu_2S/CdS coaxial nanowire has shown improved performance in photovoltaic devices due to the piezo-phototropic effect [75]. Yang et al. synthesized CdS/Cu_2S core-shell single-crystal nanowires as an impressive p-n transition to separate generated charge carriers and minimize their recombination. According to the authors, the use of hybrid CuS nanotubes-ITO Schottky transitions in photovoltaic devices demonstrated efficiency of 1.46%. In other papers, authors could utilize Cu_2S as an effective electrode counter due to their higher electrocatalytic activity [76].

1.4.4 Biomedical applications

CuS nanostructures are broadly utilized to detect biomolecules such as DNA, metabolites such as glucose, food pathogens, hydrogen peroxide, and others. The growing popularity of CuS nanoparticles for probing applications is based primarily on their metal-like electrical conductivity and ability to stimulate electron transfer reactions with biomolecules [42].

DNA detection. Recently, a large number of strategies have been developed to detect DNA hybridization [77]. Among them, the detection of chemiluminescence based on nanomaterials is of great importance. The authors mentioned that although classical chemiluminescence assays depend on the luminescence of tags (usual enzymes) attached to the probe DNA during hybridization with the target DNA [78], newer versions of assays rely on the use of metallic and semiconductor nanoparticles as a tag. Modification

of the DNA probe by CuS nanostructures requires a much shorter time than Ag nanoparticles (13 h vs. 116 h).

Thereafter, an improved sensor with a lower detection limit and higher sensitivity was reported in [79]. Using a similar approach, Ding et al. [80] have developed a more sensitive and accurate method for the quantitative determination of single nucleotide polymorphisms (SNPs) up to the attomolar concentration. Higher sensitivity was obtained by combining Au nanoparticles, each of which was loaded with ~80 CuS nanostructures for chemiluminescence detection of Cu^{2+} ions (generated by dissolution of CuS nanoparticles).

Glucose Biosensors. The first biosensor for glucose was created about half a century ago to control glucose oxidation based on the enzyme glucose oxidase (GOX) [81]. Since then, great strides have been made and numerous glucose biosensors based on the nanoscale and mesoporous electrode surfaces containing metallic and/or semiconductor nanoparticles have been developed. These strategies allow direct electron transfer between the electrode and the enzyme that is captured in the pair, thereby eliminating the need for mediators. And CuS nanoparticles with metal-like conductivity provide inexpensive alternatives to noble metal-based detectors and are of considerable interest in this field.

In the work [63], glass-carbon electrodes coated with multi-walled carbon nanotubes (MWNT) modified with nanocrystals of monocrystalline copper (I) sulfide (from spherical to triangular plate morphology) were used to create glucose sensors. The authors found that the created sensor was found to be much more sensitive to H_2O_2 (released by GOX glucose oxidation) with a detection limit of 50 nm, as opposed to 10 μm for a conventional GOX-based sensor. A possible mechanism for such enhanced photocurrents was referred to direct and efficient electron transfer from catalytic, photoexcited Cu_2S nanocomposites to the MWNTs, forming an electrical network through direct contact.

1.4.5 Antibacterial applications

The antibacterial activity of copper sulfide nanoparticles for the first time has been successfully tested in the work of Wang et al. [82]. Here, to study the bactericidal effect, authors have compared the antibacterial activity of CuS nanoparticles with free Cu^{2+} ions and MUH molecules against *E. Coli* bacteria. Results that are presented in their work show that CuS nanoparticles started to kill bacteria after 20 hours indicating the high antibacterial activity effect.

In addition to the OD_{600} monitoring analysis, the number of viable bacterial cells after 48-hour treatment was measured using CFU counting. The number of viable cells in the group receiving MUH is almost the same as in the control group, which is in good agreement with the result of OD_{600}. The authors were interested that although cells treated with CuS NCs have an OD_{600} ~0.5 value after treatment for 48 hours, no colonies formed on the LB agar plate, causing almost all cells to be dead.

Thus, for the first time, CuS NCs were used as an antibacterial agent and 800 μm (76.4 μg/mL) of CuS NCs could completely destroy *E. coli* cells by damaging their cell walls.

1.5 Preparation methods, properties and application fields of sulfur-containing nanocomposites

In addition to the synthesis of semiconductor copper sulfide (CuS) and sulfur nanoparticles, which are used for various purposes (e.g. in solar cells, cathode material in lithium batteries, agriculture (fungicides and pesticides), optical filters, antibacterial agent or in photocatalysis) [43, 83], the synthesis of binary [84, 85], ternary [86] and quaternary nanocomposites [87-89] based on them is intensively studied. This is explained by the fact that nanocomposites, unlike nanoparticles, have a wider range of application fields and improved properties [86, 90-92].

There are many reports on the synthesis of sulfur-containing semiconductor nanoparticles with preparation methods such as chemical vapor deposition, hydrothermal route, *in situ* deposition, sol-gel route, green solvent-free, size control, Pechini, and solvothermal method, etc.

The resulting nanocomposites based on sulfur and copper sulfide semiconductor nanoparticles can be used in many fields such as photoluminescence and cathodoluminescence, photocatalysis, battery technology, fluorescent sensing, and thermoelectric materials, etc. [93].

In the work [94], high-density ZnO nanowires doped with 4 atom % sulfur (S) and pure ZnO nanowires were grown vertically aligned on a silicon matrix via chemical vapor deposition of a Zn or Zn/S powder mixture at 500 °C. The form of sulfur-doped ZnO nanowires was usually beam-like. Authors set that the average diameter of sulfur-doped ZnO nanowires and simple ZnO nanowires was 20 and 50 nm, respectively. The results of elemental mapping analysis showed that the sulfur doping occurs mostly at the surface of the nanowires with a thickness of a few nanometers. In the part of the application of the work, authors found that the photoluminescence and cathodoluminescence of sulfur-doped ZnO nanowires exhibit a significantly enhanced green emission band that comes from the sulfur-doped surface region of the nanowires.

Composite nanomaterials on the basis of sulfur and carbon, exactly graphene are becoming promising materials in the fluorescent sensing field. Bian et al. [95] have successfully synthesized sulfur-doped graphene quantum dots (S-GQDs) with bright blue emission via a facile one-pot hydrothermal method. Results of experiments showed that S-GQDs possessed a single-layer graphene structure with an average size of about 2.5 nm and revealed an excitation-independent photoluminescence behavior with maximum excitation and emission wavelength at 360/450 nm, respectively. Authors mentioned that doping GOD with sulfur greatly improved their electronic and chemical properties, giving S-GQDs a sensitive response to Ag^+ ions. In addition, S-GQDs have been successfully investigated as a sensitive probe for Ag^+ detection with high

sensitivity and selectivity. In the end, authors concluded that the easy production method and high performance of S-GQDs present a promising potential for their application in sensing, biological imaging, and catalysis.

Nitrogen-sulfur co-doped fluorescent carbon nanocomposites (NSCPs) have been successfully synthesized via the simple, green, and solvent-free technique by the Huang et al. [96] for cellular imagining. The as-synthesized NSCPs showed high water solubility, long lifetime (14.01 ns), high quantum yield (27.2%), excellent stability and low cytotoxicity and can be used as a probe for cell imaging.

Hamal et al. [97] using a modified sol-gel method could prepare a new photocatalyst nanocomposite material on the basis of silver, carbon, and sulfur-doped TiO_2 with a high surface area. The influence of experimental parameters on the reactivity of visible light catalysts was estimated for the photodecomposition of acetaldehyde gas as a household model contaminant. Authors found that Ag/(C, S)–TiO_2 photocatalysts decompose acetaldehyde 10 times faster in visible light and 3 times faster in ultraviolet light than the accredited P25-TiO_2 photocatalyst.

Similar work has been performed on the synthesis of sulfur-doped titanium dioxide nanoparticles by Hussain et al. [98]. By controlling the size of nanoparticles, sulfur-doped anatase TiO_2 nanoparticles (3-12 nm) were prepared via the reaction of titanium tetrachloride, distilled-deionized water and sulfuric acid with the addition of 3M NaOH at RT. The photocatalytic and electro-optical properties of the as-synthesized sulfur-doped TiO_2 nanoparticles were investigated together with commercial TiO_2 nanoparticles with the average size around 24 nm. The results of photocatalytic activity under UV and solar radiation show the maximum conversion of phenol at a particle size of 4 nm at 4.80% sulfur doping. Also, similar results are obtained using ultraviolet energy for both phenol conversion and CO_2 + H_2O, where the formation of methanol, ethanol, and propanol is observed. It was found that for 4 nm TiO_2 particles without S-doping, the production of methanol, ethanol, and propanol was lower compared to S-doped particles.

Thermoelectric properties of sulfur-containing nanocomposites are well studied in the work of Zhou et al. [99]. Authors prepared sulfur-doped n-type Ag_2Te nanoparticles using a solvothermal method. The authors found that the use of dodecanthiol during synthesis effectively introduces sulfur doping into the sample, which optimizes the concentration of charge carriers in the nanoparticles to $>1\times1020$ cm^{-3}. This allowed authors to reach the desired electrical resistivities of $<5\times10^{-6}$ Ω·m. When as-synthesized sulfur-doped Ag_2Te nanocomposites were tested as thermoelectric materials, the 15 nm Ag_2Te nanoparticles showed a maximum *ZT* value of ~0.62 at T = 550 K, which is higher than the bulk Ag_2Te prepared by the authors.

Lately, sulfur-containing nanocomposites are widely used as a cathode material in lithium-ion batteries technology. Bakenov et al. have prepared very many variations of sulfur-containing nanocomposites with high specific energy and low cost of production such as sulfur/dehydrogenated polyacrylonitrile/ketjen black (S/DPAN/KB) [100],

sulfur/polyacrylonitrile/graphene oxide (S/PAN/GO) [101], sulfur/activated carbon/graphene (reduced graphene oxide) aerogel (S/AC/GA) [102], sulfur/graphene oxide (S/GO) [103], carbon-coated sulfur/polyacrylonitrile (C@S/PAN) [104], sulfur/nitrogen-doped carbon nanotube (S/N-CNT) [105], sulfur/nitrogen-doped graphene (S/N-G) [106], etc. All these abovementioned nanocomposites have been synthesized via the methods such as electrospinning technique, simple vacuum filtration, spray drying, novel solution processing, and simple sonicated mixing.

2 EXPERIMENTAL PART

2.1 Reagents and techniques

2.1.1 Chemical reagents and their descriptions

Descriptions of selected reagents that are necessary to perform experiments are given in Table 4.

Table 4 – Descriptions of reagents

№	Substance name	Chemical formula	Density, g/cm^3	Molar mass, g/mol	Company and country of production
1	Calcium polysulfide solution	CaS_4	1.250	168.342	*In situ* prepared
2	Carbon dioxide	CO_2	1.95×10^{-3} at STP	44.0098	*In situ* prepared
3	Thiourea	$(NH_2)_2CS$	1.405	76.1222	Sigma-Aldrich, Germany
4	Copper acetate monohydrate	$Cu(CH_3COO)_2\times H_2O$	1.882	199.6493	Acros Organics, Belgium
5	Copper chloride dihydrate	$CuCl_2\times2H_2O$	3.386	170.4826	Sigma-Aldrich, Germany
6	Elemental copper	Cu	8.960	63.5460	Pometon, Italy
7	Elemental sulfur	S	2.070	32.0660	CG-Chemikalien, Germany
8	Sodium thiosulfate pentahydrate	$Na_2S_2O_3\times5H_2O$	1.670	248.1841	ITES, Slovakia
9	Citric acid	$C_6H_8O_7$	1.665	192.1240	Liana, Slovakia
10	Sodium sulfide nonahydrate	$Na_2S\times9H_2O$	1.427	240.1820	Acros Organics, Belgium

2.1.2 Equipment for the solid-phase synthesis

Mechanochemical syntheses of CuS nanoparticles and sulfur-containing nanocomposites have been performed using a Pulverisette 6 classic ball mill (Fritch, Germany).

The Pulverisette 6 classic line planetary ball mill is a high-performance planetary ball mill with a single seat for the grinding cup and a practical, easily adjustable balance. The advantage of a mill is a very simple operation and high energy consumption with speeds up to 650 rpm. This provides high grinding performance with very small footprint for grinding results without loss when grinding hard, medium-hard, brittle and wet materials in a dry environment, in suspension or in a shielding gas atmosphere.

The sample to be crushed is mainly crushed by the high-energy impact of grinding balls. To do this, grinding cups with crushed material and balls rotate on a rotating planetary disk in the opposite direction around its axis. Starting at a certain speed, the centrifugal force leads to the separation of the crushed material and balls from the inner wall of the grinding Cup. The grinding balls cross the glass diagonally at maximum speed and grind the material both by crushing against the opposite wall of the glass and by colliding the balls with each other. Due to the rotation speed of the planetary disk up to 650 rpm, Pulverisette 6 classic ball mill develops centrifugal acceleration up to 29 G.

The performance characteristics of Pulverisette 6 ball mill are:

- high grinding power thanks to the number of revolutions up to 650 rpm;
- small footprint and ergonomic design;
- very simple operation;
- programming the timer to the second;
- simultaneous processing of up to 2 samples;
- useful volume up to 225 mL;
- a large range of rpm with a precise indication;
- sealed, easy to open working chamber;
- cooling of the crushing chamber with built-in fan for continuous grinding;
- precisely reproducible grinding results by means of an adjustable drive, precise gear ratios (gear belt), programmable microprocessor control electronics;
- programmable interval and break times.

Pulverisette 6 classic line planetary ball mill with 1 grinding seat works with 1 or 2 grinding cups in sizes 80, 250 or 500 mL, rotating with a ratio of 1: -1.82 relative to the planetary disk. For best grinding results, grinding cups and grinding balls are available in 7 different sizes and materials. This allows you to purposefully avoid contamination of samples with unwanted chips. For grinding in the atmosphere of the protective gas and for mechanical activation and alloying, it is recommended to use gas covers.

2.2 Liquid-phase preparation of sulfur and sulfur-containing S/$CaCO_3$ nanocomposites

Sulfur (S) and calcium carbonates ($CaCO_3$) were co-precipitated by bubbling CO_2 through aqueous solutions of CaS_4 polysulfide, which were prepared by the procedure described in [107-109]. When CO_2 was passed through a flask with a CaS_4 solution, a suspension containing a mixture of $CaCO_3$ and S particles was obtained via the following reaction (Figure 5):

$$MS_x + 2H_2O + CO_2 \rightarrow MCO_3 \downarrow + (x-1)S \downarrow + H_2O + H_2S \uparrow \quad (11)$$

In particular, calcium carbonate and sulfur were formed as follows:

$$CaS_4 + 2H_2O + CO_2 \rightarrow CaCO_3 \downarrow + 3S \downarrow + H_2O + H_2S \uparrow \quad (12)$$

The precipitates resulting from reaction (12) were isolated by filtration. Then, they were, in addition, used for the preparation of individual sulfur and $CaCO_3$ powders. To separate sulfur particles from $CaCO_3$, the precipitates were treated with hydrochloric acid and sulfur was obtained as a yellow powder on a filter.

For example, mixed sulfur and calcium carbonate particles (25.9 g) were precipitated from a calcium polysulfide solution (100 mL, 125 g) by bubbling carbon dioxide. Accordingly, the concentration of the particles in the mixture was 259 g/L. After mixture separation, it was found that it consisted of sulfur (16.3 g) and calcium carbonate (9.6 g).

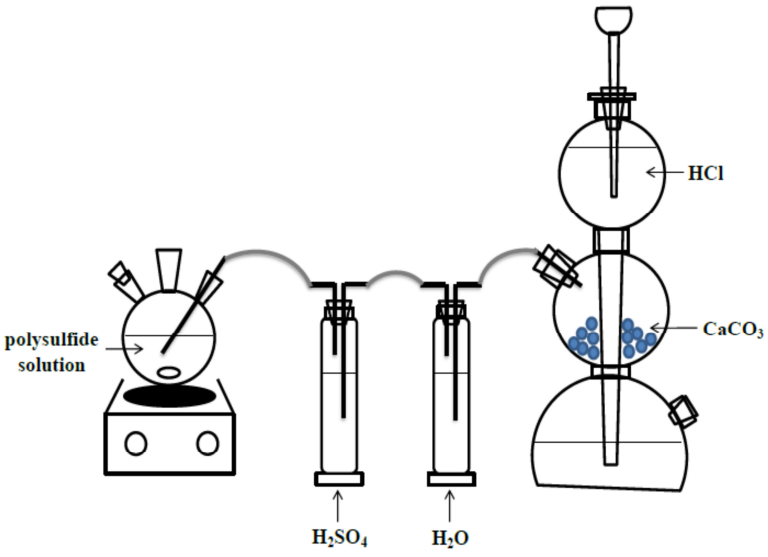
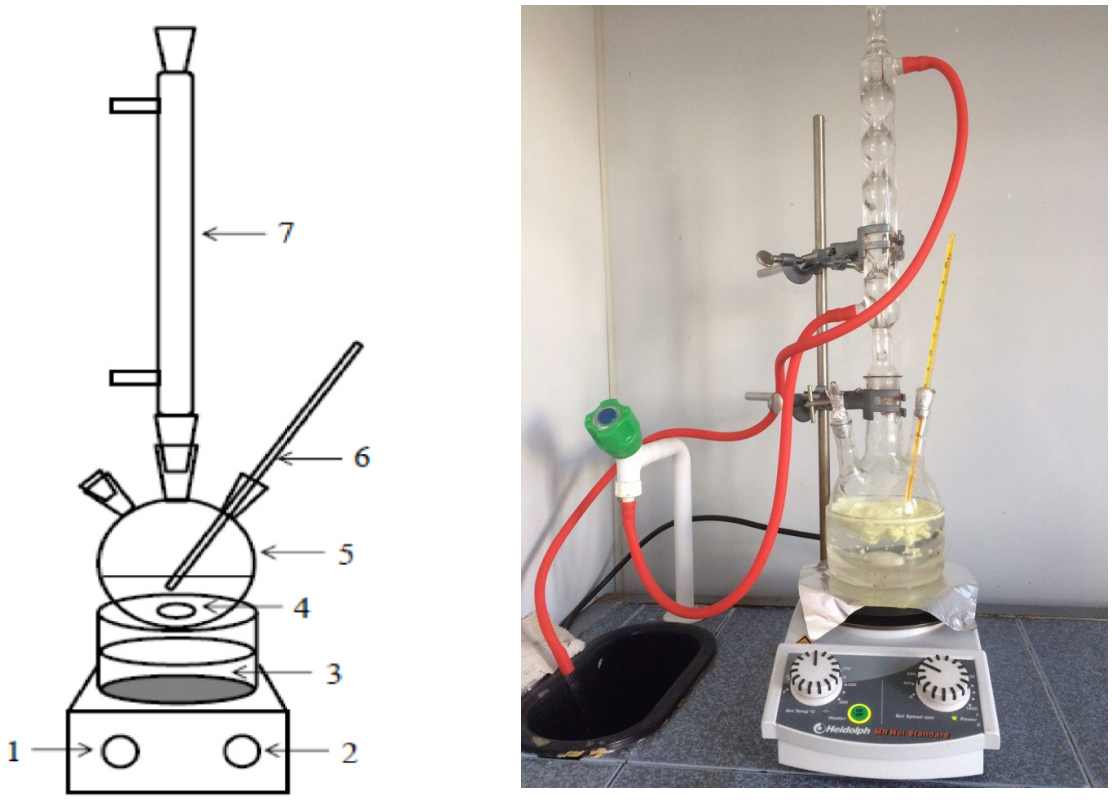


Figure 5 – Device for the liquid-phase synthesis of sulfur-containing S/$CaCO_3$ nanocomposite

2.3 Hydrothermal synthesis of CuS/S nanocomposites

CuS/S nanocomposites preparation procedure carried out as follows: 100 mL of distilled ultra-pure water was taken in a 250 mL three-necked round bottom flask equipped with a condenser and it was placed over a magnetic stirrer (see Figure 6). The temperature was raised to 80 °C and then 10 mL of thiourea solution (0.2 M) was added to the water under vigorously stirred condition. After that, also 10 mL of copper acetate solution (0.1 M) was added by dripping to the solution with the view to produce copper sulfide. Solution color is started turning from colorless to black. Then 5 mL of thiourea solution was dripped to the system in order to react with copper acetate residues. Hereupon, like in previous procedures, 10 ml of copper chloride solution was added dropwise to the above solution to obtain sulfur nanoparticles. All these step reactions were repeated twice to produce enough amount of samples for further characterization analyses. After synthesis, obtained greenish-black precipitants were centrifuged at 4000 rpm (Rotina-380R, Germany) and dried at 50 ºC for 6 h.



a b

1-temperature regulator; 2-speed regulator; 3-silicon oil; 4-magnetic stirrer; 5-three-necked flask; 6-thermometer; 7-reflux condenser.

Figure 6 – Device for the hydrothermal synthesis of sulfur-containing CuS/S nanocomposites: a – principal scheme of the device; b – constructed device

2.4 Mechanochemical synthesis of CuS/S composites

In order to synthesis CuS/S composite, elemental copper and sulfur were used without further purification. Ball milling procedure was realized in a Pulverisette 6 planetary ball mill under the following conditions: 250 mL steel milling chamber containing 50 steel balls with 10 mm diameter, milling time from 2.5 to 30 min, rotational speed 500 rpm and air atmosphere. The mixture of reactants (4 grams altogether) consisted of 1.9908 g copper and 2.0092 g sulfur, according to the reaction below:

$$\mathrm{Cu} + 2\mathrm{S} \rightarrow \mathrm{CuS/S} \tag{13}$$

After milling, the powder was collected from the milling chamber. The residual powder present on the lid was not taken for analysis, as its participation in the milling process is questionable.

The content of non-reacted elemental sulfur in the samples was determined by a gravimetric method using a Soxhlet extraction analysis employing CS_2 as a solvent. After its evaporation, the percentage of non-reacted sulfur was calculated using the following equation:

$$\mathrm{S}\ (\%) = \frac{\mathrm{m_{f1}} - \mathrm{m_{f0}}}{\mathrm{m_{s0}}}.100 \tag{14}$$

where S(%)- the content of non-reacted sulfur, m_{so} - the starting amount of sulfur in the reaction mixture (g), m_{fl} – mass of the flask after extraction (g), m_{f0} – mass of the flask before extraction (g).

2.5 Sulfur-mediated mechanochemical synthesis of spherical and needle-like copper sulfide nanoparticles

For all milling experiments, the reactants (5 g) in stoichiometric amounts were transferred into a 250 mL steel milling chamber containing 50 steel balls with 10 mm diameter and milled for 5, 10 and 15 min using the Pulverisette 6 planetary ball mill (Fritsch, Germany) using rotational speed 550 rpm, ball-to-powder ratio 37 and air atmosphere. After milling, the obtained product was washed with 1.5 L of water in order to remove the undesirable side-products and dried at 70 ºC.

Sulfur particles were mechanochemically synthesized by the reaction of sodium thiosulfate pentahydrate with citric acid, thus mirroring the procedure reported in [2], according to the following reaction:

$$Na_2S_2O_3 \times 5H_2O + C_6H_8O_7(catalyst) \rightarrow \mathrm{S} + Na_2SO_3 + C_6H_8O_7(catalyst) + 5H_2O \tag{15}$$

Citric acid has been used as a catalyst. In a typical procedure, 2.8133 g of sodium thiosulfate and 2.1817 g of citric acid was homogenized and milled.

Copper sulfide nanocrystals were prepared by the so-called acetate route [110]. In this synthesis, copper acetate monohydrate and sodium sulfide nonahydrate were co-milled in a stoichiometric amount (2.2727 g and 2.7273 g, respectively), according to the chemical reaction:

$$Cu(CH_3COO)_2 \times H_2O + Na_2S \times 9H_2O \rightarrow CuS + 2CH_3COONa + 10H_2O \quad (16)$$

In order to obtain nCuS, the reactions (15) and (16) were realized simultaneously.

2.6 Preparation of sulfur nanoparticles in dimethyl sulfoxide (DMSO)

In order to prepare sulfur nanoparticles in DMSO, first of all, the solubility of sulfur in DMSO was studied. The sulfur solubility tests in DMSO were carried out in a flask, which was immersed in an oil thermostat, with constant stirring with a magnetic stirrer (Figure 6). A small amount of sulfur powder was weighed on an analytical balance (accurate to 0.0001 g) and transferred to a round bottom flask with a magnetic stirrer. Then, 50 mL of a DMSO solution (part by volume) was measured with a cylinder and added to a round bottom flask. The flask with a solution of DMSO and powdered sulfur was fixed with a foot on a tripod and mounted on an oil bath. The temperature was adjusted in an oil bath and the desired temperature in the mixture was reached, the temperature of the mixture in the flask was observed through a thermometer. With constant stirring with a magnetic stirrer (250 rpm) at different temperatures, this mass of powdered sulfur was dissolved in 50 mL of DMSO for 30 minutes. Upon complete dissolution of sulfur, an additional portion of sulfur with a known mass was poured into the flask with the solution (this was repeated until sulfur ceases to dissolve).

After stirring was stopped, but the temperature was maintained. When all the sulfur settled to the bottom, the upper transparent solution was poured into a graduated cylinder, preventing the ingress of undissolved sulfur into the cylinder. Then we measured the mass of the remaining flask and the cylinder with the solution and the volume of the solution in the cylinder to calculate the mass of undissolved sulfur and how much DMSO remained in the flask. And the cylinder (1) was left overnight to cool to room temperature. The next day, by decantation, from the cylinder (1) merged the upper transparent solution onto another measuring cylinder (2). The masses of both cylinders (1) and (2) the volume of the final DMSO + sulfur solution at room temperature were measured to determine the amount of sulfur in the DMSO solution at room temperature. The undissolved sulfur in the flask and the precipitated sulfur contains a small amount of DMSO (this is taken into account in the calculations), and to determine the net mass of sulfur, the flask and cylinder1 were kept at a temperature of 200 °C to get rid of DMSO (boiling temperature of DMSO 189 °C), and the mass again measured.

The synthesis of nano sulfur occurs upon dilution of the obtained saturated solutions of sulfur in DMSO with water, acetone or ethyl alcohol. The sizes of sulfur particles in suspension solutions were determined by dynamic light scattering (DLS) at an angle of 90 ° using a helium-neon laser with a wavelength of 633 nm and a power of 4 mW (Malvern Zetasizer Nano ZS90) as a radiation source. Dilution of the sulfur solution in DMSO was performed at the location of the device. For each diluted solution, the initial hydrodynamic diameter of nanoparticles r_0 and the dynamics of its change were measured, up to reaching a slightly changing stabilized size r_C at measurement time t.

2.7 Characterization methods and techniques

2.7.1 XRD analysis

The structural characteristics of the sulfur nanoparticles separated from S/$CaCO_3$ nanocomposite (liquid-phase synthesis) were studied by XRD analysis using a Rigaku Ultima IV diffractometer (Rigaku, Japan).

X-ray diffraction patterns of CuS/S nanocomposites (hydrothermal route) were obtained on a MiniFlex 600 diffractometer (Rigaku, Japan) in a digital form using copper radiation. Sample analysis modes are as follows: X-ray tube voltage is 40 kV, the tube current is 15 mA, goniometer movement step is 0.02 2θ, and intensity measurement time at the point is 0.12 sec. During shooting, the sample was rotated in its own plane at a speed of 60 rpm. For phase analysis, the ICCD-PDF2 Release 2016 database and the PDXL2 software has been used.

XRD patterns of CuS/S nanocomposites (mechanochemical synthesis) were recorded by a D8 Advance diffractometer (Bruker, Germany) with CuKα (40 kV, 40 mA) radiation. XRD patterns were measured in the 2 theta range 10-65° with step size 0.03° and step time 10 s. For phase analysis, the JCPDS-PDF2 database and the Diffrac^{plus} EVA software has been used.

XRD patterns of S, CuS and nCuS (sulfur-mediated mechanochemical synthesis) were recorded by a D8 Advance diffractometer (Bruker, Germany) with CuKα (40 kV, 40 mA) radiation. XRD patterns were measured in the 2 theta range 10-60° with step size 0.03° and step time 6 s. For phase analysis, the JCPDS-PDF2 database and the Diffrac^{plus} EVA software has been used.

2.7.2 Raman spectroscopy analysis

The Raman data were obtained using a combined system Solver Spectrum (NT-MDT Spectrum Instruments, Russia), equipped with a photomultiplier tube (PMT) detector, a high-stability fast confocal laser (Rayleigh) imaging and 600/600 grating, 473 nm solid-state laser excitation. In all experiments, laser power at the sample was 35 mW and the exposure time was 60 s. Continuously tunable filters ND = 0.5 which reduce the laser intensity by 30% were also used. Without the use of a filter, the sulfur

sample is decomposed by the laser action. When using a blue laser, an error of ±4 cm^{-1} is provided.

2.7.3 TG-DSC analysis

Thermal analyses (thermogravimetry (TG) and differential scanning calorimetry (DSC)) were carried out under nitrogen with a NETZSCH 449F3A-0372 M (NETZSCH, Germany) instrument at temperatures up to 750 °C and a heating rate of 20 K/min.

2.7.4 Particle size analysis

The particle sizes of sulfur nanoparticles separated from $S/CaCO_3$ nanocomposite were measured by the method of light diffraction using a SALD 7101 laser analyzer (Shimadzu, Japan). The SALD 7101 analyzer measured particle-size distributions in a wide range of sizes from 10 nm to 300 μm in the real-time mode with a minimum time of the analysis equal to 1 s. This made it possible to monitor variations in the particle sizes due to aggregation or disaggregation in the dispersions. For this purpose, a liquid medium was placed into the 10-mL cell of the analyzer and light diffraction was observed when particles were present in the medium. The integral and differential particle size distribution functions were calculated every 4 s from the results of measuring the intensity of laser radiation scattered in different directions. When measuring sulfur or carbonate particle sizes, corresponding samples were placed into the cell in an amount of 3 mg per 1 mL water under stirring. Before measuring the sizes of hydrophobic particles, they were wetted with ethanol or isopropanol and, then, placed into the water-containing cell.

The particle size distribution of S microparticles, CuS, and nCuS nanocrystals was measured by photon cross-correlation spectroscopy (PCCS) using a particle size analyzer Nanophox (Sympatec, Germany). The powdered samples were dispersed in distilled water and sonicated before measurements. A portion of each sample was subsequently diluted with distilled water to achieve a suitable concentration for measurement. This analysis was performed using a dispersant refractive index of 1.33. The measurements were repeated 3 times for each sample.

2.7.5 Elemental analysis

Overall sulfur content in the CuS/S samples (mechanochemical synthesis) was determined using a CHNS Vario MACRO cube elemental analyzer (Elementar Analysensysteme GmbH, Hanau, Germany) equipped with a thermal conductivity detector. The combustion and reduction tubes were set to 1150 and 850 °C, respectively. Sulphanilamide (41.81% C, 16.26% N, 4.65% H, and 18.62% S) was used as a CHNS standard.

2.7.6 XPS spectroscopy

X-ray photoelectron spectroscopy (XPS) measurements of S, CuS and nCuS nanocrystals were performed using XPS instrument (SPECS) equipped with PHOIBOS 100 SCD and non-monochromatic X-ray source. The survey surface spectrum was measured at 70 eV transition energy and core spectra at 20 eV at room temperature. All spectra were acquired at a basic pressure of 9×10^{-9} mbar with AlK_{α} excitation at 200 W. The data were analyzed by SpecsLab2 CasaXPS software (Casa Software Ltd). A Shirley and Tougaard type baseline was used for all peak-fits. The spectrometer was calibrated against silver (Ag 3d). All samples showed variable degrees of charging due to their insulating nature. The problem was resolved by the calibration of carbon.

2.7.7 AFM analysis

The particle shapes and sizes of $CaCO_3$/S nanocomposites were determined by atomic force microscopy (AFM) with a Solver PRO-M scanning probe microscope (NT-MDT, Russia). The AFM images of particles were obtained using mica (muscovite) as a substrate which was fastened to a sapphire plate with double-sided scotch tape. The powders to be examined were thoroughly suspended in ultra-pure water (>18 MΩ) in a concentration of 10 mg powder per 200 μL water; a dispersion thus obtained was centrifuged at 2000 rpm for 30 s. A supernatant (10 μL) was applied onto a freshly cleaved mica and exposed in air for 2 min. The sample was then dried for 1 min in a nitrogen flow to remove the liquid from its surface. The samples were scanned in the contact mode. CSG 01 cantilevers (NT-MDT, Russia) with a tip apex curvature radius of 10 nm were used. The images were obtained using the Nova software (Version 1138) and processed with the help of the embedded Image Analysis software.

2.7.8 SEM and EDAX analysis

Scanning electron microscopic (SEM) analysis of the CuS/S nanocomposites (hydrothermal route) and S, CuS and nCuS samples (sulfur-mediated mechanochemical synthesis) was carried out with an SEM Quanta 3D 200i instrument (FEI, the Netherlands). Conducting carbon adhesive tape was used as a substrate for the samples.

SEM images of the not washed and dried filtrate samples of nCuS system were recorded using a MIRA3 FE-SEM microscopy (TESCAN, Czech Republic) equipped with EDX detector (Oxford Instrument, United Kingdom).

2.7.9 TEM and SAED analysis

Nanoscale analyses of the S, CuS and nCuS samples (sulfur-mediated mechanochemical synthesis) were performed by transmission electron microscopy (TEM). For TEM analyses, the samples were ultrasonically dispersed in absolute ethanol and the fine fraction of each sample was carefully applied onto a carbon-coated nickel grid. The dried grids were additionally carbon-coated to prevent charging under the high-energy electron beam. TEM analyses were performed using a 200-kV microscope JEM 2100 (JEOL, Japan) with LaB_6 electron source.

2.7.10 UV-Vis spectroscopy

The absorption spectra of S, CuS and nCuS samples were measured using a UV-Vis spectrophotometer Helios Gamma (Thermo Electron Corporation, Great Britain) in the range of 300-900 nm using a 1 cm path length quartz cuvette. The samples were diluted in absolute ethanol by ultrasonic stirring.

2.7.11 PL spectroscopy

The PL spectra of S, CuS and nCuS samples at room temperature were recorded at the right angle on a photon-counting spectrofluorometer PC1 (ISS, USA) with an excitation wavelength of 350 nm. A 300 W xenon lamp was used as the excitation source. Excitation and emission slit widths were set to 1 and 2 mm, respectively.

2.8 Antibacterial activity analysis of as-synthesized S, CuS and nCuS nanocrystals

The antibacterial activity of the samples was evaluated by the agar well diffusion method by a slight modification of the process reported in [111]. The tested bacteria (*S. aureus* CCM 4223, and *E. coli* CCM 3988*)* were obtained from the Czech collection of microorganisms (CCM).

In brief, bacteria were cultured aerobically at 37°C in nutrient broth (Oxoid, United Kingdom) with agitation, or on standard plate count agar (Oxoid, United Kingdom). Frozen stock cultures were maintained at -20°C. Before the experimental use, cultures were transferred to liquid media and incubated for 24 h. Cultures were then subcultured in liquid media, incubated for 24 h, and used as the source of inoculum for each experiment.

Agar media was cooled to 42°C after autoclaving, inoculated with liquid overnight bacterial culture to a cell density of 5×10^5 cfu/mL and 20 mL of this inoculated agar was pipetted into a 90-mm diameter Petri dish. Prior to the measurement, 10 mg of each sample was dispersed in 1 mL distilled water using sonication. After the solidification of agar, five millimeters diameter wells were punched into it and filled with 50 μL of samples. Distilled water was used as negative control and gentamicin sulfate (Sigma-Aldrich, USA) with the concentration of 10 mM as a positive control. The plates were incubated for 24 h at 37°C. After the incubation, the plates were photographed and the inhibition zones were measured by the ImageJ software. The values used for the calculation were the mean values of 3 replicate tests. The antibacterial activity was calculated by applying the formula:

$$\%RIZD = [(IZD\ sample - IZD\ negative\ control)/IZD\ gentamicin] \times 100 \quad (17)$$

where, RIZD is the percentage of relative inhibition zone diameter and IZD is the inhibition zone diameter (mm). As a negative control, the inhibition zones of distilled water equal to 0 were taken. The inhibition zone diameter (IZD) was obtained by

measuring the diameter of the transparent zone and subtracting the size of the wells (5 mm).

2.9 Biological activities of $S/CaCO_3$ nanocomposites

The biological activity, which manifested itself as a stimulating action on the growth of plants (acceleration of shoot and root growth upon seed germination), was determined by soaking wheat seeds with water and aqueous media containing nanoparticles of S, $CaCO_3$, and $S/CaCO_3$ nanocomposite in Petri dishes. Initially, some amount of seeds were soaked with water on a pan, which was, then, exposed in a thermostat at 25°C for 24 h. After that, ungerminated seeds were removed from the pan and 15 germinated seeds were placed in each Petri dish. Water was poured into some of the Petri dishes (blank samples), and compositions containing nano sulfur, calcium nano carbonated, or $S/CaCO_3$ nanocomposite was poured into the other dishes. Afterward, the Petri dishes were again exposed in the thermostat at 25°C. In 3 days, the Petri dishes were removed from the thermostat and the lengths of the shoots and roots of each seed were measured with a ruler.

The main goal of the experiments on the stimulation of plant growth was to determine the optimal concentration of the studied nanopowders. For this purpose, different amounts of the samples were placed into the Petri dishes containing water (6 mL). Then, the powder-to-water ratio that provided the maximum growth of shoots and roots was determined. Previously, we found [112] that some organic compounds (alcohols, glycols, and glycerol) added to aqueous nanodispersions enhanced the growth of roots and shoots. Therefore, in this study, we also added glycerol to each Petri dish. As a result, the maximum growth of shoots and roots was observed, when the content of sulfur (including that in the $S/CaCO_3$ nanocomposite) was 25 mg per 8 mL glycerol and 1 L water. The experiments on the germination of seeds in a medium containing only 8 mL glycerol per 1 L water revealed no acceleration in the growth of shoots and roots. When the nanoparticles were added, the growth increased, on average, by 11%. It should also be kept in mind that, in the experiments on the germination of seeds, we used powders of nanoparticles of sulfur, carbonates, and composites separated from the mother polysulfide solutions containing 0.5 wt % surfactant (neonol). These measurements were carried out for each composition in ten Petri dishes to increase the accuracy of the data; in other words, the lengths of roots and shoots were averaged over 150 seeds, with a root-mean-square error in the measurements being 3−4%.

2.10 Hydrophobic properties of $S/CaCO_3$ nanocomposites

The hydrophobic properties of the samples were determined by measuring the contact angle of a water droplet on the surface of a compacted powder using a horizontal optical microscope. The powders were compacted using a laboratory press under a low pressure sufficient to obtain a smooth and dense surface of the compacted sample in a

manner such that the surface was suitable for measuring the contact angles in taken photographs with an error of ±3°.

2.11 Detection of iron wear in the mechanochemically synthesized CuS/S sample using magnetometry

Magnetometry measurements were performed by using a vibrating sample magnetometer (VSM) installed on a cryogen-free superconducting magnet (Cryogenic Limited). The samples were measured in powder form packed in a specialized capsule.

3 RESULTS AND DISCUSSIONS

3.1 Liquid-phase synthesis of S/$CaCO_3$ nanocomposites

3.1.1 XRD analysis

The diffraction pattern of a nano sulfur powder separated from carbonates identifies only its orthorhombic phase (Figure 7) [113], which is inherent in sulfur nanoparticles and has been described in, e.g., [2].

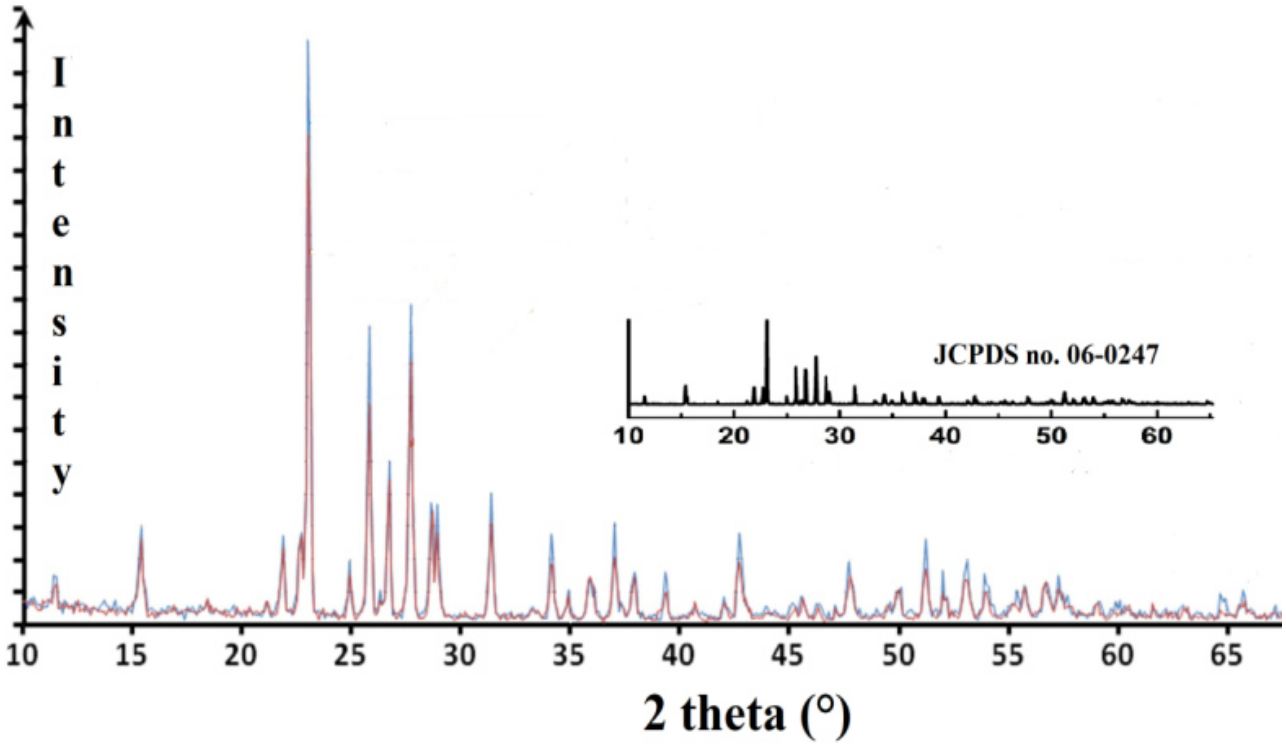


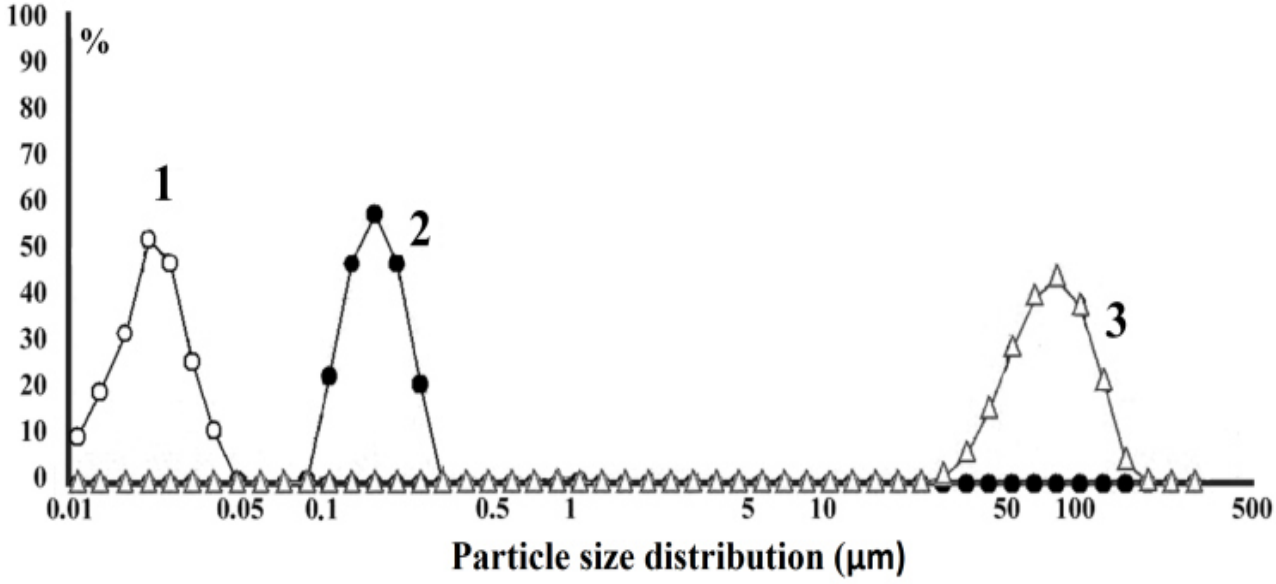
Figure 7 – Diffraction patterns of the separated sulfur sample from the composite [113, p. 412]

3.1.2 Particle size analysis

The integral and differential particle-size distributions were measured for each sample [113]. Previously, it was found [3] that sulfur nanoparticles with an average size of about 20 nm were precipitated from acidified solutions of polysulfide. Then, these nanoparticles enlarged in two stages to reach micron sizes. This took place when a polysulfide solution contained no surfactant, but the situation markedly changed when it was added to the solution [3, 56].

Figure 8 shows the differential size distributions of sulfur particles after their separation from $CaCO_3$ in the absence of the surfactant. It is seen that, at the initial stage, sulfur nanoparticles with an average size of about 20 nm are formed and that they are stable for a certain time (≈ 15 min). At the second stage, the nanoparticles begin to

form aggregates with sizes of 80–300 nm. In the third stage, these aggregates gradually grow to sizes of 30−170 μm for nearly 7 h. It has been found that being subjected to ultrasound, these submicron- and micron-sized aggregates are disrupted into primary sulfur particles with sizes of about 20 nm. At the same time, the addition of a surfactant (neonol, 0.5 wt %) into a mother polysulfide solution stabilizes the dispersion of sulfur particles with the average size of 20 nm for a period of more than 10 h. Therefore, polysulfide solutions containing neonol (0.5%) were, in all cases, used to produce nano sulfur, nano carbonated, and S/$CaCO_3$ nanocomposite.



1-primary nanoparticles immediately after their separation from calcium carbonate; 2-distribution measured 15 min after the separation (the first stage of enlargement); 3-distribution measured 7 h after the separation

Figure 8 – Dynamics of the differential size distribution of sulfur particles [113, p. 410]

3.1.3 AFM spectroscopy

We have determined the sizes and shapes of the particles of both kinds [113]. Figure 9 shows the AFM images of sulfur and calcium carbonate nanoparticles. As is seen in Figure 9a, sulfur nanoparticles have a quasi-spherical shape. Using special image-processing software, it has been found that the average particle size is about 50 nm. This size may be considered to be corresponding to the data represented by curve 1 in Figure 8. Two types of particles are seen in the image of $CaCO_3$ particles (Figure 9b).

It may be stated that the AFM images are in qualitative agreement with the laser diffraction data, while the differences are caused by the resolving power of the Solver PRO-M microscope and the specific features of sample preparation.

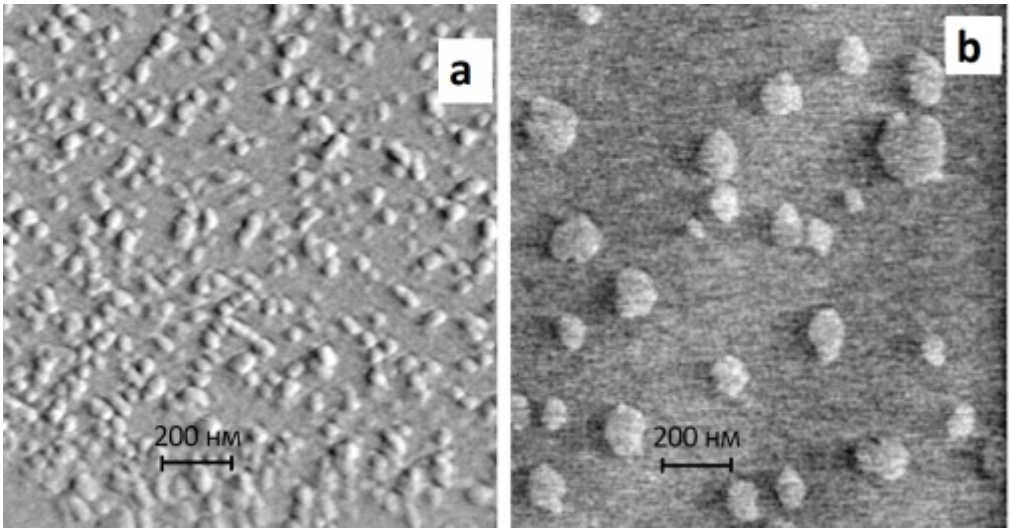


Figure 9 – AFM images taken from particles of (a) sulfur, and (b) calcium carbonate [113, p. 412]

3.1.4 Hydrophobic properties of S, $CaCO_3$ nanoparticles and S/$CaCO_3$ nanocomposites

The surface of a solid is of great importance at all levels of size. At the nanoscale level, surface phenomena are most pronounced and interesting. So it is known that the lotus leaf exhibits super-hydrophobicity, allowing water drops to roll in an almost perfect spherical state. The ability of the nanostructured surface of a lotus leaf to repel water has become a symbol for environmentally friendly technologies.

Measuring the wetting angle of water droplets gave the following results: 140±3° for the compacted surface of the separated sulfur nanoparticles; 147±3° for the surface of the separated calcium carbonate nanoparticles; 133±3° for the $CaCO_3$/S composite surface. It is known that sulfur is hydrophobic, and the mineral calcite is hydrophilic. In this regard, we note (Figure 10) that a drop of water on the surface of the nano sulfur (Figure 10a) is transparent and evaporates without leaving visible marks at the location. Drops of water on the surface of $CaCO_3$ (Figure 10b) and S/$CaCO_3$ (Figure 10c) always capture an insignificant portion of the substrate material to their periphery, and upon drying leave a visible trace – a tiny unevenness at the location compared to the original surface. We explain this by the fact that calcite nanoparticles partially retain hydrophilicity. The hydrophobic properties of calcium nano carbonated and S/$CaCO_3$ nanocomposite observed in this work are most likely caused by the neonol molecules that were present in polysulfide solutions in the amount of 0.5%. Moreover, this factor can also explain the hydrophobization of shell limestone with polysulfide solutions.

The largest wetting angle, close to the super-hydrophobicity, was inherent in the surface of calcium nano carbonated in the structure of calcite, and this is consistent with the results of [114, 115], in which calcium and barium carbonate nanoparticles were obtained in the presence of surfactants.

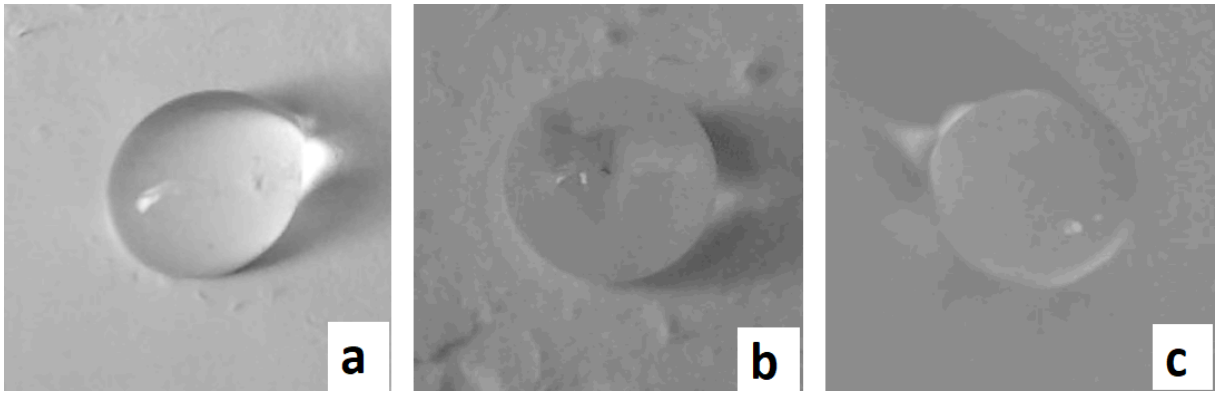


Figure 10 – Water droplets on the surface of the samples of nano sulfur (a), calcium carbonate (b) and S/$CaCO_3$ nanocomposite (c)

3.1.5 Biological activity of S, $CaCO_3$ nanoparticles and S/$CaCO_3$ nanocomposites

We considered the effect of the obtained samples of suspensions based on nano sulfur, calcium nano carbonate and S/$CaCO_3$ nanocomposite on the germination of wheat seeds according to the above method [113].

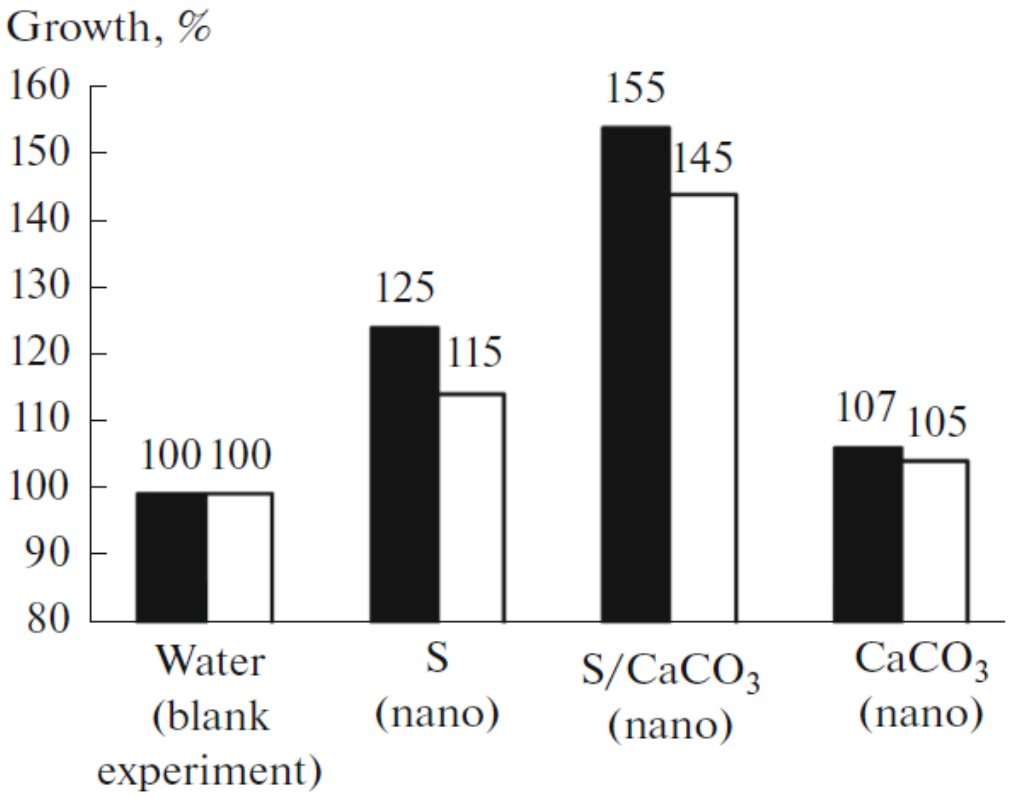


Figure 11 – The dependence of the length of the shoots and roots of wheat grains on the composition of aqueous suspensions for their treatment [113, p. 415]

The task was to determine which of the components prepared from calcium polysulfide and at what concentrations has the greatest effect on the growth of wheat grain. The assessment of the action of nano sulfur, nano calcite, and $S/CaCO_3$ composite was carried out by measuring the length of shoots and roots of grains grown in various media. The results are presented in the form of a diagram shown in Figure 11, from which it is clear that nano carbonated has the least impact on seed development (an increase in the length of the shoots by only 7%), the average value shows the nano sulfur (25%), and the greatest – $S/CaCO_3$, which accelerates the growth of shoots by 55% and the roots on 45% compared with control data.

We also carried out similar experiments with micron sulfur particles and the $S/CaCO_3$ composite. It was found that in this case, sulfur and the composite at concentrations lower than 25 mg/L do not affect the growth of wheat seeds, and at high concentrations, they do lead to its slowing down.

3.2 Hydrothermal synthesis of CuS/S nanocomposites

3.2.1 XRD analysis

Figure 12 shows the XRD patterns of the CuS/S nanocomposites [116]. The diffraction peaks of the CuS/S nanocomposites closely matched the standard copper sulfide and sulfur peaks. It is observed that in the case of sulfur, the peaks observed at 2θ = 11.47º, 15.55º, 18.43º, 21.17º, 23.07º, 25.83º indexed as (111), (022), (202), (115), (222) and (026) planes corresponding to orthorhombic phase with space group Fddd (70) (ICCD PDF-2 card №00-064-0585). From the patterns, it is also noticed that copper sulfide particles have diffraction peaks at 2θ values 27.12º, 27.67º, 29.27º, 31.78º, 47.92º, 52.73º, 59.32º indexed as (100), (101), (102), (103), (110), (108) and (116) planes corresponding to the hexagonal covellite phase with space group P63/mmc (194) (ICCD PDF-2 card №01-078-0877). No other peaks were detected, indicating the high purity of the sample.

The average crystallite size of copper sulfide and sulfur particles in the composite was calculated by Williamson-Hall formula (Equation 18) as follows:

$$\Delta K = \frac{0.9}{D} + K\varepsilon \tag{18}$$

where $\Delta K = \beta cos\theta/\lambda$ and β is the instrumental corrected full width at half maximum (FWHM), θ is the Bragg's angle, λ is the wavelength of CuKα radiation (1.5406 Å), $K = 4sin\theta/\lambda$, D is the average crystallite size and ε is the lattice strain [117]. According to the noted equation, the average crystallite size of copper sulfide and sulfur particles was about 3.5 and 3.6 nm, respectively.

Similar composite materials which consist of sulfur and copper sulfide compounds early have been synthesized via the reaction sodium polysulfide solution and Cu^{2+} ions. XRD analysis confirmed the presence of sulfur and copper sulfide phases in the sample [118].

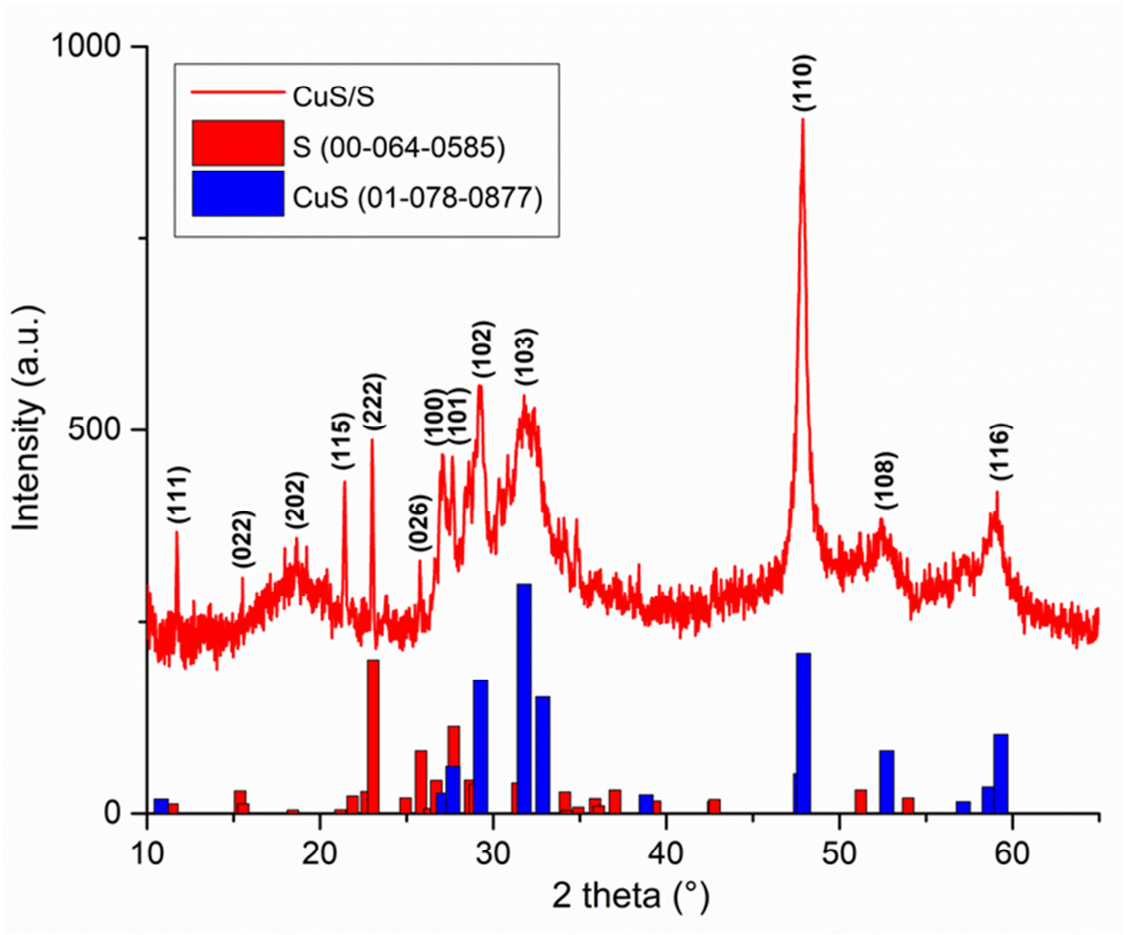


Figure 12 – XRD pattern of as-synthesized CuS/S nanocomposites by the hydrothermal route [116, p. 132]

3.2.2 Raman spectroscopy analysis

A typical Raman spectrum of CuS is shown in Figure 13 [116]. The peak is pronounced at 468 cm^{-1}, which corresponds to the vibrational (stretching) modes of the S–S covalent bond [119] and the much weaker peak at 260 cm^{-1} is explained by the fluctuation of the Cu–S bond [119]. In the works of Munce and Safrani et al. [120, 121], Raman spectra of covellite with the sharp band at 468 cm^{-1} which is attributed to S–S stretching vibration and a weak band at 263 cm^{-1} correspondings to A_{1g} TO mode are presented. However, according to their results, both of these peaks have been associated with the covellite phase of CuS.

Usually, sulfur has three distinct peaks in the Raman spectrum. According to [122, 123], the main wavenumbers determining sulfur are around 152, 220, and 474 cm^{-1}. However, in our case, apart from the characteristic peaks of the covellite, the sulfur peaks are not present in the Raman spectrum. This can be explained by the fact that sulfur could burn under the action of a laser beam or with the too-small size of sulfur crystals, which makes it difficult to measure with Raman spectroscopy due to the

phonon confinement effect [124]. Other explanations of this phenomenon are not considered since the other characterizing methods (XRD and TG-DSC) confirm the presence of sulfur in the composite material.

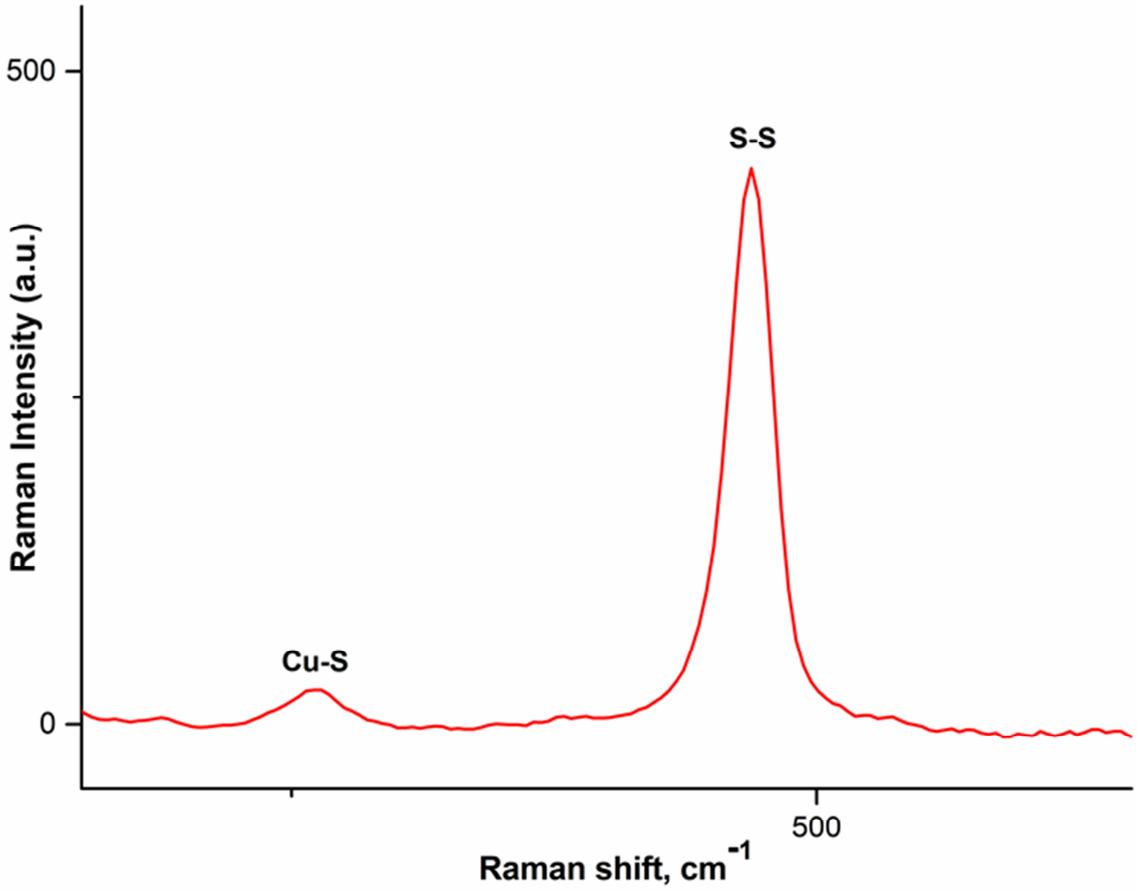


Figure 13 – Raman spectra of as-synthesized CuS/S nanocomposite [116, p. 133]

3.2.3 TG-DSC analysis

Thermal analysis of CuS/S sample was performed in a nitrogen environment, which is shown in Figure 14 [116]. From the DSC curve can be seen the small endothermic effect at 115°C, which shows the phase transformation of sulfur from S_α to S_β [125]. The decomposition proceeds in the following steps: TGA curve shows that the first loss up to 260°C with a mass loss of around 16.16 % due to the sulfur content removal and corresponding endothermic peak emerged at 260 °C. CuS nanoparticles are desulfurized at around 450°C to obtain the Cu_2S product [126]. According to the reaction (19), 12.29 % mass decrement is observed between 260 °C and 455 °C with small and sharp exothermic peaks, which point out 385 and 455 °C respectively.

$$2CuS \rightarrow Cu_2S + S \quad (19)$$

After 455 °C, from the curve can be seen a fluent mass decrement (12.55 %) with an exothermic peak at 525 °C. This weight reduction goes to around 720 °C and then stabilizes to a plateau. In this temperature range, the Cu_2S can decompose, forming copper and sulfur. This decomposition can be expressed by the following reaction (20):

$$Cu_2S \rightarrow 2Cu + S \quad (20)$$

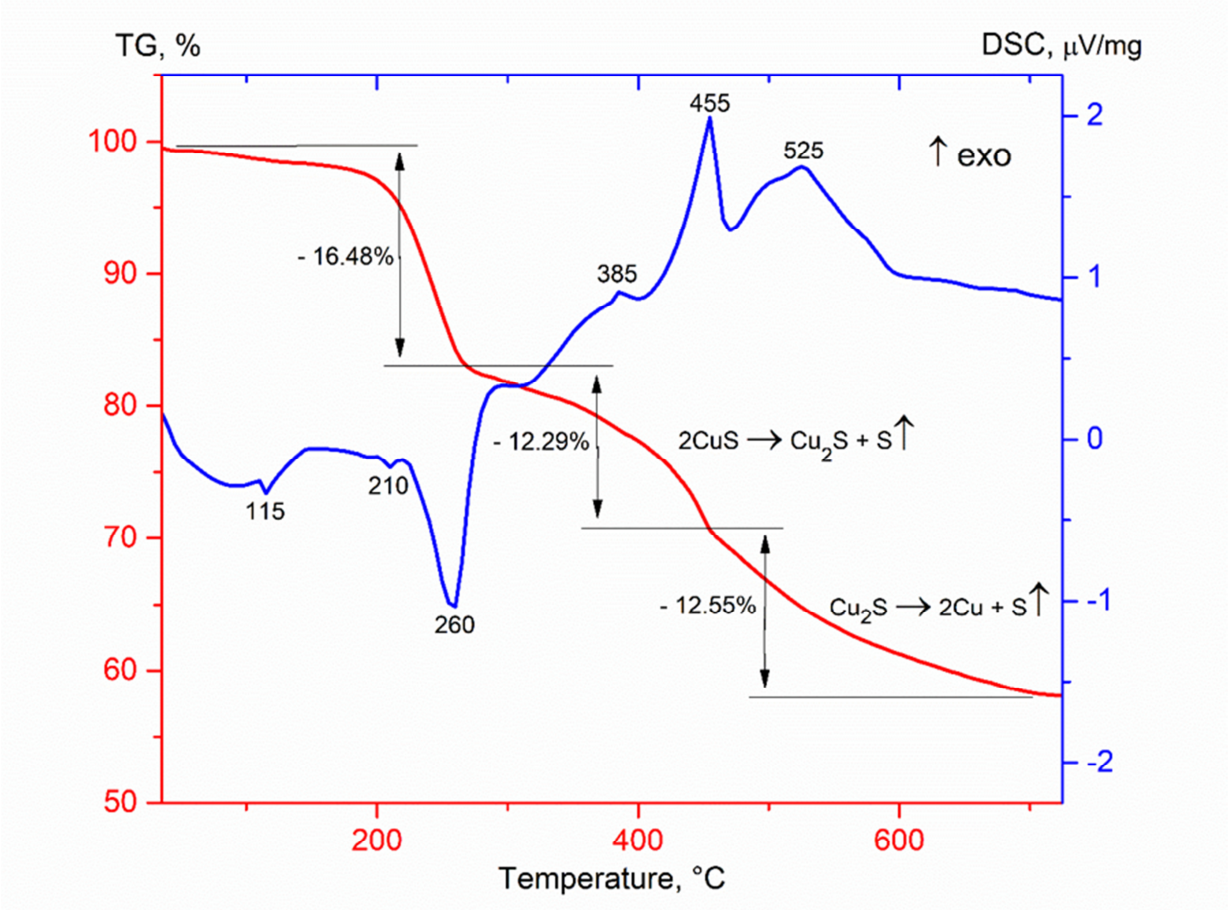


Figure 14 – TG-DSC curves of CuS/S nanocomposite sample [116, p. 134]

3.2.4 SEM analysis

To study the morphology of the obtained CuS/S nanocomposites, scanning electron microscopy analysis was used [116]. In Figure 15, we can see sample particles with non-uniform sizes. It can be clearly seen (see Figure 15b) two shapes of particles: spherical and elongated (needle-like) ones. As Raman spectroscopy could not detect sulfur from the composite material, we can definitely say that it is amorphous and has a non-structured shape. In the case of CuS nanoparticles, it is observed elongated needle-like CuS (nCuS) structures with the thickness from c.a.160 nm to 300 nm. Length of the nCuS particles exceeds their width around 20-30 times.

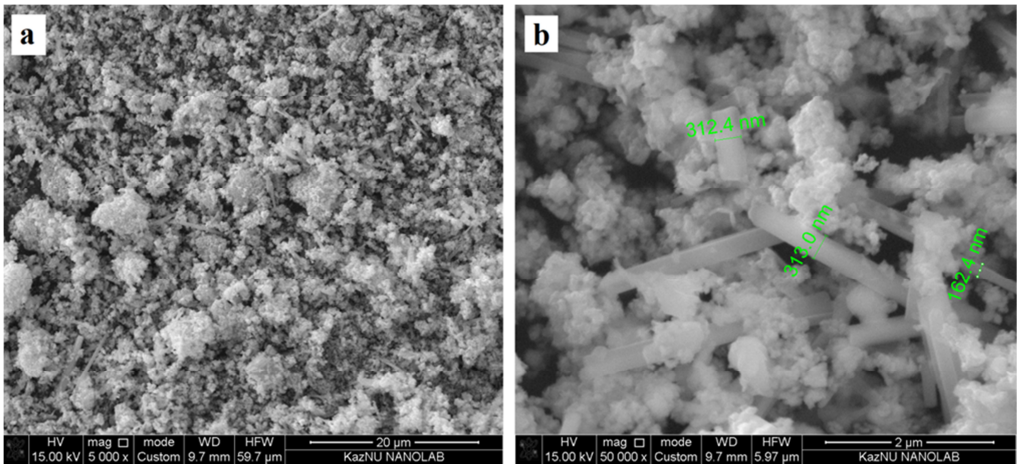


Figure 15 – SEM images of CuS/S nanocomposite: a – 5000×, b – 50 000× [116, p. 135]

3.3 Mechanochemical synthesis of CuS/S composites

3.3.1 XRD analysis

The progress of the reaction can be well seen from the XRD patterns presented below (Figure 16) [127].

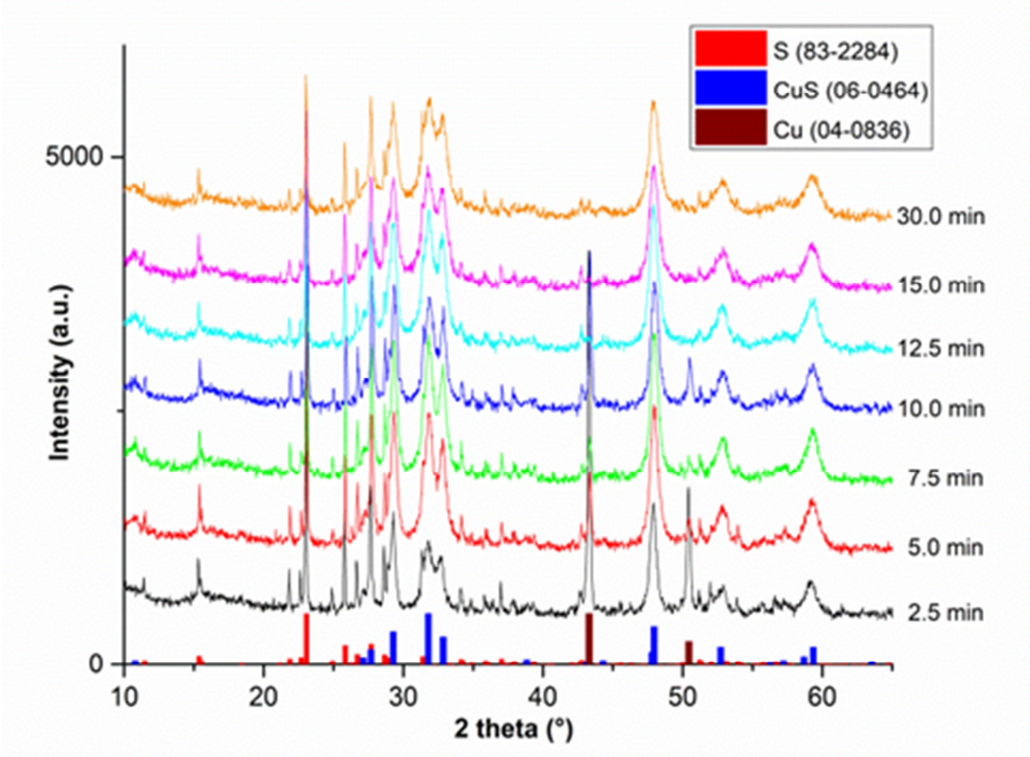


Figure 16 – XRD patterns of the powders milled for different times (time and identified phases are provided in the figure)

On the contrary to the study [57], the peaks of starting copper did not disappear within a second range in this case but were still visible until 10 minutes. As Cu peaks diminish, those of CuS become more intensive. After 12.5 min, Cu could no longer be identified. Sulfur peaks are visible throughout the whole process, so they are involved in the composite structure with the as-synthesized CuS at the end.

3.3.2 Elemental analysis

The content of overall and elemental sulfur was investigated by CHNS analysis and Soxhlet extraction, respectively (see Table 5).

The overall sulfur content remained constant throughout the experiment, although some discrepancies were detected in the early stages. These are most probably due to the inhomogeneous distribution of reactants. Especially at the very beginning (after 2.5 min), sulfur as a lighter element was most probably present as a major substance in the powder on the lid, which resulted in its lower content in the analyzed sample (45%). However, the elements became homogeneously distributed within the milled powder with time.

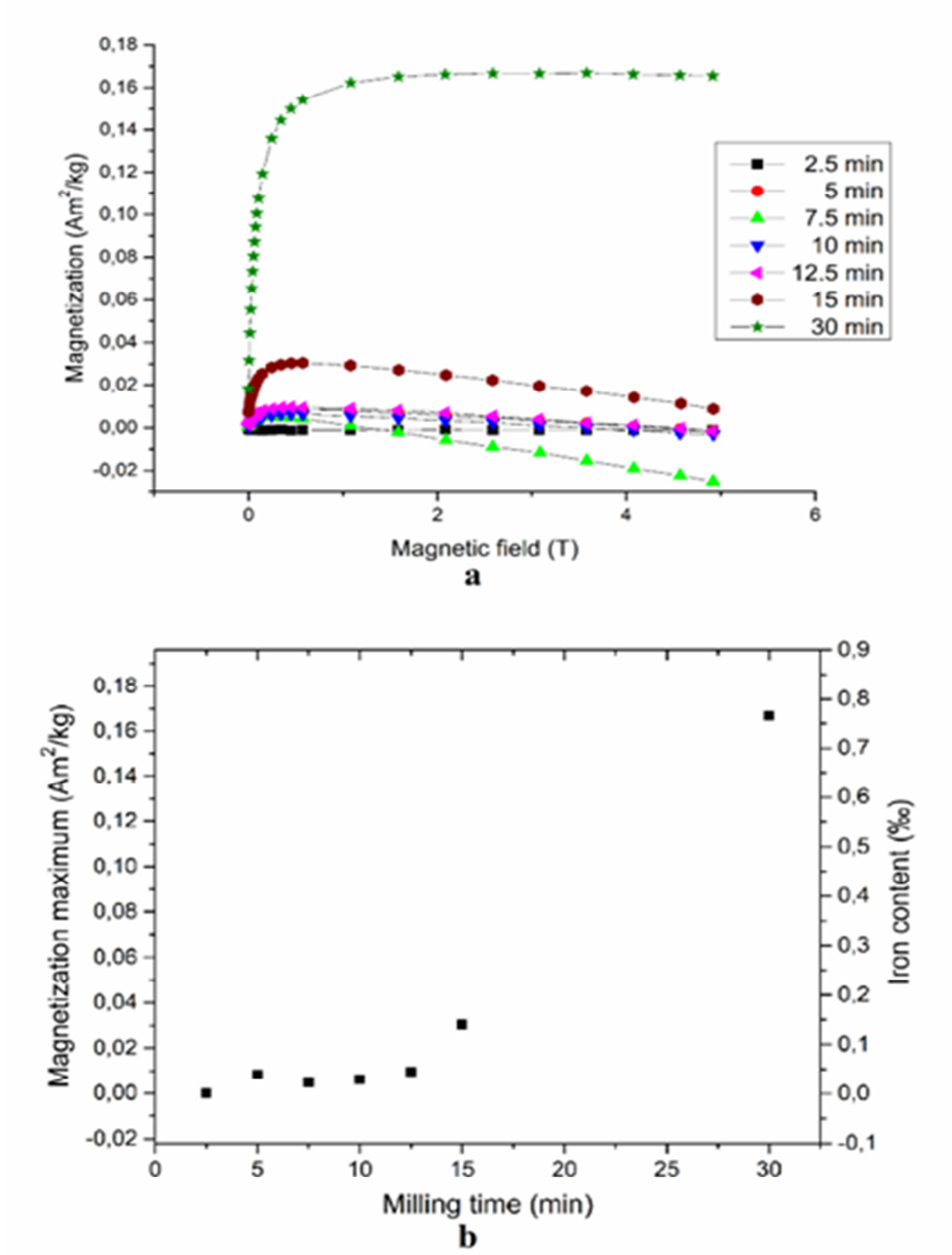
Table 5 – Overall and free sulfur content in the samples milled for different times [127]

Time (min) T	Overall sulfur content (%)	Free sulfur content (%)
2.5	45.2	31.2
5	52.1	24.9
7.5	52.0	23.1
10	54.7	21.5
12.5	50.7	23.6
15	50.3	20.0
30	50.7	18.7

The content of non-reacted sulfur decreased during the process. The decrease in the first stages of milling is more significant due to the progress of the CuS formation reaction. According to XRD (Figure 71), this process seems to be finished after 12.5 min. Upon the last 15 minutes of treatment, only a slight decrease in free S content was observed, which could be due to the measurement error. This means that it is no longer used for the reaction. Theoretically, the content of free sulfur should be 25% upon complete CuS formation, but sulfur is volatile and a small amount can easily evaporate during the Soxhlet analysis.

3.3.3 Results of magnetometry measurements

The magnetic response of the milled mixture was checked for each sample. The magnetization curves are presented in Figure 17a and the maximum magnetization is plotted as a function of milling time in Figure 17b.



a – magnetization curves; b- magnetization maximum and iron content vs. milling time

Figure 17 – Magnetometry results for the powders milled for different time (time of milling is given in figure)

The increase of magnetization value with milling time can be observed. As both reactants and products are diamagnetic, it can be only ascribed to the wear coming from the milling media, which is becoming larger when the duration of the process is increased. Most probably, small fragments are being torn down from the milling chamber walls and balls. This is evidenced by a sensitive magnetometer device as the negative diamagnetic signal is gradually suppressed by the emerging positive ferromagnetic contribution.

In order to quantify the wear, we assumed that no other component contributes to the magnetic signal. Using this assumption and the fact that the saturation magnetization value of pure iron is 216 Am^2/kg, the content of iron in the samples can be calculated. It can be seen that even ten-thousandths of per mille can be detected (for the sample treated for 2.5 min the value $6.77.10^{-4}$ ‰ was evidenced), which demonstrates the great sensitivity of this method. After the CuS formation is finished, the production of wear seems to increase significantly (from 0.13 ‰ to 0.76 ‰ for the powder treated for 15 and 30 min, respectively). It seems that during the CuS formation, the energy is spent mostly on this process, however, after its completion, the presence of a significant amount of more refractory CuS material boosts the wear production by its collisions with the balls.

3.4 Sulfur-mediated mechanochemical synthesis sulfur, spherical and needle-like copper sulfide (nCuS) nanoparticles

3.4.1 XRD analysis

As a first step, it was necessary to prepare sulfur particles to serve as a nucleation agent. In Figure 18, the X-ray diffraction patterns of sodium thiosulfate pentahydrate (STS) milled for 1, 3, 5, 10 and 15 min in the presence of citric acid (CA) are shown [128]. The patterns were recorded after the washing procedure.

It can be clearly seen that almost all diffraction peaks can be surely ascribed to sulfur and there seems to be no difference with respect to milling time. However, in addition to sulfur peaks, there are some diffuse peaks present around 45° for the samples milled for more than 5 min. These two peaks at 43.60° and 44.66° can be ascribed to chromium and iron respectively and are a result of contamination from the milling chamber. Their intensity increases with prolonged milling. It seems that this reaction causes a significant amount of chromium and iron from milling media to enter the reaction mixture after a very short time. The intensity of these peaks increases with milling time, which supports the hypothesis about wear [129].

Results of XRD analysis of not washed sulfur sample for a different time are presented below in Figure 19. The diffractions characteristic for sulfur corresponding to standard JCPDS card №83-2284 were identified in all samples. In addition, also various other diffractions are present.

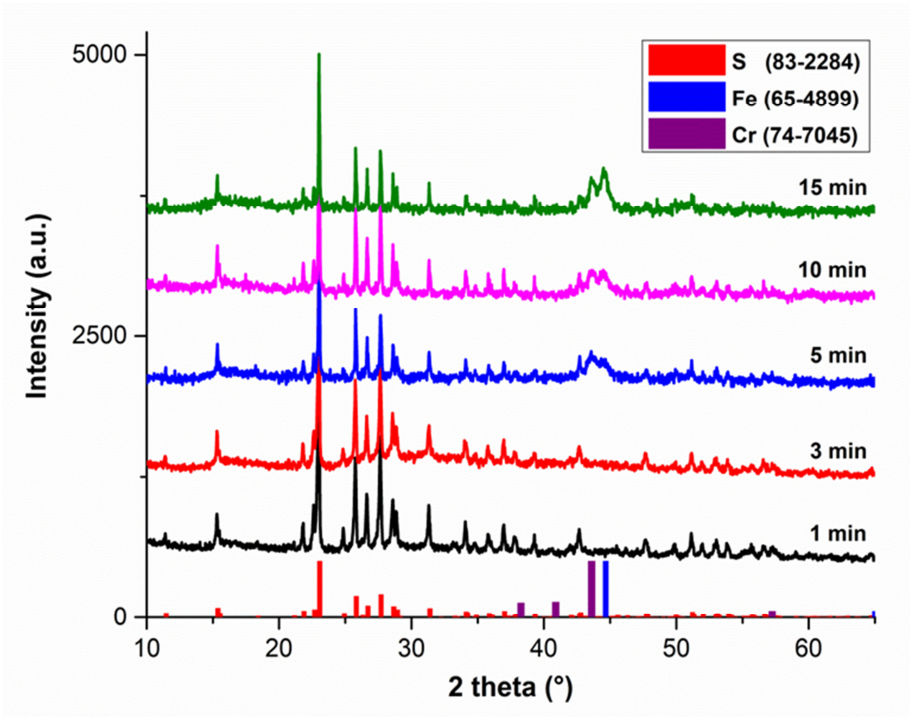


Figure 18 – XRD patterns of sulfur prepared by milling of STS and CA for a different time [128, p. 12899]

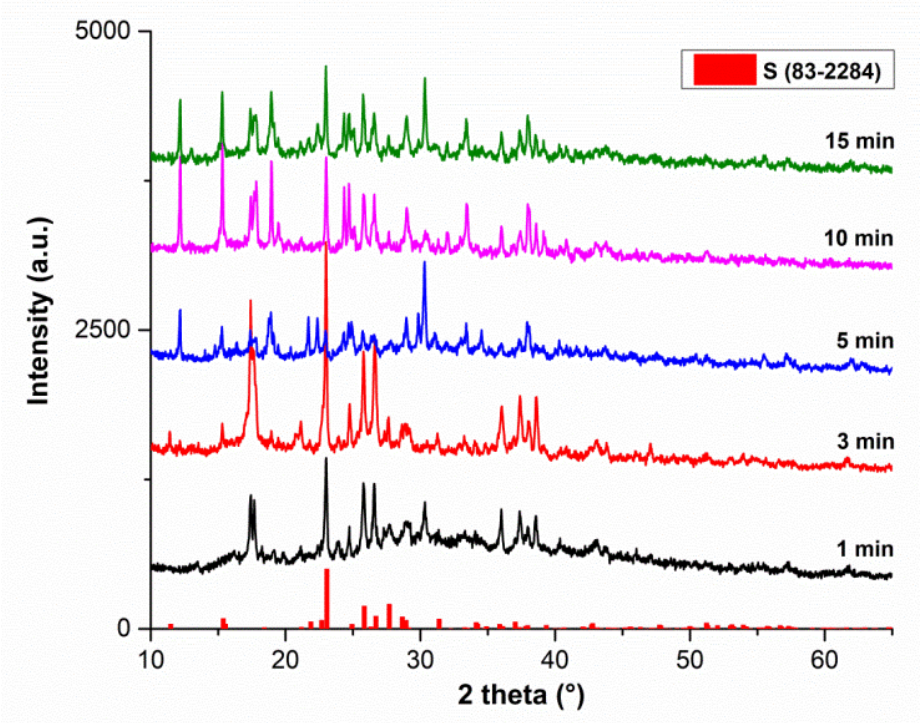


Figure 19 – XRD patterns of the not washed sulfur samples prepared by milling of STS and CA for a different time [128, ESI p. S2]

Using a similar approach, Urakaev et al. synthesized sulfur nanoparticles via the reaction of sodium thiosulfate pentahydrate with crystalline succinic acid ($C_4H_6O_4$) [2]. In their work, the concept of the diluent agent (side final product, Na_2SO_3) was used. The main idea of this approach is a dilution of the initial reaction system by a compound, which will not react with reagents and products, and thus dilutes the product to form smaller nanocrystallites [130, 131]. Also, using this approach we have shown the possibility of using organic crystalline acids as a catalyst to the synthesis of sulfur nanoparticles with the mechanochemical method [132].

In comparison with Urakaev et al. [2], the synthesis time was significantly reduced. However, as the diffraction peaks seem to be very sharp in our case, the size of crystallites is most probably in the micrometer range.

Subsequently, the synthesis of copper sulfide using the acetate route was realized. Figure 20 shows the XRD patterns of the washed powders after milling copper acetate and sodium sulfide at different times.

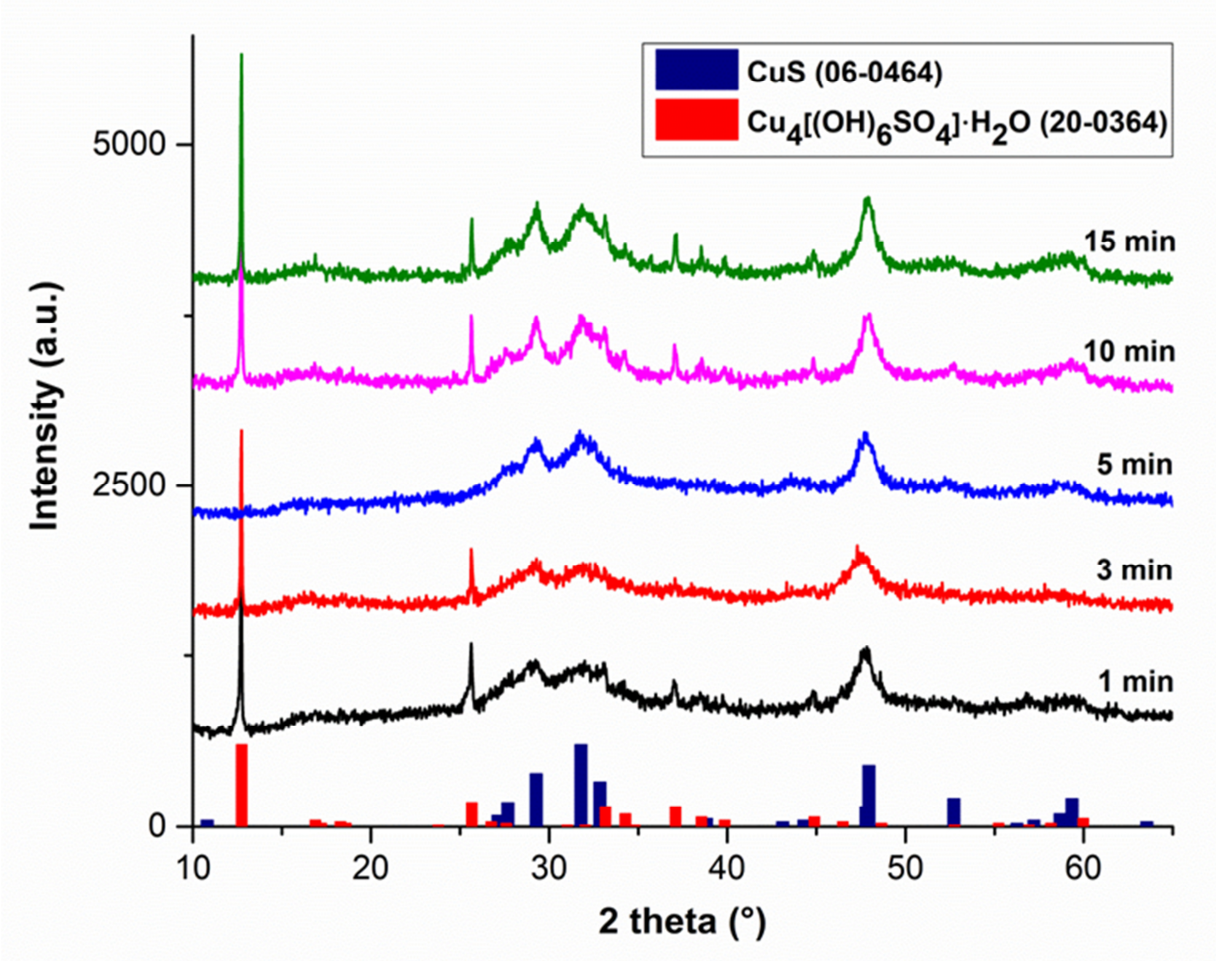


Figure 20 – XRD patterns of copper sulfide prepared by milling of copper acetate and sodium sulfide for a different time [128, p. 12899]

The diffraction peaks in the patterns of the washed samples closely match those of copper sulfide from the database (JCPDS 06-0464). As shown in the XRD pattern, only 5 minutes of milling are satisfactory for the reaction, as no other peaks were detected, indicating the high purity of the sample. All the other samples contain posnjakite phase ($Cu_4[(OH)_6SO_4]\cdot H_2O$) (JCPDS 20-0364). We are unable to explain this phenomenon at the moment, but it was observed also upon repeated experiments. The presence of hydrated copper sulfates (namely chalcanthite and bonattite phases) was also detected upon the semi-industrial mechanochemical synthesis of CuS using this approach before [133]. From the XRD pattern (Figure 20) it seems that the size of nanocrystals changes with milling time, as the intensity of the peaks increases (the finest particles are most probably present after 5 minutes of treatment).

In Figure 21, XRD patterns of not washed samples of CuS synthesis using the acetate route for the different times are shown. The content of CuS (JCPDS 06-0464) is really low. The patterns contain very intensive reflections most probably corresponding to hydrated forms of copper sulfates.

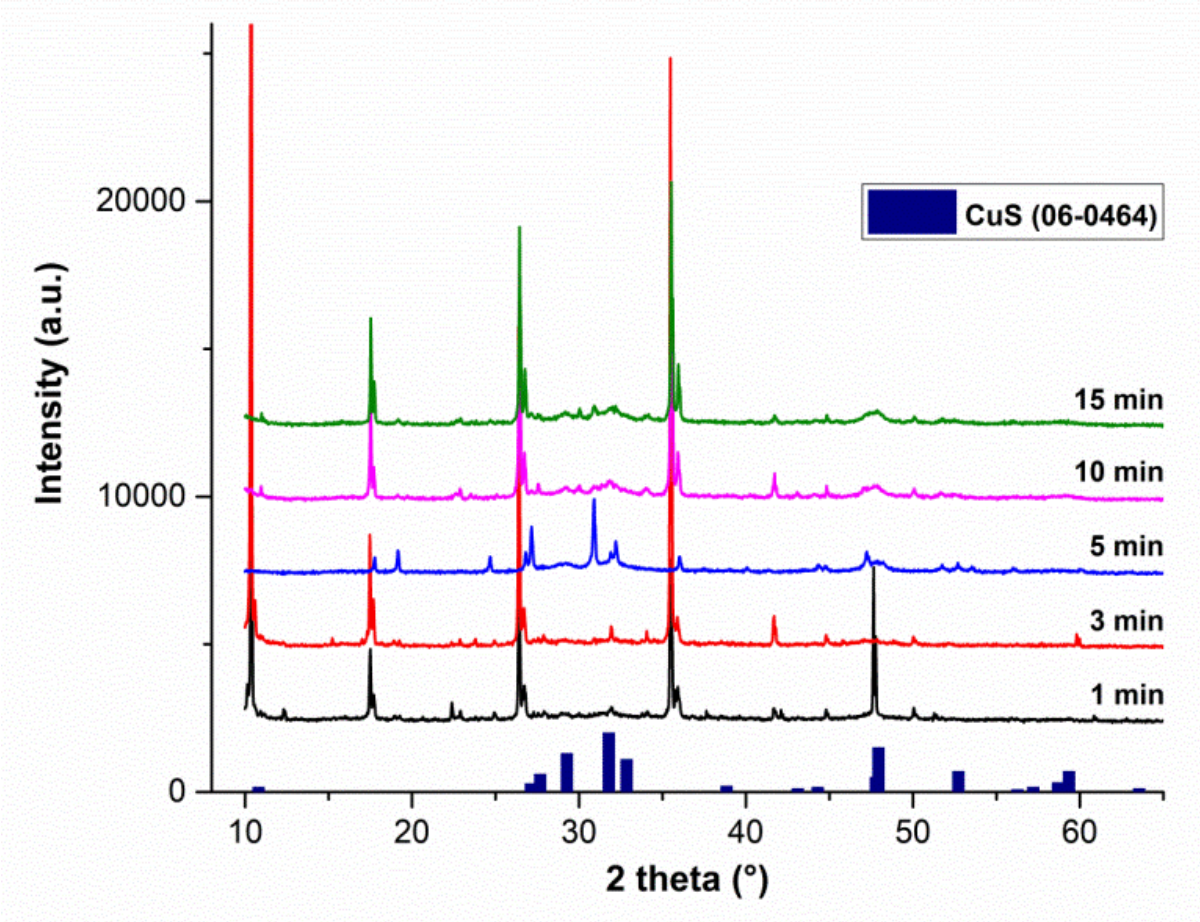


Figure 21 – XRD patterns of not washed copper sulfide sample prepared by milling of copper acetate and sodium sulfide for a different time [128, ESI p. S3]

The above-mentioned facts suggest that for both S and CuS formation, 5 minutes of milling seem to be the best option. Both reactions were performed simultaneously in the range between 1 and 15 minutes. The XRD patterns of the washed powders after this combined approach are present in Figure 22. The XRD patterns prior to washing procedures are provided in Figure 23. Standard copper sulfide peaks (JCPDS 06-0464) distinctly confirm the presence of copper sulfide particles in all the washed samples. The size of nanocrystals seems to be larger than when solely acetate route was used (Figure 20), as the peaks are sharper and more intensive. Sulfur was not identified in either XRD patterns. The reason for this could be its quick amorphization during the milling process [134], or the fact that it *in situ* undergoes further reaction. As the iron contamination was not detected in this case, it is probable that the phenomena taking place during this combined approach are different from the situation when each step is performed individually. This point will be discussed later.

In Figure 23, XRD patterns of not washed samples of nCuS synthesis using a combined approach are shown. The patterns are very complicated for identification, as the content a vast amount of diffraction peaks.

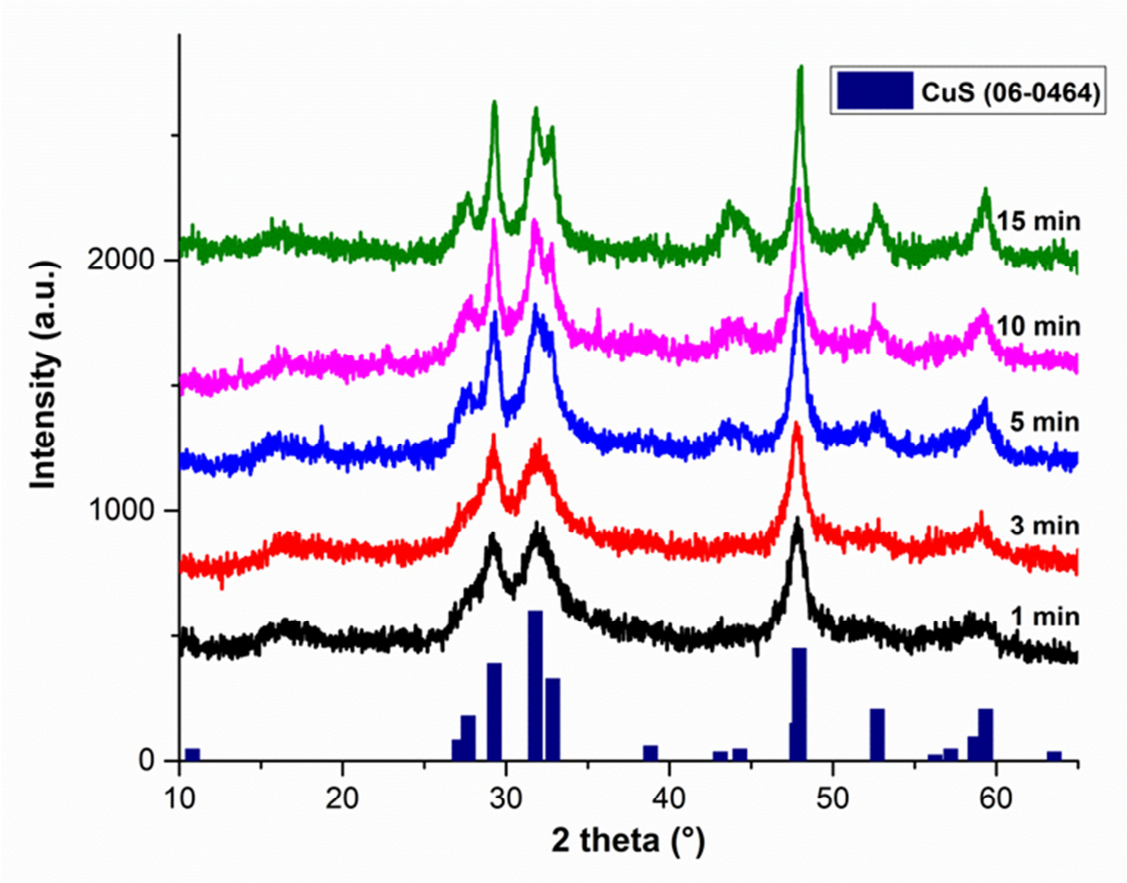


Figure 22 – XRD pattern of mechanochemically synthesized copper sulfide prepared by a combined approach for a different milling time (nCuS) [128, p. 12899]

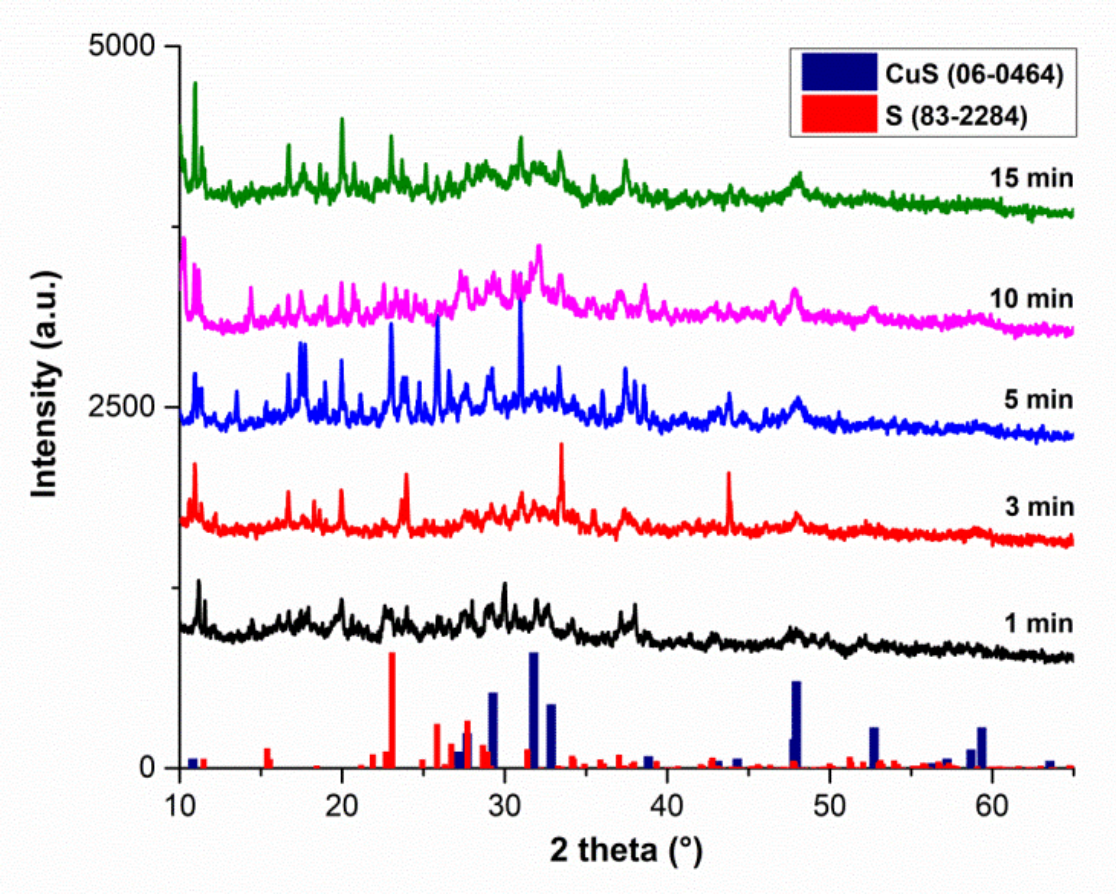


Figure 23 – XRD pattern of mechanochemically synthesized not washed copper sulfide sample prepared by a combined approach for different milling time (nCuS) [128, ESI p. S3]

3.4.2 Raman spectroscopy analysis

Raman spectroscopy was used to characterize the three samples prepared by mechanochemical synthesis (sulfur (S), and copper sulfide prepared either by acetate route (CuS) or and by a combined approach (nCuS)) [128].

As can be seen in Figure 24, three strong peaks were evidenced for the S sample. According to [122, 123], the main sulfur peaks should be located at 152, 220, and 474 cm^{-1}. In our case, the bands at 153.03; 218.77; 474.12 cm^{-1} were found, which definitely confirm its presence.

The Raman spectrum of copper sulfide prepared by acetate route (CuS) contains two distinguishable peaks at 266.00 and 470.57 cm^{-1}. According to literary data, the main wavenumbers defining peaks of copper sulfide are located at 265 and 473.5 cm^{-1} [135-137], so our results match with these values providing another proof of successful CuS synthesis.

In the nCuS sample, sulfur signals are absent, similarly to the XRD results of this sample. We could observe only copper sulfide peaks at wavenumbers 258.75 and 470.57

cm^{-1}. Although the absence of sulfur peaks in the nCuS sample can be explained by too small size of sulfur crystals, which makes it difficult to measure with Raman spectroscopy due to the phonon confinement effect [124], its absence could also mean its transformation into some water-soluble compound and its washing out during the post-treatment of the milled mixture with distilled water (this will be discussed later).

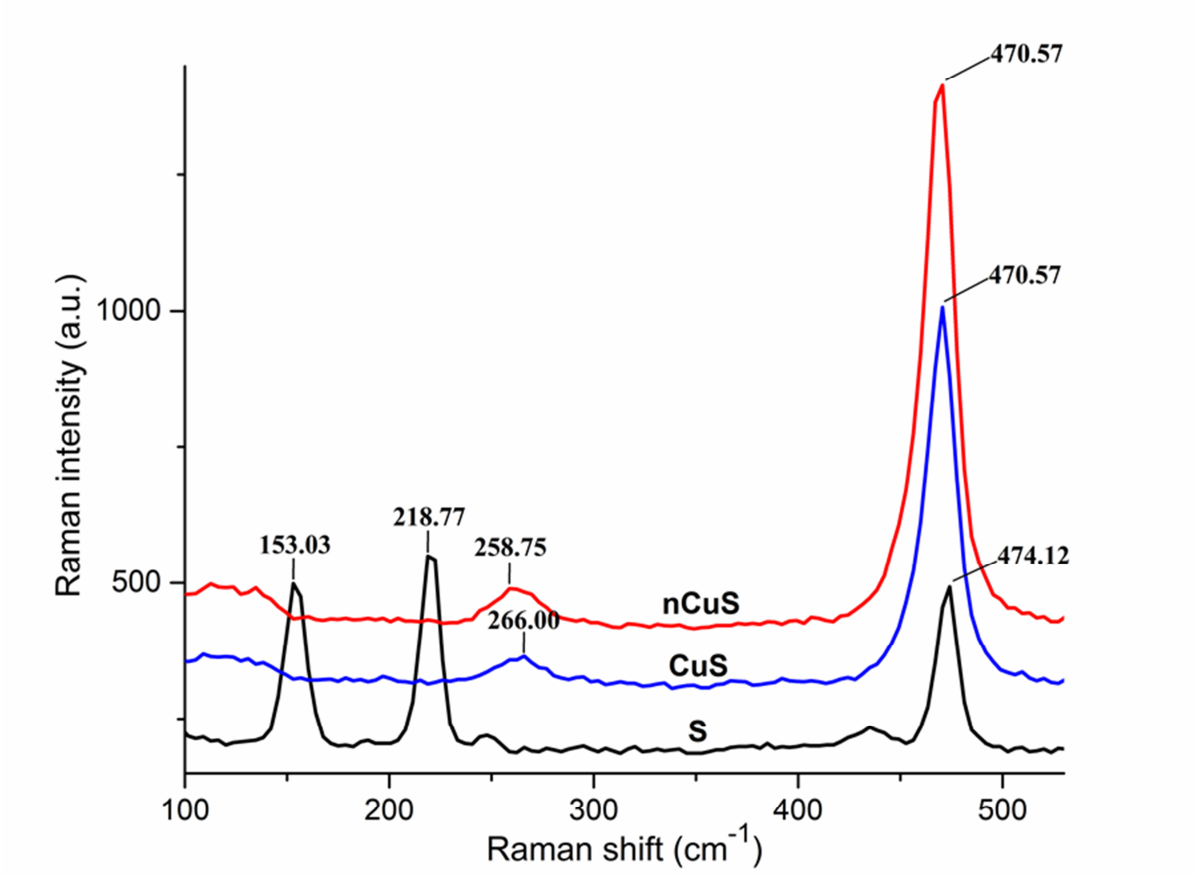


Figure 24 – Raman spectra of S, CuS and nCuS samples [128, p. 12900]

3.4.3 UV-Vis spectroscopy analysis

Figure 25 shows the differences in the visible range of UV–Vis absorption spectra of S, CuS and nCuS samples with clearly higher intensity of light absorbance for CuS-containing samples [128]. The optical band gap, Eg was estimated based on Tauc equation for directly allowed optical transition $\alpha h\nu=A(h\nu-Eg)^{1/2}$ by the plotting $(\alpha h\nu)^2$ against photon energy and extrapolating the slope in the band edge region to zero, as shown in the inset of Figure 25. The optical band gap was determined to be 2.12 eV for CuS and 2.0 eV for nCuS, respectively. In the wavelength of the optical spectra, a blue shift was not found in comparison with the bulk CuS which has a characteristic bandgap energy of about 2.2 eV [138]. The determined band gaps are in accordance with the results published in previous papers [139-141].

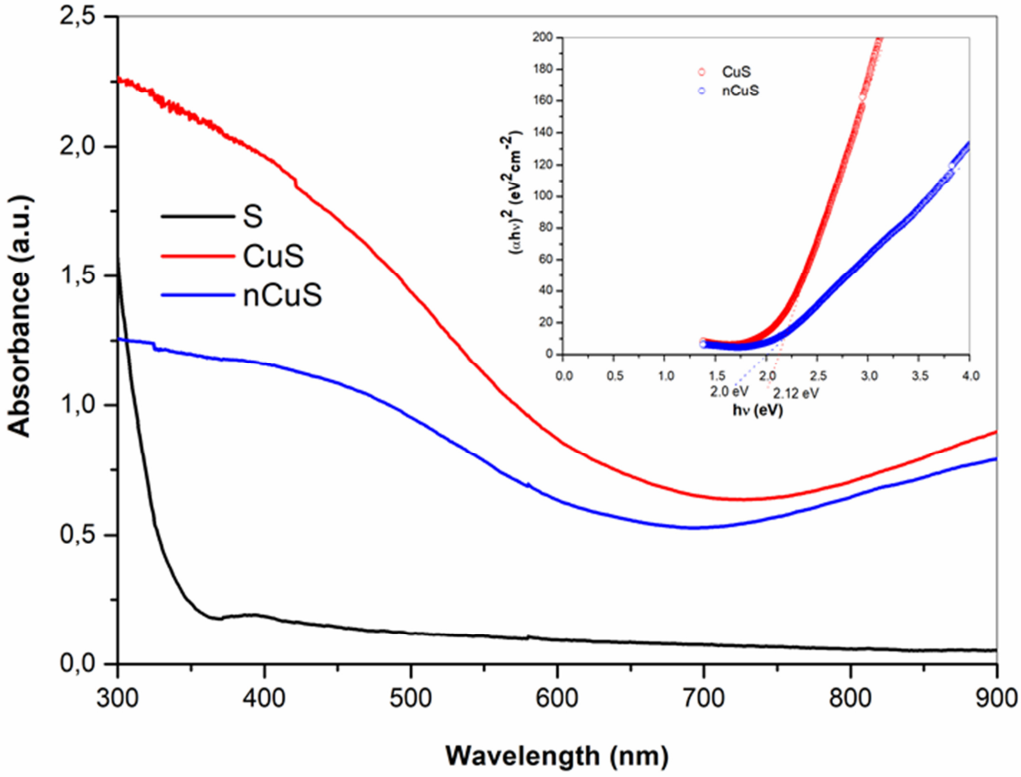


Figure 25 – UV-Vis absorption spectra of S, CuS and nCuS samples (Tauc's plots with the determined energy band gaps are presented in the inset) [128, p. 12900]

3.4.4 PL spectroscopy

The room temperature PL spectra of S, CuS and nCuS samples were taken using excitation wavelength 350 nm and are displayed in Figure 26. CuS and nCuS samples exhibit a very weak emission at about 398 and 397 nm (3.096 eV and 3.104 eV) almost consistent with the literature [142]. Our results are different from previous papers, where no emission was reported [143], but on the other hand, are in accordance with results reported in our earlier papers [66, 144]. The observed photoluminescence intensity of nCuS sample is higher than in the case of CuS. The behavior of S with an emission peak at 400 nm (3.08 eV) and a very slight peak at 470 nm (2.63 eV) in comparison with CuS and nCuS is also different similarly to absorption spectra (Figure 25). The peak intensity is influenced by several parameters such as shapes, crystallinities, size effects of the products, which, in turn account for the increase in the content of surface oxygen vacancy and defects with a decrease in dimension [145].

It can be seen that the synthesized S, CuS and nCuS samples have a little bit different optical properties. The bandgap energy depends on the crystalline structure, size as well as morphology of the CuS nanostructures.

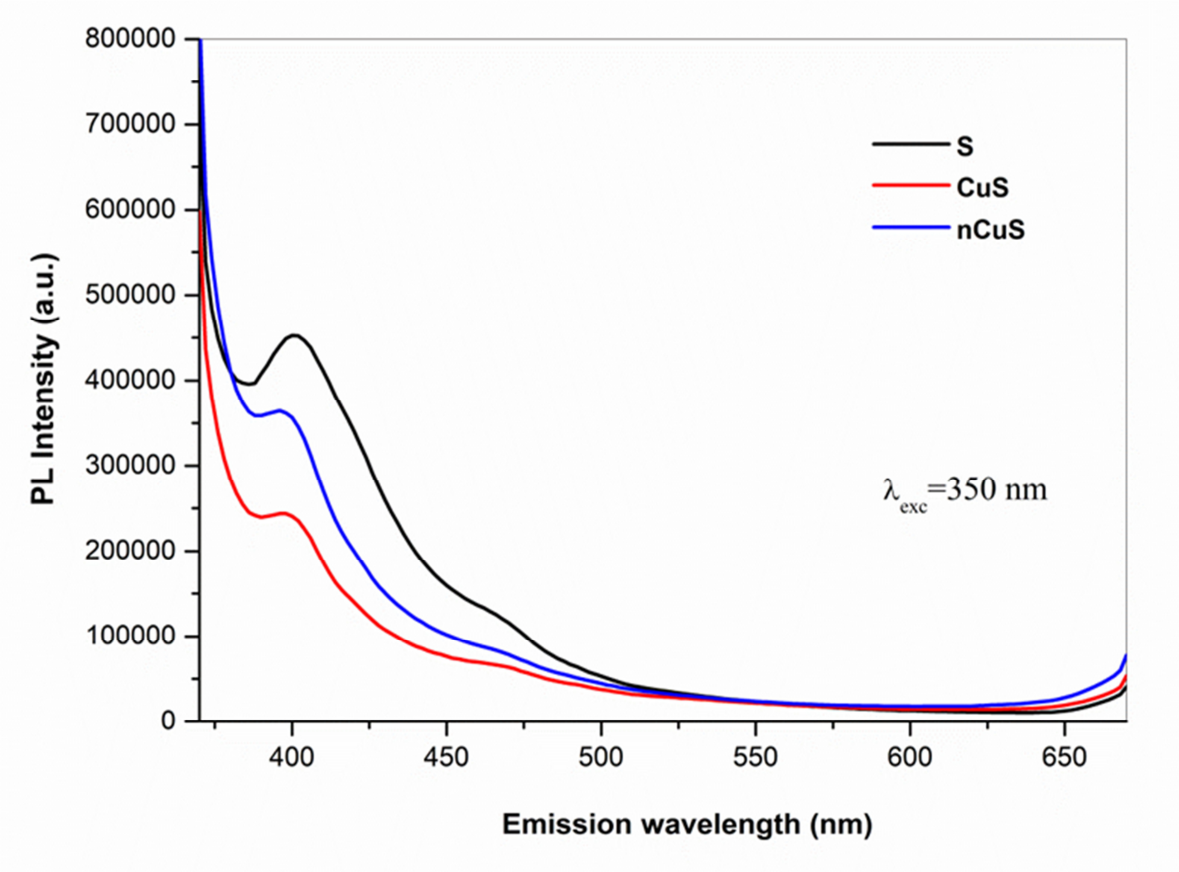


Figure 26 – PL emission spectra of S, CuS and nCuS samples at an excitation wavelength of 350 nm [128, p. 12901]

3.4.5 XPS analysis

In order to investigate the oxidation states of the most abundant elements, the XPS spectra were recorded (Figure 27) [128].

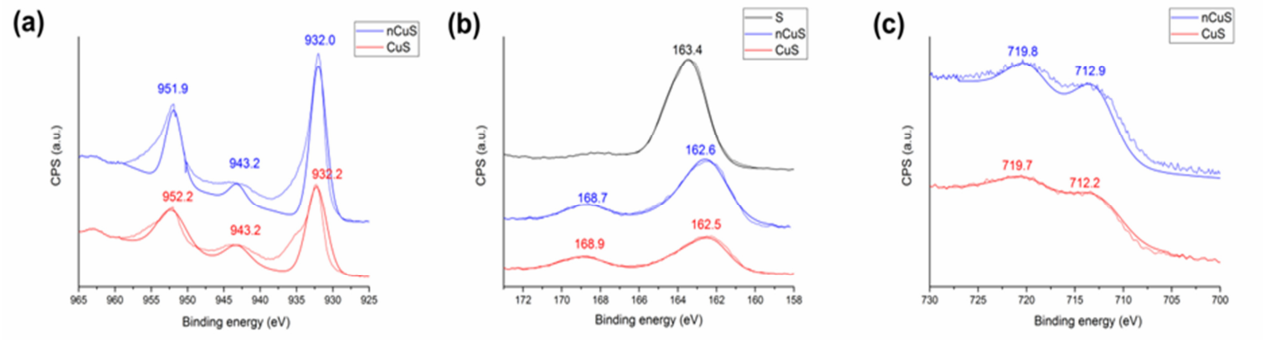


Figure 27 – XPS spectra of S, CuS and nCuS samples: (a) Cu2p, (b) S2p, (c) Fe2p. Bold lines show the results of fitting and the thin lines of the experimental data [128, p. 12901]

The XPS spectra showed the anticipated results in terms of oxidation states of all elements. In the case of copper (Figure 27a), the spectra are practically identical, showing the Cu in oxidation state +II (peaks around 952 and 932 eV). The satellite peak at 943.2 eV further confirms this[66, 146, 147]. There is a dispute about the presence of Cu in the oxidation state (I) in this compound, which cannot be overlooked [148]. In the case of sulfur (Figure 27b), the presence of S(-II) is clear (the peak around 162.5 eV) [66, 146, 147]. However, also some oxidized species are present on the surface, as the peak around 168.8 correspondings to S(+VI) was found for both samples [149]. The sulfur sample exhibits a peak at 163 eV, which is in accordance with the binding energy reported for elemental sulfur in other studies [150, 151]. Regarding iron coming from milling media, it was registered only in the case of CuS and nCuS samples. Its content seems to be higher in the case of nCuS. The results are different from XRD, where Fe was detected also for pure sulfur, but it was not detected in the CuS sample (Figures 18 and 20). However, XPS is a surface method, so the distribution of elements can be different in comparison with the bulk analyzed by XRD. Iron was definitely oxidized into ionic form. It cannot be surely claimed whether it is in (+II) or (+III) state, as the XPS peaks are quite close and the binding energy depends also on the anion in the compound [152]. Nevertheless, its interaction with the milled powder and incorporation into some compound, mostly in the form of sulfate is in accordance with the results of XRD of the dried filtrate (Figure 33) and with the presence of sulfate peak in the S2p spectrum (Figure 27b).

3.4.6 PCCS analysis

Particle size distributions of the prepared samples are shown in Figure 28 [128].

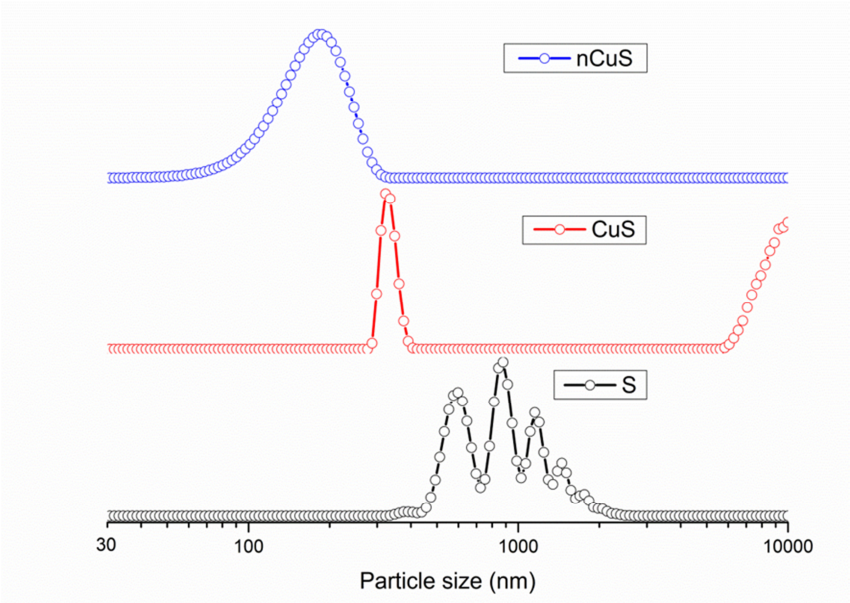


Figure 28 – The particle size distribution of S, CuS and nCuS samples [128, p. 12902]

Sulfur particles (S sample) are characterized by the polymodal distribution composed of several more-or-less discrete fractions. The sizes of particles are of a wide range (from 330 nm to 2600 nm).

In the case of CuS nanoparticles synthesized by acetate route (CuS), the polymodal distribution was obtained in the measured range. The sample consists of particles with very fine sizes (from 280 nm to 410 nm) as well as of the coarse (or agglomerated) ones with the sizes of several micrometers.

The unimodal particle size distribution was obtained for the sample prepared by a combined approach (nCuS). The fraction is very fine (from 40 nm to 330 nm) with the average hydrodynamic diameter of 170 nm.

3.4.7 Microstructural and morphological analyses

Figure 29 shows the results of the SEM analysis of mechanochemically synthesized S, CuS and nCuS samples [128]. SEM images of the sulfur sample (Figure 29a, b) showed that the sulfur particles are slightly larger than in the case of the other samples, thereby confirming the results of the PCCS analysis. The SEM-EDS results (see Figure 30a, S sample) also confirmed the results of XRD analysis showing the presence of iron and chromium in the sample. Also, nickel and silicon are present in small amounts in the sample. Silicon can be present as a result of the cleaning procedure applied before the experiment, in which grinding balls and steel chambers are cleaned using abrasive SiO_2. The presence of Cr and Ni could be due to wear coming from the steel milling chamber, as these elements are introduced to steel when it is produced.

In the case of both CuS samples, it is evident that the individual nanoparticles are agglomerated into large grains. SEM images of CuS produced by the acetate route (Figure 29c, d) show that the copper sulfide particles have non-uniform sizes. It was already shown by PCCS analysis of this sample that it exhibits the polymodal distribution of particles (Figure 28). On the contrary to the produced sulfur, the EDS results did not show any impurities indicating high purity of the sample.

The SEM results of CuS produced by sulfur-mediated acetate route synthesis (Figure 29e, f), it can be seen that the particles exhibit significantly different morphology from CuS samples produced by a simple acetate route. More light on the shape of particles will be shed in the next paragraph (TEM analysis). The EDS results revealed the presence of wear and impurity in this sample, documented by Si, Fe and Cr peaks in the spectra. However, the intensity of the corresponding peaks is smaller compared to the sulfur sample, so the wear is not so significant in the case. Its concentration is most probably too low to be detected by the XRD (Figure 22).

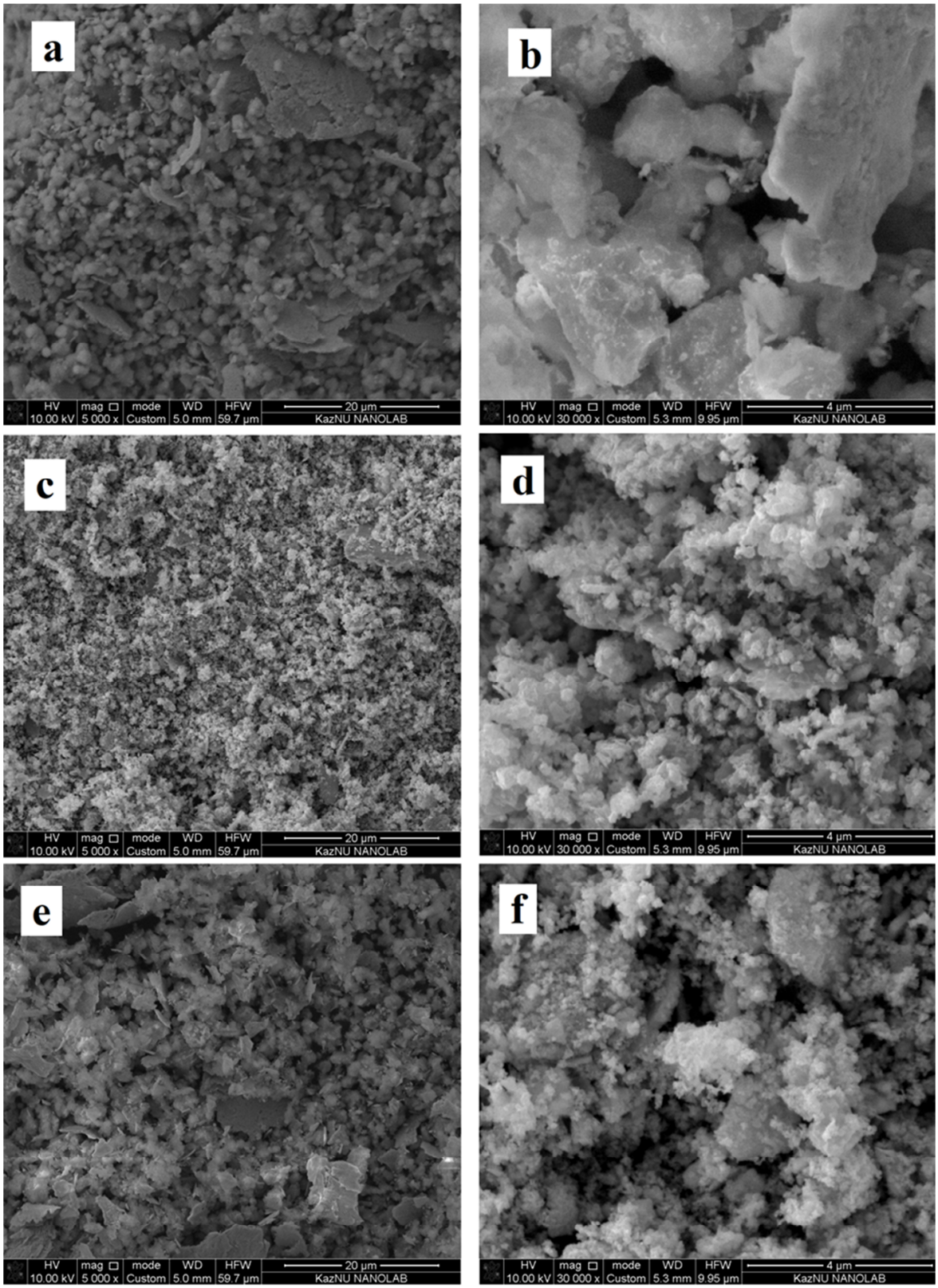


Figure 29 – SEM images of mechanochemically synthesized sulfur (a, b), CuS (c, d) and nCuS (e, f) samples [128, p. 12903]

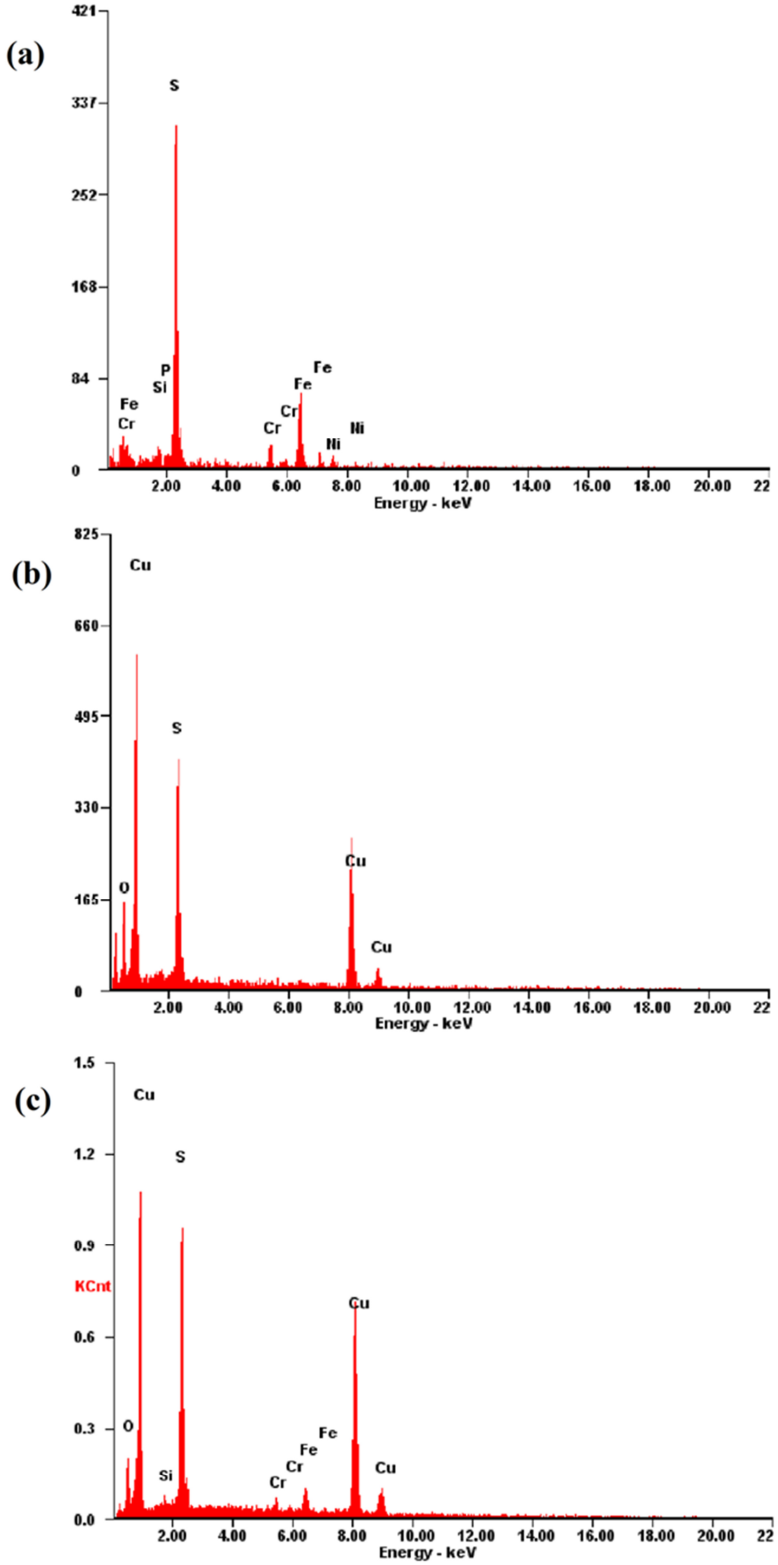


Figure 30 – EDS results of mechanochemically synthesized S (a), CuS (b) and nCuS (c) samples [128, p. 12904]

In order to reveal the morphology of CuS nanoparticles in the products, TEM analysis was performed [128]. The sulfur particles underwent detrimental changes under the high-energy electron beam, therefore, only CuS and nCuS samples were analyzed. Low-magnification images (Figure 31a, b) confirmed the observations by SEM that both samples are composed of agglomerated nanoparticles. Selected-area electron diffraction (SAED) patterns were recorded and only reflections from the covellite (CuS) phase were found in both samples. The difference in the morphology of nanoparticles between the samples was revealed at higher magnifications. HRTEM images (Figure 31c, d) show that in the CuS sample, the crystallites are tightly packed; they have more or less isometric morphology and size (diameter) in the range of 20 nm. The morphology of individual CuS crystallites is different in the nCuS sample. Here, most of the crystallites show elongated or needle-like shape with a thickness in the range between 6 and 8 nm and lengths up to 60 nm (aspect ratio up to 1:10). HRTEM analysis of the crystallites revealed that the particles are elongated along the basal planes of the covellite structure.

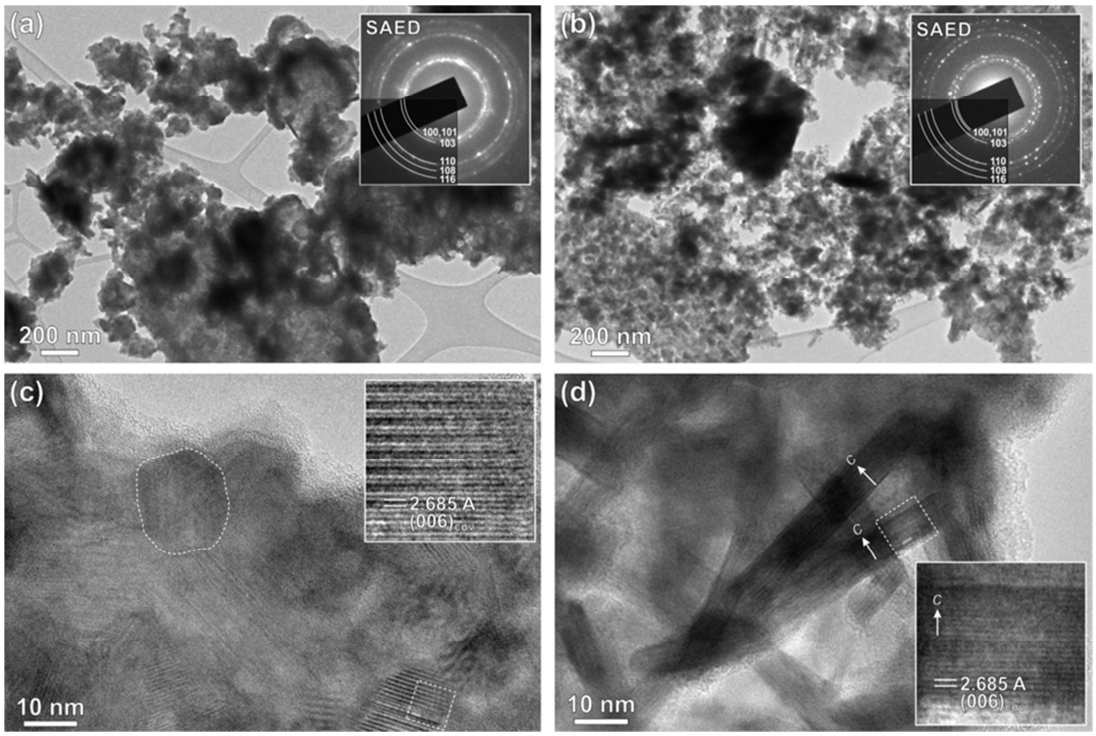


Figure 31 – Low-magnification images with SAED patterns in the insets of (a) CuS and (b) nCuS samples confirm that both samples are composed of agglomerated nanoparticles. All rings in the SAED pattern belong to covellite (JCPDS 06-0464), (*hkl*) of lattice planes for the most intense rings are given. (c, d) High-resolution TEM images of both samples reveal the difference in the morphology of nanoparticles in both samples. (c) In the CuS sample, the NPs are nearly isometric, while in the (d) nCuS sample, the particles are elongated along basal (00l) planes (perpendicular to the c-axis, denoted by arrows) of the CuS covellite structure [128, p. 12905]

The difference in morphology of CuS NPs in both samples implies differences in the nucleation and growth mechanism of CuS under different synthesis conditions. The reasons may lie in the unique properties of the covellite structure (Figure 32a), which is composed of main structural units including Cu atoms in tetrahedral and triangular planar coordination and S-S bonds between these main units [153]. In the CuS sample prepared via the acetate route, the reaction between the precursors results in relatively uniform growth rates in all directions or a slightly faster growth rate in the *c*-direction (Figure 32b). On the other hand, the presence of elemental sulfur shows a significant effect on the crystal growth of CuS NPs. The nanoparticles have a needle-like shape with a uniform thickness of around 6 nm length of up to 60 nm (aspect ratio 1:10) as shown in Figure 32c. The presence of elemental sulfur may enhance the S-S bonding and preferential growth of CuS along the basal planes (Figure 32c). This could be potentially interesting for applications since CuS exhibits superconducting-like behavior at temperatures below 40 K due to the structural characteristics [153].

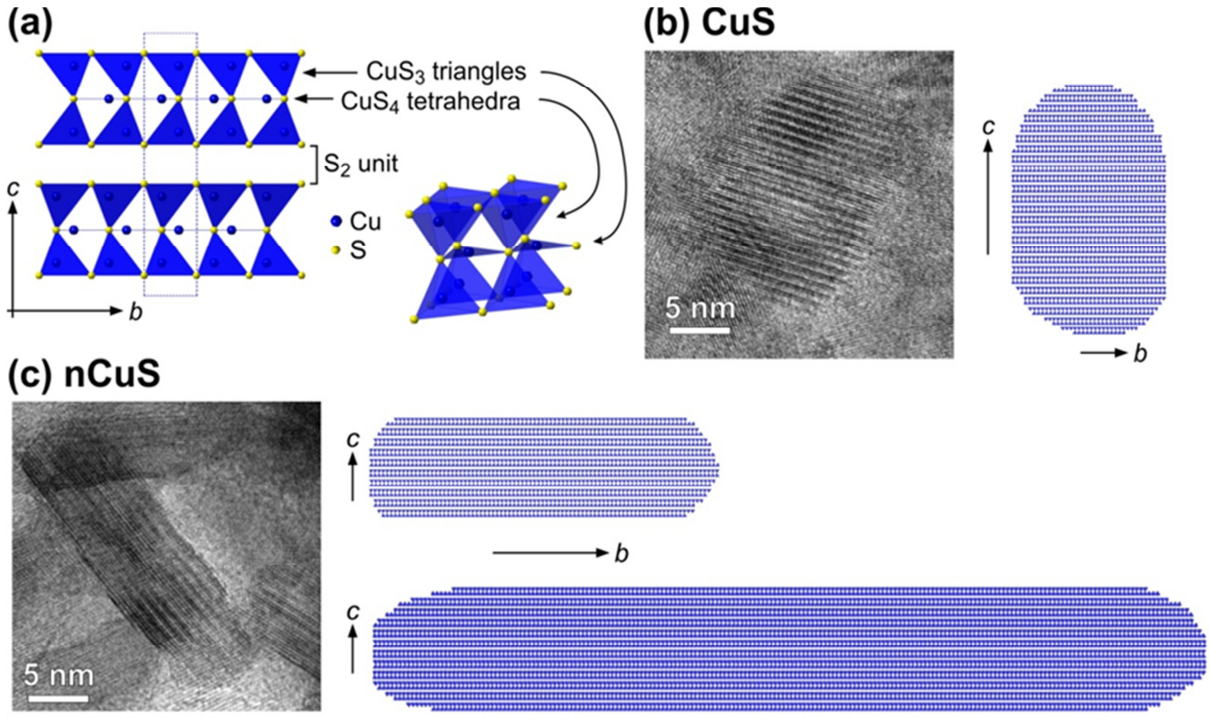


Figure 32 – (a) Crystal structure of CuS. (b) Nearly isometric CuS NPs in the sample obtained by acetate route. (c) Elongated, needle-like CuS NPs with an aspect ratio up to 1:10 are observed in the sample synthesized in the presence of elemental sulfur [128, p. 12905]

As elemental sulfur was not detected in the nCuS produced by a combined approach, it is highly probable that it reacted *in situ* to form a water-soluble compound. From our point of view, the following reaction can occur:

$$2Cu(CH_3COO)_2 \times H_2O + Na_2S_2O_3 \times 5H_2O + C_6H_8O_7 + Na_2S \times 9H_2O + 8O_2 \rightarrow 2CuS + Na_2SO_4 + Na_2CO_3 + 22H_2O + 7CO_2 + C_6H_8O_7 \quad (21)$$

According to this reaction, there are three sulfur atoms entering the reaction. Two of them end in CuS products. The first one comes from the acidic decomposition sodium thiosulfate (reaction 15). We are of the opinion that it is present also in elemental form for a short time, thus serving as a nucleation agent. The second one comes from sodium sulfide. The last one is oxidized from sodium sulfite (product of reaction (15) into sodium sulfate. In order to prove this hypothesis, we recorded the XRD pattern of the dried filtrate (Figure 33). A small amount of CuS (JCPDS 06-0464) was identified. In addition to this, also Na_2SO_4 (JCPDS 79-1553) and $Na_2CO_3 \times 10H_2O$ (JCPDS 01-0938) were found, thus supporting the idea about the reaction (21). Possibly, also CuC_4O_4 (JCPDS 76-4595) and $Fe_4(OH)_{10}SO_4$ (JCPDS 21-0419) could be present [128]. The presence of $Fe_4(OH)_{10}SO_4$ could be a result of the reaction between iron coming from milling media and side-products of reaction (21) in acidic conditions (due to the presence of citric acid). CuC_4O_4 can be hypothetically formed as a result of the reaction between Cu(+II) cations and acetate anions. For further information, the XRD patterns of the dried filtrates after 1 and 3 minutes are provided in Figure 34.

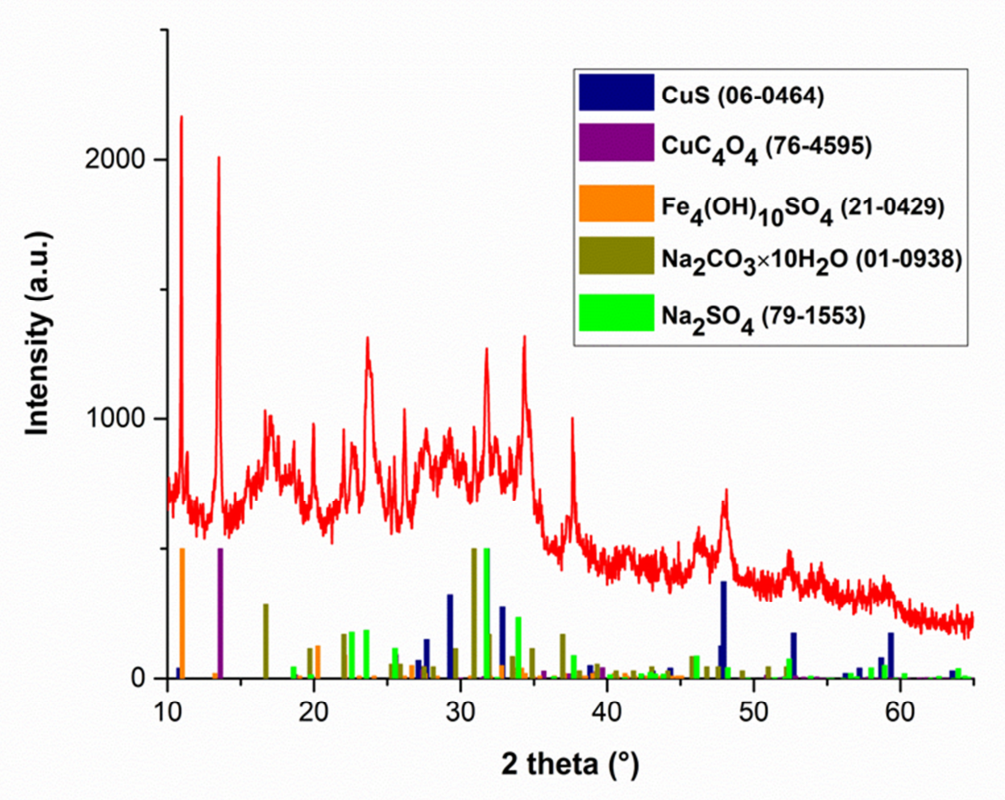


Figure 33 – XRD pattern of dried filtrate of mechanochemically synthesized copper sulfide sample prepared by a combined approach for 5 min (nCuS) [128, p. 12906]

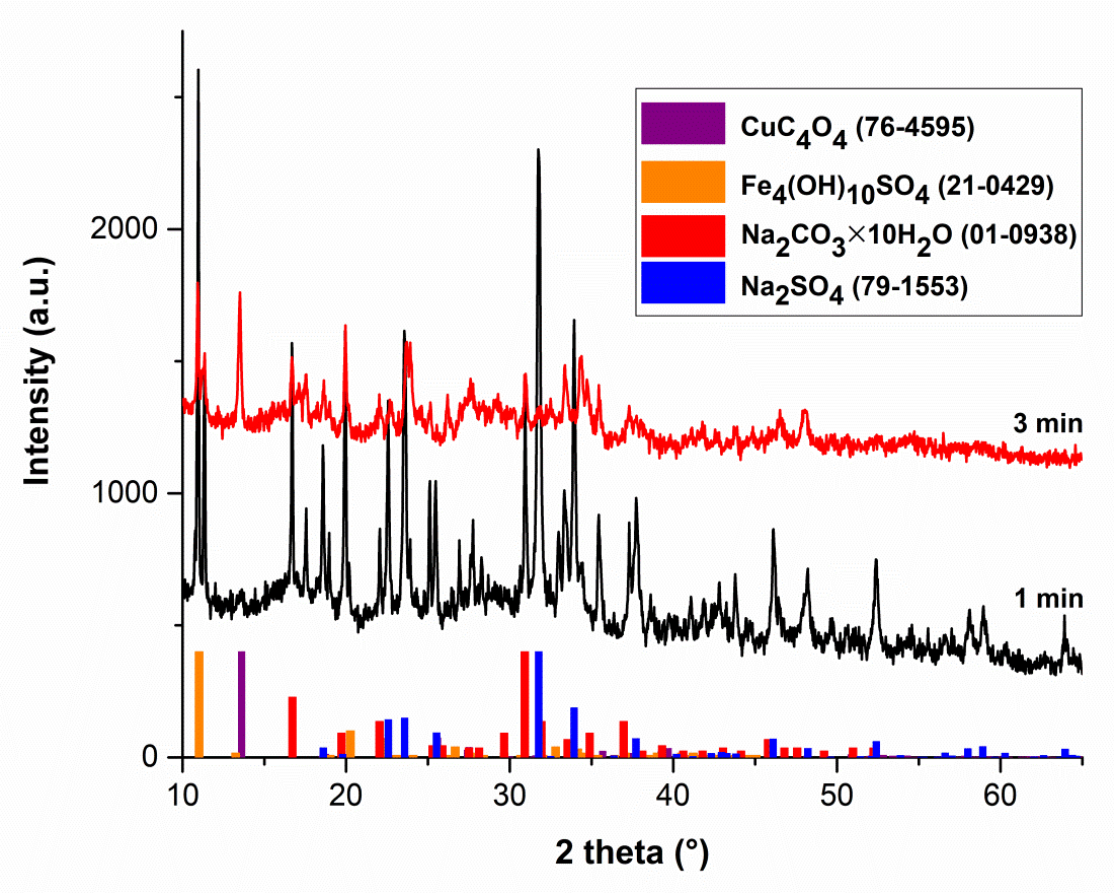


Figure 34 – XRD pattern of dried filtrates of mechanochemically synthesized copper sulfide (nCuS) sample prepared by a combined approach for 1 and 3 min [128, ESI p. S4]

3.4.8 SEM, EDS and elemental mapping analysis of not washed samples and dried filtrates

In order to examine the chemical changes going on during the nCuS formation (namely the absence of elemental sulfur in the final nCuS sample), the tools of SEM, EDS, and elemental mapping were utilized. Namely, the not washed sample taken directly from the milling chamber and the dried filtrate obtained after the washing procedure of this sample were compared. The SEM images of both samples are provided in Figures 35 and 36. Although the morphology is of secondary importance in this case, some phenomena can be observed. The not washed sample contains large particles of hundreds of microns with quite smooth morphology (Figure 35). The dried filtrate seems to be more structured with particles from a few microns up to 100 micrometers (Figure 36). The cracks observed in the image are most probably present due to the manual crashing of the obtained sample prior to analysis.

The chemical composition of both samples was investigated by means of EDS analysis. The results are summarized in Table 6.

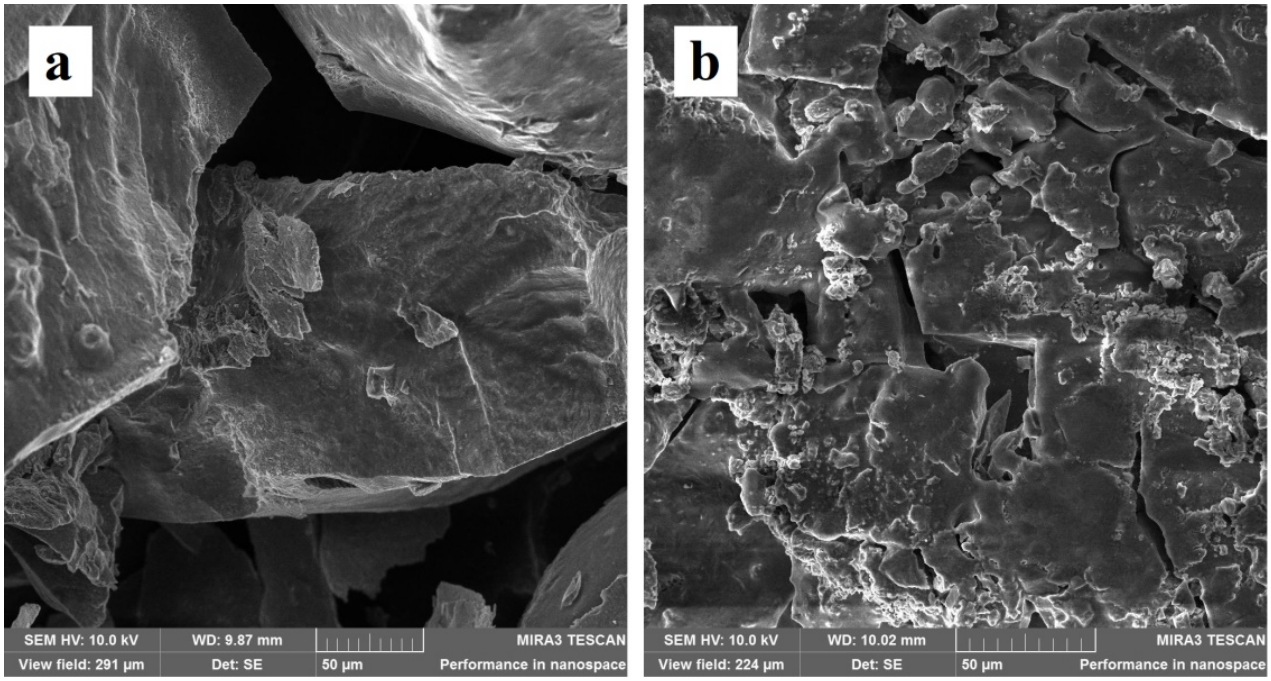


Figure 35 – SEM image of the not washed (a) and dried filtrate which is obtained after washing nCuS sample (b) [128, ESI p. S5, S6]

Table 6 – Results of the EDS analysis of not washed powder and dried filtrate from nCuS synthesis (values are in atomic %)

Sample	Region	Na	S	O	Cu	Fe
Not washed	1	21.9	13.2	60.3	4.5	0.2
	2	22.4	11.8	61.5	4.2	0.2
	Average	22.2	12.5	60.9	4.4	0.2
Dried filtrate	1	24.1	14.1	60.2	1.5	0.2
	2	23.2	12.9	60.0	3.6	0.2
	3	26.2	10.0	61.8	1.6	0.5
	Average	24.5	14.1	60.2	2.2	0.3

The difference between the two samples is not large. Both of them contain a significant amount of sodium, sulfur, and oxygen. The atomic ratio of these elements is quite close to the theoretical stoichiometry of sodium sulfate Na_2SO_4 (namely 28.6% of Na, 14.3 % of S and 57.1 % of O). This compound was identified in the XRD pattern of the dried filtrate (Figure 35), so sulfur formed *in situ* by equation (15) is most probably transformed into sodium sulfate upon further processing (21). The only significant difference is in the copper content, which was two times higher for the not washed sample. As copper sulfide remained in the solid-state during the washing process, the

significant decrease of Cu content in the dried filtrate is logical. However, the content of sulfur was slightly lower for the not washed sample, which is contradictory and we are unable to explain this phenomenon at the moment. Iron content was on the borderline of the detection limit, so the contamination from milling media was not very significant in the analyzed regions.

The results of the elemental mapping of the dried filtrate after nCuS synthesis are shown in Figure 36. Distribution of Na, S, and O is completely matching, which points to the fact that they are present in the same compound. This further supports the presence of Na_2SO_4. Copper seems to be concentrated in the area close to the middle of the image. The sulfur distribution in this region is also slightly richer, which points to the presence of a small amount of CuS (which was not effectively separated from the liquid phase during filtration). Its presence was also mentioned in the XRD pattern of the dried filtrate (see Figure 33). Iron seems to be evenly distributed, with some larger particles on the right side of the map. These particles can be fragments either from milling balls of the chamber.

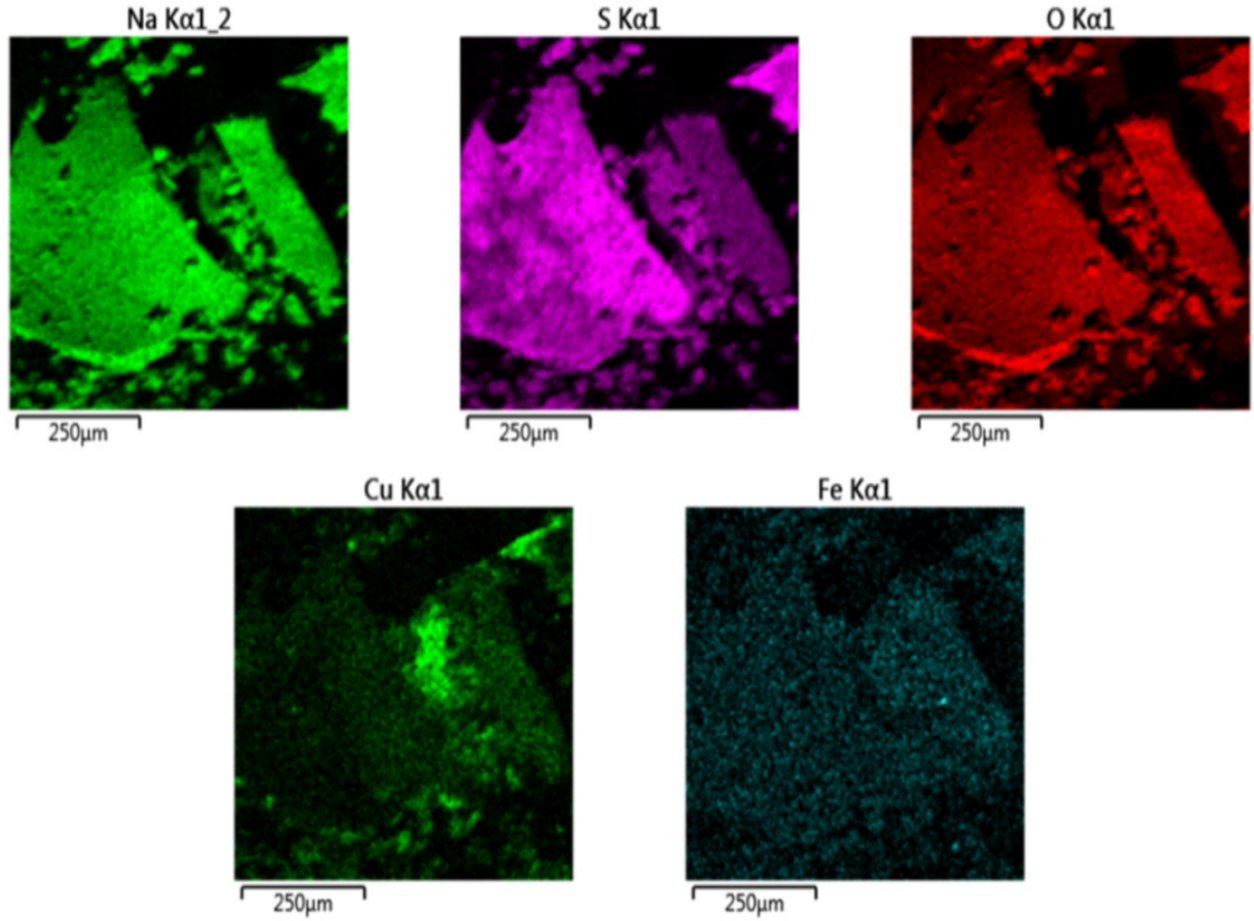


Figure 36 – Elemental mapping of the dried filtrate after nCuS synthesis for Na, S, O, Cu, and Fe elements [128, ESI p. S7]

3.4.9 Results of antibacterial activity measurements

Three final samples (S, CuS and nCuS) in concentration 10 mg/mL were subjected to tests of antibacterial activity using agar well plate method on one Gram-negative (*E. coli*) and one Gram-positive (*S. aureus*) bacteria [128]. The results are summarized in Figure 37.

It can be seen that three studied samples exhibit significantly different antibacterial activity. The sulfur sample did not show any activity. However, the produced particles in our case are micro-sized and the antibacterial activity was reported to significantly increase upon the reduction of particle size into the nano-range [154]. The crystal structure, size and capping agent of sulfur NPs can have a significant effect on the antibacterial activity of sulfur [154, 155].

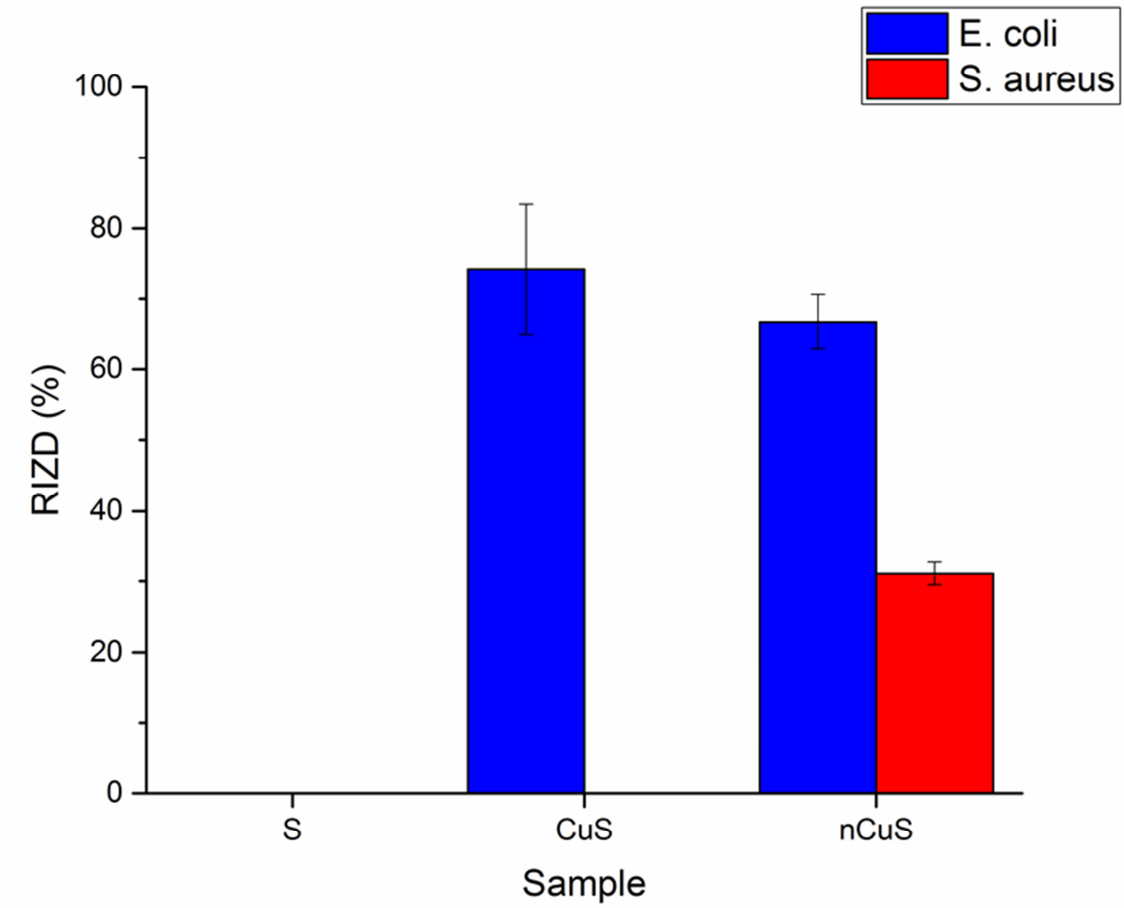


Figure 37 – Antibacterial activity of S, CuS and nCuS samples expressed as relative inhibition zones diameter (RIZD) [128, p. 12906]

Copper sulfide prepared by acetate route has shown very strong antibacterial activity against gram-negative *E. coli*, however, no activity for the gram-positive *S. aureus* was evidenced. Although the formation of the even larger zone than for *E. coli*

was evidenced in this case, the zones were not transparent and the borders were not strict so it was concluded that it is just some kind of reaction between the sample and the bacterial colonies, but it cannot be interpreted as antibacterial activity. On the contrary to the specificity of CuS sample, the nCuS one has shown the effect against both *E.coli* and *S. aureus*. Although the effect was approximately two times lower against *S. aureus*, the sulfur-mediated synthesis brought about an improvement of antibacterial activity in terms of being less selective. This creates a space for the investigation of the effect of CuS nanoparticles of various shapes on the antibacterial activity in the future.

3.5 Preparation of sulfur nanoparticles in dimethyl sulfoxide (DMSO)

The solubility of sulfur in DMSO at a different temperature is presented in Table 7 [156].

Table 7 – The solubility of sulfur in DMSO depending on the temperature and concentration of sulfur in DMSO after cooling the resulting solutions for 24 hours to room temperature (~ 25 °C)

№	Temperature,°C	Solubility, g/L	Solubility at RT, g/L
1	25	0.918	0.918
2	50	4.554	1.592
3	75	7.634	2.308
4	100	33.102	3.378
5	125	52.554	14.152
6	150	74.690	14.246
7	175	98.764	14.708

3.5.1 Results of DLS analysis

The following conclusions can be drawn from the analysis of the data in Figure 38. The narrowest size distribution of sulfur nanoparticles, both initial and stabilized, occurs when water is used as a diluent: the distribution intervals of the average values were r_0 = 54 ÷ 109 nm, r_C = 63 ÷ 130 nm; the size stabilization time interval was equal to t = 70 ÷ 108 minutes. In cases of using acetone and ethyl alcohol as diluents, there is a significant variation in the values of these indicators: in the case of acetone, r_0 = 9 ÷ 615 nm, r_C = 59.5 ÷ 2519 nm, t = 14 ÷ 51 minutes were measured; and in the case of ethyl alcohol - r_0 = 19 ÷ 1365 nm, r_C = 370 ÷ 2014 nm, t = 25 ÷ 34 minutes.

Thus, the developed method allows obtaining colloidal solutions of sulfur nanoparticles in aqueous-organic systems [156]. The advantages of the present invention

are the use of a saturated solution of sulfur in dimethyl sulfoxide as a precursor and the achievement of the goal by subsequent multiple dilutions of this solution with water, acetone or alcohol, which can greatly simplify and reduce the cost of preparing sulfur nanoparticles. The resulting aqueous-organic solution of a suspension of sulfur nanoparticles, as an antifungal drug, can be used, for example, for spraying seeds and shoots of cultivated plants. Organic suspension solutions based on volatile acetone and ethyl alcohol can be used to hydrophobize the surface of various materials, including porous. Also, aqueous-organic solutions of a suspension of sulfur nanoparticles have prospects for widespread use in biomedicine.

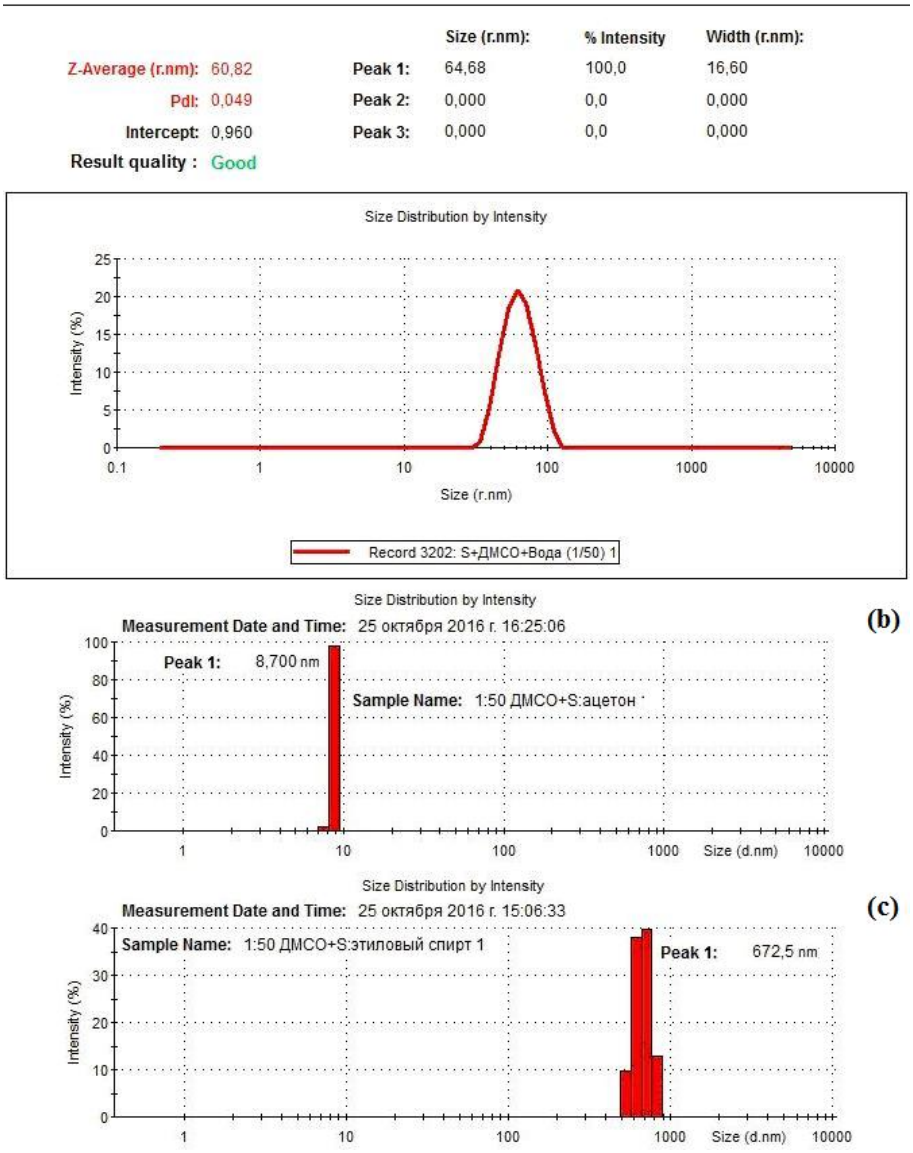


Figure 38 – The initial size distribution functions of sulfur nanoparticles after diluting a saturated sulfur solution in DMSO 50 times: (a) dilution with water; (b) -acetone; (c) - ethyl alcohol [155, p. 5]

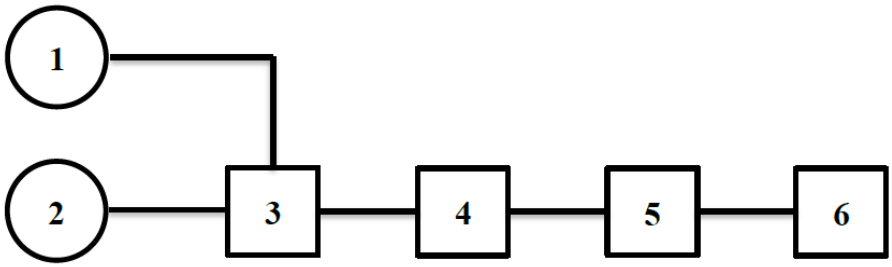
4 APPLIED ASPECTS OF THE DEVELOPED METHODS FOR PRODUCING SULFUR, COPPER SULFIDE NANOPARTICLES, AND SULFUR-CONTAINING NANOCOMPOSITES

As shown above, in this thesis liquid-phase and solid-phase methods for the synthesis of sulfur, copper sulfide (CuS) nanoparticles, and sulfur-containing nanocomposites are proposed.

Using liquid-phase synthesis methods sulfur-containing $S/CaCO_3$ and CuS/S nanocomposites have been successfully synthesized. As in the hydrothermal synthesis of CuS/S nanocomposites is not presented application areas of composite, the principal scheme of production technology of this composite material is not developed.

1. Scheme for the production of sulfur nanoparticles, and sulfur-containing $S/CaCO_3$ nanocomposites using a pilot reactor.

Using a pilot production reactor, from 10 liters of a calcium polysulfide (CaS_4) solution with a density of 1.25 g/cm^3, 1630 g of sulfur nanopowders or 2590 g of sulfur-containing $S/CaCO_3$ nanocomposite in each charge can be produced. We proposed to use the reactor R-620 for pilot production, with a capacity of up to 20 L (manufacturer: SELECTA, Spain). A principle scheme of production target nanoparticles and nanocomposites in a pilot reactor is shown in Figure 39.



1 – CO_2 gas tank; 2 – calcium polysulfide (CaS_4) solution (ρ=1.25 g/cm^3); 3 – liquid-phase synthesis of sulfur-containing $S/CaCO_3$ nanocomposites using a pilot production reactor; 4 – separating nanocomposite product from the solution via filtration; 5 – obtaining sulfur nanoparticles by treating nanocomposite with hydrochloric (HCl) acid; 6 – drying as-obtained sulfur nanoparticles.

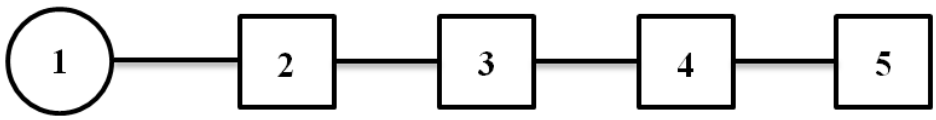
Figure 39 – Principle scheme of the production of sulfur nanoparticles and sulfur-containing $S/CaCO_3$ nanocomposites by the liquid-phase method using a reactor for pilot production

In addition to the preparation of sulfur, and sulfur-containing nanocomposites, in this thesis sulfur-mediated successful mechanochemical synthesis of elongated needle-like copper sulfide (nCuS) nanocrystals in a planetary ball mill are presented. The

advantage of a planetary mill is a higher speed of the process of mechanical activation to obtain the target product (due to the fact that the speed of the mechanochemical process is determined by the speed of impact of grinding media). Below is a developed principle scheme for the sulfur-mediated mechanochemical synthesis of needle-like copper sulfide (nCuS) nanocrystals.

2. Scheme for the production of elongated needle-like copper sulfide (nCuS) nanocrystals using a planetary ball mill.

Using a planetary mill, it is possible to obtain copper sulfide nanopowders of 10 g in each charge. We suggested using a four-chamber planetary mill with a chamber volume of 500 mL (Retsch - 400; Pulverisette - 6) and high energy planetary ball mill Pulverisette 5 PREMIUM with a unique capacity of up to 450 mL. A principle scheme of production elongated needle-like copper sulfide (nCuS) nanocrystals in a planetary ball mill are presented in Figure 40.



1 – preparation of powder precursors charge; 2 – mechanochemical synthesis of charge in the stainless steel chamber; 3 – washing with distilled water as-obtained mixture; 4 – separation of target solid product from the solution via filtration; 5 – drying as-filtrated target product

Figure 40 – Principle scheme of production elongated needle-like copper sulfide (nCuS) nanocrystals by the mechanochemical method using a planetary ball mill

Information about prices and descriptions of sulfur nanoparticles is openly available in two offering companies. The product of the first company (US Research Nanomaterials Inc, USA) is orthorhombic yellow sulfur nanopowders with a purity of 99.99% and an average particle size of 47 nm synthesized via laser gas phase method. The price for sulfur nanopowders is 85, 265, and 595 US dollars (USD) for 5, 25, and 100 g, respectively [157]. The website of the second company (SkySpring Nanomaterials Inc, USA) also openly lists prices for sulfur nanoparticles with a purity of 99.99% and an average particle size of <55 nm. The price for sulfur nanopowders in this company is 110, 190, and 360 US dollars (USD) for 25, 100, and 500 g, respectively [158].

The price for commercial copper sulfide (CuS) nanoparticles is not provided on the official website of the abovementioned companies and other nanomaterial producing companies. However, the cost of micro-sized CuS presented on the website of US Research Nanomaterials Inc. The price of copper sulfide microparticles with purity of

99% and an average particle size of 15 μm was 198 US dollars (USD) for 25 g of nanopowder [159].

Estimated costings for production 100 g of sulfur nanoparticles and copper sulfide nanocrystals are shown in Table 8.

Table 8 – Estimated costings for production 100 g of sulfur and copper sulfide nanoparticles

Name of compound	Sulfur nanoparticles		Copper sulfide (nCuS) nanoneedles	
	Amount, g	Expenses, tenge	Amount, g	Expenses, tenge
Calcium polysulfide (CaS_x) solution (ρ=1.25 g/cm^3)	767	2 050	-	-
Carbon dioxide (CO_2) gas	26	750	-	-
Surfactant neonol	<1	200	-	-
Hydrochloric acid (HCl)	120	3 500	-	-
Sodium thiosulfate pentahydrate ($Na_2S_2O_3 \times 5H_2O$)	-	-	130	39 000
Citric acid ($C_6H_8O_7$)	-	-	100	18 000
Copper acetate monohydrate ($Cu(CH_3COO)_2 \times H_2O$)	-	-	105	37 000
Sodium sulfide nonahydrate ($Na_2S \times 9H_2O$)	-	-	125	22 000
Electricity and rental premises	-	1500	-	12 000
Mill consumables	-	-	-	5000
Employee salary	-	10 000	-	30 000
Other expenses	-	2 000	-	10000
Total cost	-	20 000	-	173 000

Calculations show that the price for 100 g of sulfur nanoparticles from the manufacturer (SkySpring Nanomaterials Inc, USA) is more than 74 thousand tenges. Even if we take into account the costs of preparing the solution and promoting it on the market (not included in the table), the cost of sulfur nanoparticles by the proposed method is three times cheaper than the cost of a well-known commercial product. In the case of CuS, as we mentioned before, no copper sulfide (CuS) nanoparticles in the sale were found. Only on the website of US Research Nanomaterials Inc, we found copper

monosulfide microparticles with average particle size of 15 μm which cost more than 300 thousand tenges. In our case we could synthesize copper sulfide (CuS) nanocrystals with needle-like shape in nano size. So, in both case, upon realizing the production of the above nanoparticles will be very rentable.

CONCLUSION

1. The optimal conditions for solid-phase (mechanochemical) and liquid-phase preparation of sulfur, semiconductor spherical and needle-like copper sulfide (nCuS), and sulfur-containing nanocomposites ($S/CaCO_3$ and CuS/S) were found.

2. All as-obtained products have been characterized using vast of modern methods of physicochemical analysis.

3. The physicochemical, biological, and anti-biological properties of as-obtained sulfur, CuS nanoparticles, and sulfur-containing nanocomposites are determined.

The hydrophobic properties of sulfur, calcium carbonate nanoparticles, as well as sulfur-containing $S/CaCO_3$ nanocomposites are evaluated. The measurements of the contact angles of water droplets yielded the following results: $140^{\circ}\pm3^{\circ}$, $147^{\circ}\pm3^{\circ}$, and $133^{\circ}\pm3^{\circ}$ for the densified surface of sulfur, calcium carbonate nanoparticles, and $S/CaCO_3$ nanocomposites, respectively.

The biological activity of sulfur, calcium carbonate nanoparticles, and $S/CaCO_3$ nanocomposites on wheat-seed germination are tested. It was found that calcium carbonate nanoparticles have the weakest effect on seed germination. Sulfur nanoparticles have a moderate effect, while $S/CaCO_3$ composite has the strongest action and accelerates the growth of the shoots and roots by 55 and 45%, respectively.

The antibacterial properties of mechanochemically synthesized sulfur microparticles, spherical, and needle-like copper sulfide (nCuS) nanocrystals are studied. It was found that nCuS is a less selective agent, as it possessed activity against both *E. coli* and *S. aureus* bacteria, whereas the spherical CuS sample showed activity only against *E. coli*. Sulfur microparticles did not show any antibacterial activity against both bacteria.

4. The principal technological scheme for the production of sulfur, nCuS nanocrystals, and sulfur-containing ($S/CaCO_3$) nanocomposites are developed. Facile, quick, low-cost, and environmentally-friendly methods for production abovementioned nanostructures are developed.

5. The economic efficiency of using the developed method for producing sulfur, CuS nanostructures, and sulfur-containing nanocomposites in comparison with known methods is preliminarily assessed. Based on data from open sources, it was calculated that the cost of sulfur nanoparticles obtained by the developed method is three times cheaper than the selling price of commercial sulfur nanoparticles (SkySpring Nanomaterials Inc, USA). Also, on the website of US Research Nanomaterials Inc, we found copper monosulfide microparticles with average particle size of 15 μm which cost more than 300 thousand tenges. Typically, copper sulfide nanoparticles are one or two orders of magnitude more expensive than copper sulfide microparticles. Thus, in both case, upon realizing the production of the above nanoparticles will be very rentable.

REFERENCES

1 Tan D., Garcia F. Main group mechanochemistry: from curiosity to established protocols // Chemical Society Reviews. – 2019. – Vol. 48, Issue 8. – P. 2274-2292.

2 Urakaev F.K., Bulavchenko A.I., Uralbekov B.M., Massalimov I.A., Tatykayev B.B., Bolatov A.K., Dzharlykasimova D.N., Burkitbayev M.M. Mechanochemical synthesis of colloidal sulfur particles in the $Na_2S_2O_3$-H-2($C_4H_4O_4$)-Na_2SO_3 system // Colloid Journal. – 2016. – Vol. 78, Issue 2. – P. 210-219.

3 Shamsipur M., Pourmortazavi S.M., Roushani M., Kohsari I., Hajimirsadeghi S.S. Novel approach for electrochemical preparation of sulfur nanoparticles // Microchimica Acta. – 2011. – Vol. 173, Issue 3-4. – P. 445-451.

4 Guo Y., Zhao J., Yang S., Yu K., Zhang H., Wang Z. Preparation and characterization of monoclinic sulfur nanoparticles by water-in-oil microemulsions technique // Powder Technology. – 2006. – Vol. 162, Issue– P. 83-86.

5 Choudhury S.R., Mandal A., Chakravorty D., Gopal M., Goswami A. Evaluation of physicochemical properties, and antimicrobial efficacy of monoclinic sulfur-nanocolloid // Journal of Nanoparticle Research. – 2013. – Vol. 15, Issue 4. – P.

6 Choudhury S.R., Ghosh M., Goswami A. Inhibitory effects of sulfur nanoparticles on membrane lipids of aspergillus niger: a novel route of fungistasis // Current Microbiology. – 2012. – Vol. 65, Issue 1. – P. 91-97.

7 Choudhury R., Ghosh M., Mandal A., Chakrovarty D., Pal M., Pradhan S., Goswami A. Surface modified sulfur nanoparticles: an effective antifungal agent against *Aspergillus niger* and *Fusarium oxysporum* // Applied Microbiology and Biotechnology. – 2011. – Vol. 90, Issue 2. – P. 733-743.

8 Chaudhuri R.G., Paria S. Synthesis of sulfur nanoparticles in aqueous surfactant solutions // Journal of Colloid and Interface Science. – 2010. – Vol. 343, Issue– P. 439–446.

9 Cheng X., Cheng K., Liu J., Sun X. Synthesis and characterizations of nanoparticle sulfur using eggshell membrane as template // Materials Science Forum. – 2011. – Vol. 675-677, Issue– P. 279-282.

10 Baláž M. Eggshell membrane biomaterial as a platform for the applications in materials science // Acta Biomaterialia. – 2014. – Vol. 10, Issue 9. – P. 3827-3843.

11 Salem N.M., Albanna L.S., Awwad A.M. Green synthesis of sulfur nanoparticles using *Punica granatum* peelsand the effects on the growth of tomato by foliar spray applications // Environmental Nanotechnology, Monitoring & Management. – 2016. – Vol. 6, Issue– P. 83-87.

12 Choudhury S.R., Ghosh M., Mandal A., Chakravorty D., Pal M., Pradhan S., Goswami A. Surface-modified sulfur nanoparticles: an effective antifungal agent against *Aspergillus niger* and *Fusarium oxysporum* // Applied Microbiology and Biotechnology. – 2011. – Vol. 90, Issue 2. – P. 733-743.

13 Xie X.-y., Li L.-y., Zheng P.-s., Zheng W.-j., Bai Y., Cheng T.-f., Liu J. Facile synthesis, spectral properties and formation mechanism of sulfur nanorods in PEG-200 // Materials Research Bulletin. – 2012. – Vol. 47, Issue 11. – P. 3665-3669.

14 Kenawi M.Z., Morsy T.A., Abdalla K.F., Hady H.M. Treatment of human scabies by sulfur and permethrin // Journal of the Egyptian Society of Parasitalogy. – 1993. – Vol. 23, Issue 3. – P. 691-696.

15 Jha D.K., Debata L. A case of vitiligo treated by sulphur // Indian Journal of Research In Homoeopathy. – 2009. – Vol. 3, Issue 3. – P.

16 Chen H., Dong W., Ge J., Wang C., Wu X., Lu W., Chen L. Ultrafine sulfur nanoparticles in conducting polymer shell as cathode materials for high performance lithium/sulfur batteries // Scientific Reports. – 2013. – Vol. 3, Issue– P.

17 Barkauskas J., Juškėnas R., Milerienė V., Kubilius V. Effect of sulfur on the synthesis and modification of carbon nanostructures // Materials Research Bulletin. – 2007. – Vol. 42, Issue 9. – P. 1732-1739.

18 Lin A.N., Reimer R.J., Carter D.M. Sulfur revisited // Journal of the American Academy of Dermatology. – 1988. – Vol. 18, Issue 3. – P. 553-558.

19 Lee Z.W., Zhou J., Chen C.-S., Zhao Y., Tan C.-H., Li L., Moore P.K., Deng L.-W. The slow-releasing hydrogen sulfide donor, GYY4137, exhibits novel anti-cancer effects *in vitro* and *in vivo* // One Plos. – 2011. – Vol. 6, Issue 6. – P.

20 Nishimura S.I., Hato M., Hyugaji S., Feng F., Amano M. Glycomics for drug discovery: metabolic perturbation in androgen-independent prostate cancer cells induced by unnatural hexosamine mimics // Angewandte Chemie - International Edition. – 2012. – Vol. 51, Issue 14. – P. 3386-3390.

21 Griffith C.M., Woodrow J.E., Seiber J.N. Environmental behavior and analysis of agricultural sulfur // Pest Management Science. – 2015. – Vol. 71, Issue 11. – P. 1486-1496.

22 Venkataraman K., The chemistry of synthetic dyes, Academic press, New York1974.

23 Suleiman H.Y., Roth R., Jain S., Heuser J.E., Shaw A.S., Miner J.H. Injury-induced actin cytoskeleton reorganization in podocytes revealed by super-resolution microscopy // Jci Insight. – 2017. – Vol. 2, Issue 16. – P.

24 Basu S., Choudhury S.R., Roy S., Goswami A. Polyethylene glycol-stabilized sulphur nanoparticles: an effective antimicrobial agent against multidrug-resistant bacteria // Journal of Antimicrobial Chemotherapy. – 2012. – Vol. 67, Issue 5. – P. 1134–1137.

25 Choudhury S.R., Mandal A., Ghosh M., Basu S., Chakravorty D., Goswami A. Investigation of antimicrobial physiology of orthorhombic and monoclinic nanoallotropes of sulfur at the interface of transcriptome and metabolome // Applied Microbial and Cell Physiology. – 2013. – Vol. 97, Issue 13. – P. 5965-5978.

26 Choudhury S.R., Nair K.K., Kumar R., Gogoi R., Srivastava C., Gopal M., Subhramanyam B.S., Devakumar C., Goswamia A. Nanosulfur: A potent fungicide

against food pathogen, Aspergillus niger. International conference on advance nanomaterials and nanotechnology // AIP Conference Proceedings. – 2010. – Vol. 1276, Issue 154. – P.

27 Deshpande A.S., Khomane R.B., Vaidya B.K., Joshi R.M., Harle A.S., Kulkarni B.D. Sulfur Nanoparticles Synthesis and Characterization from H2S Gas, Using Novel Biodegradable Iron Chelates in W/O Microemulsion // Nanoscale Research Letters. – 2008. – Vol. 3, Issue 6. – P. 221-229.

28 Gogoi R., Singh P.K., Kumar R., Nair K.K. Suitability of nano-sulfur for biorational management of powdery mildew of okra (*Abelmoschus esculentus* Moench) caused by *Erysiphe cichoracearum* // Journal of Plant Pathology and Microbiology. – 2013. – Vol. 4, Issue 4. – P. 171.

29 Lee J., Lee H.-J., Park J.-D., Lee S.-K., Lee S.-I., Lim H.-D., Lee Y.-M., Yun Y.-G., Jeon B.-H., Ree I.-S., Jung C.-D., Lee S.-K., Kim E.-C. Anticancer activity of highly purified sulfur in immortalized and malignant human oral keratinocytes // Toxicology In Vitro. – 2008. – Vol. 22, Issue 1. – P. 87-95.

30 Al-Ali A., Suleiman M., Hussein A. Preparation of sulfur nanoparticles and investigating their activities against cancer cell // M.Sc Thesis, An- Nijah National University, Nablus, Palestine. – 2013. – Vol. Issue– P.

31 Rai M., Ingle A.P., Paralikar P. Sulfur and sulfur nanoparticles as potential antimicrobials: from traditional medicine to nanomedicine // Expert Review of Anti-infective Therapy. – 2016. – Vol. 14, Issue 10. – P. 969-978.

32 Beyth N., Houri-Haddad Y., Domb A., Khan W., Hazan R. Alternative antimicrobial approach: Nanoantimicrobial material // Evidence-Based Complementary and Alternative Medicine. – 2015. – Vol. 2015, Issue– P. 16.

33 Kandi V., Kandi S. Antimicrobial properties of nanomolecules: potential candidates as antibiotics in the era of multi-drug resistance // Epidemiology and Health. – 2015. – Vol. 37, Issue– P.

34 Gupta A.K., Nicol K. The use of sulfur in dermatology // Journal of Drugs in Dermatology –2004. – Vol. 3, Issue 4. – P. 427-431.

35 Choudhury S.R., Goswami A. Supramolecular reactive sulfur nanoparticles: a novel and efficient antimicrobial agent // Journal of Applied Microbiology. – 2013. – Vol. 114, Issue 1. – P. 1-10.

36 Owens R.G. Chemistry and physiology of fungicidal action // Annual Review of Phytopathology. – 1963. – Vol. 1, Issue– P. 77-100.

37 Schneider T., Baldauf A., Ba L.A., Jamier V., Khairan K., Sarakbi M.-B., Reum N., Schneider M., Röseler A., Becker K., Burkholz T., Winyard P.G., Kelkel M., Diederich M., Jacob C. Selective antimicrobial activity associated with sulfur nanoparticles // Journal of Biomedical Nanotechnology. – 2011. – Vol. 7, Issue 3. – P. 395-405.

38 Jabir N.R., Tabrez S., Ashraf G.M., Shakil S., Damanhouri G.A., Kamal M.A. Nanotechnology-based approaches in anticancer research // International Journal of Nanomedicine. – 2012. – Vol. 7, Issue– P. 4391–4408.

39 Danhier F., Feron O., Préat V. To exploit the tumor microenvironment: Passive and active tumor targeting of nanocarriers for anti-cancer drug delivery // Journal of Controlled Release. – 2010. – Vol. 148, Issue 2. – P. 135-146.

40 An Y.-l., Nie F., Wang Z.-y., Zhang D.-s. Preparation and characterization of realgar nanoparticles and their inhibitory effect on rat glioma cells // International Journal of Nanomedicine. – 2011. – Vol. 6, Issue– P. 3187–3194.

41 Zefirov N.S., Chimicheskaya enciklopedia, Moskva: Bolshaya enciklopedia1995.

42 Goel S., Chen F., Cai W.B. Synthesis and biomedical applications of copper sulfide nanoparticles: From sensors to theranostics // Small. – 2014. – Vol. 10, Issue 4. – P. 631-645.

43 Baláž P., Baláž M., Achimovičová M., Bujňáková Z., Dutková E. Chalcogenide mechanochemistry in materials science: insight into synthesis and applications (a review) // Journal of Materials Science. – 2017. – Vol. 52, Issue– P. 11851-11890.

44 Naveed M., Younas W., Zhu Y., Rafai S., Zhao Q., Tahir M., Mushtaq N., Cao C. Template free and facile microwave-assisted synthesis method to prepare mesoporous copper sulfide nanosheets for high-performance hybrid supercapacitor // Electrochimica Acta. – 2019. – Vol. 319, Issue– P. 49-60.

45 Chen W., Xie Y., Hu C., Zeng T., Jiang H., Qiao F., Gu J., Dong X., Zhao X. Room temperature synthesis of aqueous soluble covellite cus nanocrystals with high photothermal conversion // CrystEngComm. – 2018. – Vol. 20, Issue 30. – P. 4283-4290.

46 Wang X., He Y., Hu Y., Jin G., Jiang B., Huang Y. Photothermal-conversion-enhanced photocatalytic activity of flower-like CuS superparticles under solar light irradiation // Solar Energy. – 2018. – Vol. 170, Issue– P. 586-593.

47 Hessein A., Wang F., Masai H., Matsuda K., El-Moneim A.A. Improving the stability of CdS quantum dot sensitized solar cell using highly efficient and porous CuS counter electrode // Journal of Renewable and Sustainable Energy. – 2017. – Vol. 9, Issue 2. – P.

48 Rokade A.A., Jin Y.E., Park S.S. Facile synthesis of plate-like CuS nanoparticles and their optical and photo-thermal properties // Materials Chemistry and Physics. – 2018. – Vol. 207, Issue– P. 465-469.

49 Qin Y., Kong X., Lei D., Lei X. A facial grinding method for the synthesis of high-purity CuS nanosheets // Industrial & Engineering Chemistry Research. – 2018. – Vol. 57, Issue 8. – P. 2759-2764.

50 Islam D.A., Chakraborty A., Bhattacharya B., Sarkar U., Acharya H. Tailored synthesis of CuS nanodisks from a new macrocyclic precursor and their efficient

catalytic properties on methylene blue dye degradation // Journal of Nanoparticle Research. – 2016. – Vol. 18, Issue 5. – P.

51 Li J., Jiu T., Tao G.-H., Wang G., Sun C., Li P., Fang J., He L. Manipulating surface ligands of copper sulfide nanocrystals: synthesis, characterization, and application to organic solar cells // Journal of Colloid and Interface Science. – 2014. – Vol. 419, Issue– P. 142-147.

52 Darouie M., Afshar S., Zare K., Monajjemi M. Investigation of different factors towards synthesis of CuS spherical nanoparticles // Journal of Experimental Nanoscience. – 2013. – Vol. 8, Issue 4. – P. 451–461.

53 Tan C., Zhu Y., Lu R., Xue P., Bao C., Liu X., Fei Z., Zhao Y. Synthesis of copper sulfide nanotube in the hydrogel system // Materials Chemistry and Physics. – 2005. – Vol. 91, Issue 1. – P. 44-47.

54 Yang J., Jing-Hui, Zeng, Yu S.-H., Yang L., Zhou G.-e., Qian Y.-t. Formation process of CdS nanorods via solvothermal route // Chemistry of Materials. – 2000. – Vol. 12, Issue 11. – P. 3259-3263.

55 Baláž P., Boldižárová E., Godočıková E., Briančin J. Mechanochemical route for sulphide nanoparticles preparation // Materials Letters. – 2003. – Vol. 57, Issue 9-10. – P. 1585-1589.

56 Godocikova E., Balaz P., Gock E., Choi W.S., Kim B.S. Mechanochemical synthesis of the nanocrystalline semiconductors in an industrial mill // Powder Technology. – 2006. – Vol. 164, Issue 3. – P. 147-152.

57 Baláž M., Zorkovská A., Urakaev F., Baláž P., Briančin J., Bujňáková Z., Achimovičová M., Gock E. Ultrafast mechanochemical synthesis of copper sulfides // RSC Advances. – 2016. – Vol. 6, Issue 91. – P. 87836-87842.

58 Roy P., Srivastava S.K. Nanostructured copper sulfides: synthesis, properties and applications // CrystEngComm. – 2015. – Vol. 17, Issue 41. – P. 7801-7815.

59 Dibenedetto F., Borgheresi M., Caneschi A., Chastanet G., Cipriani C., Gatteschi D., Pratesi G., Romanelli M., Sessoli R. First evidence of natural superconductivity: covellite // European Journal of Mineralogy. – 2006. – Vol. 18, Issue 3. – P. 283-287.

60 Yu X.L., Cao C.B., Zhu H.S., Li Q.S., Liu C.L., Gong Q.H. Nanometer-sized copper sulfide hollow spheres with strong optical-limiting properties // Advanced Functional Materials. – 2007. – Vol. 17, Issue 8. – P. 1397-1401.

61 Tanveer M., Cao C., Ali Z., Aslam I., Idrees F., Khan W.S., But F.K., Tahir M., Mahmood N. Template free synthesis of CuS nanosheet-based hierarchical microspheres: an efficient natural light driven photocatalyst // CrystEngComm. – 2014. – Vol. 16, Issue 24. – P. 5290-5300.

62 Wu Y., Wadia C., Ma W., Sadtler B., Alivisatos A.P. Synthesis and photovoltaic application of copper (I) sulfide nanocrystals // Nano Letters. – 2008. – Vol. 2008, Issue 8. – P. 8.

63 Lee H., Yoon S.W., Kim E.J., Park J. In-situ growth of copper sulfide nanocrystals on multiwalled carbon nanotubes and their application as novel solar cell and amperometric glucose sensor materials // Nano Letters. – 2007. – Vol. 7, Issue 3. – P. 778-784.

64 Lai C.-H., Huang K.-W., Cheng J.-H., Lee C.-Y., Hwang B.-J., Chen L.-J. Direct growth of high-rate capability and high capacity copper sulfidenanowire array cathodes for lithium-ion batteries // Journal of Material Chemistry. – 2010. – Vol. 20, Issue 32. – P. 6638-6645.

65 Bu X., Zhou D., Li J., Zhang X., Zhang K., Zhang H., Yang B. Copper sulfide self-assembly architectures with improved photothermal performance // Langmuir. – 2014. – Vol. 30, Issue 5. – P. 1416-1423.

66 Baláž M., Dutková E., Bujňáková Z., Tóthová E., Kostova N.G., Karakirova Y., Briančin J., Kaňuchová M. Mechanochemistry of copper sulfides: Characterization, surface oxidation and photocatalytic activity // Journal of Alloys and Compounds. – 2018. – Vol. 746, Issue– P. 576-582.

67 Wang M., Xie F., Li W., Chen M., Zhaoc Y. Preparation of various kinds of copper sulfides in a facile way and the enhanced catalytic activity by visible ligh // Journal of Materials Chemistry A. – 2013. – Vol. 1, Issue 30. – P. 8616-8621.

68 Yang Z.K., Song L.X., Teng Y., Xia J. Ethylenediamine-modulated synthesis of highly monodisperse copper sulfide microflowers with excellent photocatalytic performance // Journal of Materials Chemistry A. – 2014. – Vol. 2, Issue 47. – P. 20004-20009.

69 Zhang Y.Q., Zhang B.P., Ge Z.H., Zhu L.F., Li Y. Preparation by solvothermal synthesis, growth mechanism, and photocatalytic performance of cus nanopowders // European Journal of Inorganic Chemistry. – 2014. – Vol. 2014, Issue 14. – P. 2368-2375.

70 Sahoo A.K., Srivastava S.K. Controllable architecture of CdS and CuS by single-source precursor-mediated approach and their photocatalytic activity // Journal of Nanoparticle Research. – 2013. – Vol. 15, Issue 4. – P.

71 Gao M.-R., Xu Y.-F., Jiang J., Yu S.-H. Nanostructured metal chalcogenides: synthesis, modification, and applications in energy conversion and storage devices // Chemical Society Reviews. – 2013. – Vol. 42, Issue 7. – P. 2986-3017.

72 Débart A., Dupont L., Patrice R., Tarascon J.-M. Reactivity of transition metal (Co, Ni, Cu) sulphides versus lithium: The intriguing case of the copper sulphide // Solid State Sciences. – 2006. – Vol. 8, Issue 6. – P. 640-651.

73 Chen Y., Davoisne C., Tarascon J.-M., Guéry C. Growth of single-crystal copper sulfide thin films viaelectrodeposition in ionic liquid media for lithium ion batteries // Journal of Material Chemistry. – 2012. – Vol. 22, Issue 12. – P. 5295-5299.

74 Bera A., Dey S., Pal A.J. Band mapping across a pn-junction in a nanorod by scanning tunneling microscopy // Nano Letters. – 2014. – Vol. 14, Issue 4. – P. 2000-2005.

75 Pan C., Niu S., Ding Y., Dong L., Yu R., Liu Y., Zhu G., Wang Z.L. Enhanced Cu_2S/CdS coaxial nanowire solar cells by piezo-phototronic effect // Nano Letters. – 2012. – Vol. 12, Issue 6. – P. 3302-3307.

76 Jiang Y., Zhang X., Ge Q.-Q., Yu B.-B., Zou Y.-G., Jiang W.-J., Song W.-G., Wan L.-J., Hu J.-S. ITO@Cu_2S tunnel junction nanowire arrays as efficient counter electrode for quantum-dot-sensitized solar cells // Nano Letters. – 2014. – Vol. 14, Issue 1. – P. 365-372.

77 Wang J. Survey and summary: From DNA biosensors to gene chips // Nucleic Acids Research. – 2000. – Vol. 28, Issue 16. – P. 3011–3016.

78 Chen X., Zhang X.-E., Chai Y.-Q., Hu W.-P., Zhang Z.-P., Zhang X.-M., Cass A.E.G. DNA optical sensor: a rapid method for the detection of DNA hybridization // Biosensors and Bioelectronics. – 1998. – Vol. 13, Issue 3-4. – P. 451-458.

79 Zhang S., Zhong H., Ding C. Ultrasensitive flow injection chemiluminescence detection of DNA hybridization using signal DNA probe modified with au and CuS nanoparticles // Analytical Chemistry. – 2008. – Vol. 80, Issue 19. – P. 7206-7212.

80 Ding C., Wang Z., Zhong H., Zhang S. Ultrasensitive chemiluminescence quantification of single-nucleotide polymorphisms by using monobase-modified Au and CuS nanoparticles // Biosensors and Bioelectronics. – 2010. – Vol. 25, Issue 5. – P. 1082-1087.

81 Jr. L.C.C., Lyons C. Electrode systems for continuous monitoring in cardiovascular surgery // Annals of the New York Academy of Sciences. – 1962. – Vol. 102, Issue 1. – P. 29-45.

82 Wang H.-Y., Hua X.-W., Wu F.-G., Li B., Liu P., Gu N., Wang Z., Chen Z. Synthesis of ultrastable copper sulfide nanoclusters via trapping the reaction intermediate: potential anticancer and antibacterial applications // ACS Applied Materials & Interfaces. – 2015. – Vol. 7, Issue 13. – P. 7082-7092.

83 Ryan K.M., Cabot A., Coughlan C., Ibáñez M., Dobrozhan O., Singh A. Compound copper chalcogenide nanocrystals // Chemical Reviews. – 2017. – Vol. 117, Issue 9. – P. 5865–6109.

84 Yu J., Zhang J., Liu S. Ion-Exchange Synthesis and Enhanced Visible-Light Photoactivity of CuS/ZnS Nanocomposite Hollow Spheres // Journal of Physical Chemistry C. – 2010. – Vol. 114, Issue 32. – P. 13642-13649.

85 Baláž P., Baláž M., Dutková E., Zorkovská A., Kováč J., Hronec P., Kováč Jr. J., Čaplovičová M., Mojžiš J., Mojžišová G., Eliyas A., Kostova N.G. CdS/ZnS nanocomposites: from mechanochemical synthesis to cytotoxicity issues // Materials Science and Engineering C. – 2016. – Vol. 58, Issue– P. 1016-1023.

86 Lu C., Liu C., Chen R., Fang X., Xu K., Meng D. Synthesis and characterization of ZnO/ZnS/CuS ternary nanocomposites as high efficient photocatalyst in visible light // Journal of materials science-materials in electronics. – 2016. – Vol. 27, Issue 7. – P. 6947-6954.

87 Nogueira A.F., Benedetti J.E., Bernardo D.R., Morais A., Bettini J. Synthesis and characterization of a quaternary nanocomposite based on TiO_2/CdS/rGO/Pt and its application in the photoreduction of CO_2 to methane under visible light // RSC Advances. – 2015. – Vol. 5, Issue 43. – P. 33914-33922

88 Habibi-Yangjeh A., Akhundia A. Facile preparation of novel quaternary g-C_3N_4/Fe_3O_4/AgI/Bi_2S_3 nanocomposites: magnetically separable visible-light-driven photocatalysts with significantly enhanced activity // RSC Advances. – 2016. – Vol. 6, Issue 108. – P. 106572-106583.

89 Habibi-Yangjeh A., Shekofteh-Gohari M. Fe_3O_4/ZnO/Ag_3VO_4/AgI nanocomposites: Quaternary magnetic photocatalysts with excellent activity in degradation of water pollutants under visible light // Separation and Purification Technology. – 2016. – Vol. 166, Issue– P. 63-72.

90 Dong S., Wang P., Zhai Y., Wang D. Synthesis of reduced graphene oxide-anatase TiO_2 nanocomposite and its improved photo-induced charge transfer properties // Nanoscale. – 2011. – Vol. 3, Issue 4. – P. 1640-1645.

91 Pan S., Liu X. ZnS–Graphene nanocomposite: Synthesis, characterization and optical properties // Journal of Solid State Chemistry. – 2012. – Vol. 191, Issue– P. 51-56.

92 Saranya M., Ramachandrana R., Kollub P., Jeong S.K., Grace A.N. A template-free facile approach for the synthesis of CuS–rGO nanocomposites towards enhanced photocatalytic reduction of organic contaminants and textile effluents // RSC Advances. – 2015. – Vol. 5, Issue 21. – P. 15831-15840.

93 Yang Y., Zheng G., Cui Y. Nanostructured sulfur cathodes // Chemical Society Reviews. – 2013. – Vol. 42, Issue 7. – P. 3018-3032.

94 Bae S.Y., Seo H.W., Park J. Vertically aligned sulfur-doped zno nanowires synthesized via chemical vapor deposition // Journal of Physical Chemistry B. – 2004. – Vol. 108, Issue 17. – P. 5206-5210.

95 Bian S., Shen C., Qian Y., Liu J., Xi F., Dong X. Facile synthesis of sulfur-doped graphene quantum dots asfluorescent sensing probes for Ag^+ions detection // Sensors and Actuators B: Chemical. – 2017. – Vol. 242, Issue– P. 231-237.

96 Huang H., Lu Y.-C., Wang A.-J., Liu J.-H., Chen J.-R., Feng J.-J. A facile, green, and solvent-free route to nitrogen-sulfur-codoped fluorescent carbon nanoparticles for cellular imaging // RSC Advances. – 2014. – Vol. 4, Issue 23. – P. 11872-11875.

97 Hamal D.B., Klabunde K.J. Synthesis, characterization, and visible light activity of new nanoparticle photocatalysts based on silver, carbon, and sulfur-doped TiO_2 // Journal of Colloid and Interface Science. – 2007. – Vol. 311, Issue 2. – P. 514-522.

98 Hussain S.T., Khan K., Hussain R. Size control synthesis of sulfur doped titanium dioxide (anatase) nanoparticles, its optical property and its photo catalytic reactivity for CO_2 + H_2O conversion and phenol degradation // Journal of Natural Gas Chemistry. – 2009. – Vol. 18, Issue 4. – P. 383-391.

99 Zhou W., Zhao W., Lu Z., Zhu J., Fan S., Ma J., Hng H.H., Yan Q. Preparation and thermoelectric properties of sulfur doped Ag_2Te nanoparticlesvia solvothermal methods // Nanoscale. – 2012. – Vol. 4, Issue 13. – P. 3926-3931.

100 Kalybekkyzy S., Mentbayeva A., Kahraman M.V., Zhang Y., Bakenov Z. Flexible S/DpAN/KB nanofiber composite as binder-free cathodes for Li-S batteries // Journal of the Electrochemical Society. – 2019. – Vol. 166, Issue 3. – P. A5396-A5402.

101 Peng H., Wang X., Zhao Y., Tan T., Bakenov Z., Zhang Y. Synthesis of a flexible freestanding sulfur/polyacrylonitrile/graphene oxide as the cathode for lithium/sulfur batteries // Polymers. – 2018. – Vol. 10, Issue 4. – P.

102 Li H., Sun L., Wang Z., Zhang Y., Tan T., Wang G., Bakenov Z. Three-dimensionally hierarchical graphene based aerogel encapsulated sulfur as cathode for lithium/sulfur batteries // Nanomaterials. – 2018. – Vol. 8, Issue 2. – P.

103 Tian Y., Sun Z., Zhang Y., Wang X., Bakenov Z. Micro-spherical sulfur/graphene oxide composite via spray drying for high performance lithium sulfur batteries // Nanomaterials. – 2018. – Vol. 8, Issue 1. – P.

104 Peng H., Wang X., Zhao Y., Tan T., Mentbayeva A., Bakenov Z., Zhang Y. Enhanced electrochemical performance of sulfur/polyacrylonitrile composite by carbon coating for lithium/sulfur batteries // Journal of Nanoparticle Research. – 2017. – Vol. 19, Issue 10. – P.

105 Zhao Y., Yin F., Zhang Y., Zhang C., Mentbayeva A., Umirov N., Xie H., Bakenov Z. A free-standing sulfur/nitrogen-doped carbon nanotube electrode for high-performance lithium/sulfur batteries // Nanoscale Research Letters. – 2015. – Vol. 10, Issue 1. – P. 1-6.

106 Zhao Y., Bakenova Z., Zhang Y., Peng H., Xie H., Bakenov Z. High performance sulfur/nitrogen-doped graphene cathode for lithium/sulfur batteries // Ionics. – 2015. – Vol. 21, Issue 7. – P. 1925-1930.

107 Massalimov I.A., Khusainov A.N., Zainitdinova R.M., Musavirova L.R., Zaripova L.R., Mustafin A.G. Chemical precipitation of sulfur nanoparticles from aqueous solutions // Russian Journal of Applied Chemistry. – 2014. – Vol. 87, Issue 6. – P. 700-708.

108 Massalimov I.A., Vikhareva I.N., Kireeva M.S. Use of polysulfides of alkali and alkaline-earth metals to obtain highly dispersed sulfur // Russian Journal of Applied Chemistry. – 2008. – Vol. 81, Issue 2. – P. 195-199.

109 Massalimov I.A., Shainurova A.R., Khusainov A.N., Mustafin A.G. Production of sulfur nanoparticles from aqueous solution of potassium polysulfide // Russian Journal of Applied Chemistry. – 2013. – Vol. 85, Issue 12. – P. 1832–1837.

110 Balaz P., Boldizarova E., Godocikova E., Briacin J. Mechanochemical route for sulphide nanoparticles preparation // Materials Letters. – 2003. – Vol. 57, Issue 9-10. – P. 1585-1589.

111 Rojas J.J., Ochoa V.J., Ocampo S.A., Muñoz J.F. Screening for antimicrobial activity of ten medicinal plants used in Colombian folkloric medicine: A possible

alternative in the treatment of non-nosocomial infections // BMC Complementary and Alternative Medicine. – 2006. – Vol. 6, Issue– P. 2.

112 Massalimov I.A., Khusainov A.N., Zainitdinova R.M., Musavirova L.R., Zaripova L.R., Mustafin A.G. Chemical precipitation of sulfur nanoparticles from aqueous solutions // Russian Journal of Applied Chemistry. – 2014. – Vol. 87, Issue 6. – P. 700–708.

113 Massalimov I.A., Samsonov M.R., Akhmetshin B.S., Mustafin A.G., Burkitbayev M.M., Shalabayev Z.S., Urakaev F.K. Coprecipitation of nanocomposites based on colloidal particles of sulfur and carbonates of alkaline-earth metals from polysulfide solutions // Colloid Journal. – 2018. – Vol. 80, Issue 4. – P. 407-417.

114 Du L., Wang Y., Luo G. In situ preparation of hydrophobic $CaCO_3$ nanoparticles in a gas–liquid microdispersion process // Particuology. – 2013. – Vol. 11, Issue 4. – P. 421-427.

115 Du L., Wang Y., Wang K., Luo G. Effects of nanoparticles with different wetting abilities on the gas–liquid mass transfer // Chemical Engineering Science. – 2014. – Vol. 114, Issue– P. 105-113.

116 Shalabayev Z.S., Oskenbay A.K., Orazbay P.E., Duisenkulova A.S. Synthesis of CuS/S nanocomposites by hydrothermal way and their characterization // Chemical Journal of Kazakhstan. – 2019. – Vol. 3, Issue– P. 130-139.

117 Kalita M.P.C., Kalita A. Williamson-Hall analysis and optical properties of small sized ZnO nanocrystals // Physica E. – 2017. – Vol. 92, Issue– P. 36-40.

118 Shalabayev Z., Madikassimova M., Tatykaev B., Uralbekov B., Urakaev F., Burkitbayev M., Synthesis of CuS/S nanocomposites and their application fields, The 5th International Conference on Advanced Nanomaterials and Energy Storage Systems (INESS-2017), Astana, Kazakhstan, 2017.

119 Ishii M., Shibata K., Nozaki H. Anion Distributions and Phase Transitions in $CuS_{1-x}Se_x$ (x=0-1) Studied by Raman Spectroscopy // Journal of Solid State Chemistry. – 1993. – Vol. 105, Issue– P. 504-511.

120 Munce C.G., Parker G.K., Holt S.A., Hope G.A. A Raman spectroelectrochemical investigation of chemical bath deposited Cu_xS thin films and their modification // Colloids and Surfaces A: Physicochemical and Engineering Aspects. – 2007. – Vol. 295, Issue 1-3. – P. 152-158.

121 Safrani T., Joppb J., Golan Y. A comparative study of the structure and optical properties of copper sulfide thin films chemically deposited on various substrates // RSC Advances. – 2013. – Vol. 3, Issue 45. – P. 23066-23074.

122 Jaroudi O.E., Picquenard E., Gobeltz N., Demortier A., Corset J. Raman spectroscopy study of the reaction between sodium sulfide or disulfide and sulfur: identity of the species formed in solid and liquid phases // Inorganic Chemistry. – 1999. – Vol. 38, Issue 12. – P. 2917-2923.

123 J. Wang, J. Chenb, K. Konstantinov, L. Zhaoa, S.H. Nga, G.X. Wang, Z.P. Guoa, Liu H.K. Sulphur-polypyrrole composite positive electrode materials for

rechargeable lithium batteries // Electrochimica Acta. – 2006. – Vol. 51, Issue 22. – P. 4634-4638.

124 Zuo J., Xu C., Liu Y., Qian Y. Crystallite size effects on the Raman spectra of Mn_3O_4 // Nanostructurred Materials. – 1998. – Vol. 10, Issue 8. – P. 1331-1335.

125 Černošek Z., Holubová J., Černošková E., Růžička A. Sulfur – a new information on this seemingly well-known element // Journal of Non-oxide Glasses – 2009. – Vol. 1, Issue 1. – P. 38-42.

126 Saha B., Saikia J., Das G. Correlating enzyme density, conformation and activity on nanoparticle surfaces in highly functional bio-nanocomposites // The Analyst. – 2015. – Vol. 140, Issue 2. – P. 532-542.

127 M. Baláž, Rajňák M., Shalabayev Z., Investigation of iron wear coming from milling media in mechanochemical synthesis of copper sulfide-sulfur composite using magnetometry, The 17th Czech and Slovak Conference on Magnetism, Kosice, Slovakia, 2019.

128 Shalabayev Z., Baláž M., Daneu N., Dutková E., Bujňáková Z., Kaňuchová M., Danková Z., Balážová Ľ., Urakaev F., Tkáčiková Ľ., Burkitbayev M. Sulfur-mediated mechanochemical synthesis of spherical and needle-like copper sulfide nanocrystals with antibacterial activity // ACS Sustainable Chemistry and Engineering – 2019. – Vol. 7, Issue 15. – P. 12897-12909.

129 Urakaev F.K. Preparation of $NaIn(WO_4)_2$ nanocrystals and a charge for crystal growth via the free-of-rubbing mechanical activation of the Na_2CO_3–In_2O_3–WO_3 system // Mendeleev Communications. – 2016. – Vol. 26, Issue 6. – P. 546-548.

130 Dodd A.C., McCormick P.G. Synthesis of nanocrystalline ZrO_2 powders by mechanochemical reaction of $ZrCl_4$ with LiOH // Journal of the European Ceramic Society. – 2002. – Vol. 22, Issue 11. – P. 1823-1829.

131 Tsuzuki T., Ding J., McCormick P.G. Mechanochemical synthesis of ultrafine zinc sulfide particles // Physica B. – 1997. – Vol. 239, Issue 3-4. – P. 378-387.

132 Shalabayev Z., Tatykaev B., Uralbekov B., Urakaev F., Burkitbayev M., Mechanochemical synthesis of sulfur nanoparticles via reaction of sodium thiosulfate with crystalline acids, The 9th International Conference on Mechanochemistry and Mechanical Alloying (INCOME2017), Kosice, Slovakia, 2017.

133 Godočíková E., Baláž P., Gock E., Choi W.S., Kim B.S. Mechanochemical synthesis of the nanocrystalline semiconductors in an industrial mill // Powder Technology. – 2006. – Vol. 164, Issue 3. – P. 147-152.

134 Luo H., Ruoff A.L. X-Ray-diffraction study of sulfur to 32 GPa - amorphization at 25 GPa // Physical Review B. – 1993. – Vol. 48, Issue 1. – P. 569-572.

135 Givalou L., Antoniadou M., Perganti D., Giannouri M., Karagianni C.S., Kontos A.G., Falarasa P. Electrodeposited cobalt-copper sulfide counter electrodes for highly efficient quantum dot sensitized solar cells // Electrochimica Acta. – 2016. – Vol. 210, Issue– P. 630-638.

136 Tarachand, S. Hussainb, N. P. Lallaa, Y.-K. Kuoc, A. Lakhania, V. G. Sathea, U. Deshpandea, Okrama G.S. Thermoelectric properties of Ag-doped CuS nanocomposites synthesized by a facile polyol method // Physical Chemistry Chemical Physics. – 2018. – Vol. 20, Issue 8. – P. 5926-5935.

137 K.R. Nemade, Waghuley S.A. Band gap engineering of CuS nanoparticles for artificial photosynthesis // Materials Science in Semiconductor Processing. – 2015. – Vol. 39, Issue– P. 781-785.

138 Haram S.K., Mahadeshwar A.R., Dixit S.G. Synthesis and characterization of copper sulfide nanoparticles in Triton-X 100 water-in-oil microemulsions // Journal of Physical Chemistry. – 1996. – Vol. 100, Issue 14. – P. 5868-5873.

139 Zhang Y.Q., Zhang B.P., Zhu L.F. Monodisperse CuS nanodisks: low-temperature solvothermal synthesis and enhanced photocatalytic activity // Rsc Advances. – 2014. – Vol. 4, Issue 103. – P. 59185-59193.

140 Huse N.P., Dive A.S., Gattu K.P., Sharma R. An experimental and theoretical study on soft chemically grown CuS thin film for photosensor application // Materials Science in Semiconductor Processing. – 2017. – Vol. 67, Issue– P. 62-68.

141 Tanveer M., Cao C.B., Ali Z., Aslam I., Idrees F., Khan W.S., But F.K., Tahir M., Mahmood N. Template free synthesis of CuS nanosheet-based hierarchical microspheres: an efficient natural light driven photocatalyst // Crystengcomm. – 2014. – Vol. 16, Issue 24. – P. 5290-5300.

142 Ou S.M., Xie Q., Ma D.K., Liang J.B., Hu X.K., Yu W.C., Qian Y.T. A precursor decomposition route to polycrystalline CuS nanorods // Materials Chemistry and Physics. – 2005. – Vol. 94, Issue 2-3. – P. 460-466.

143 Jiang X.C., Xie Y., Lu J., He W., Zhu L.Y., Qian Y.T. Preparation and phase transformation of nanocrystalline copper sulfides (Cu_9S_8, Cu_7S_4 and CuS) at low temperature // Journal of Materials Chemistry. – 2000. – Vol. 10, Issue 9. – P. 2193-2196.

144 Achimovicova M., Dutkova E., Tothova E., Bujnakova Z., Briancin J., Kitazono S. Structural and optical properties of nanostructured copper sulfide semiconductor synthesized in an industrial mill // Frontiers of Chemical Science and Engineering. – 2019. – Vol. 13, Issue 1. – P. 164-170.

145 Jing L.Q., Qu Y.C., Wang B.Q., Li S.D., Jiang B.J., Yang L.B., Fu W., Fu H.G., Sun J.Z. Review of photoluminescence performance of nano-sized semiconductor materials and its relationships with photocatalytic activity // Solar Energy Materials and Solar Cells. – 2006. – Vol. 90, Issue 12. – P. 1773-1787.

146 Ye M.D., Wen X.R., Zhang N., Guo W.X., Liu X.Y., Lin C.J. In situ growth of CuS and $Cu_{1.8}S$ nanosheet arrays as efficient counter electrodes for quantum dot-sensitized solar cells // Journal of Materials Chemistry A. – 2015. – Vol. 3, Issue 18. – P. 9595-9600.

147 Li S., Ge Z.H., Zhang B.P., Yao Y., Wang H.C., Yang J., Li Y., Gao C., Lin Y.H. Mechanochemically synthesized sub-5 nm sized CuS quantum dots with high

visible-light-driven photocatalytic activity // Applied Surface Science. – 2016. – Vol. 384, Issue– P. 272-278.

148 Nduna M.K., Lewis A.E., Nortier P. A model for the zeta potential of copper sulphide // Colloids and Surfaces A. – 2014. – Vol. 441, Issue– P. 643-652.

149 Krylova V., Andrulevicius M. Optical, XPS and XRD studies of semiconducting copper sulfide layers on a polyamide film // International Journal of Photoenergy. – 2009. – Vol. 2009, Issue– P. art. ID 304308.

150 Senkevich J.J., Yang G.R., Tang F., Wang G.C., Lu T.M., Cale T.S., Jezewski C., Lanford W.A. Substrate-independent sulfur-activated dielectric and barrier-layer surfaces to promote the chemisorption of highly polarizable metallorganics // Applied Physics a-Materials Science & Processing. – 2004. – Vol. 79, Issue 7. – P. 1789-1796.

151 Hao Q.Y., Cui G.L., Tian Y., Tan T.Z., Zhang Y.G. Three-Dimensional S/CeO2/RGO Composites as Cathode Materials for Lithium-Sulfur Batteries // Materials. – 2018. – Vol. 11, Issue 9. – P.

152 Grosvenor A.P., Kobe B.A., Biesinger M.C., McIntyre N.S. Investigation of multiplet splitting of Fe 2p XPS spectra and bonding in iron compounds // Surface and Interface Analysis. – 2004. – Vol. 36, Issue 12. – P. 1564-1574.

153 Duarte H.l.A., Morales-García A., Antonio Lenito Soares J., Santos E.C.D., Abreu H.A.d. First-principles calculations and electron density topological analysis of covellite (CuS) // The Journal of Physical Chemistry A. – 2014. – Vol. 118, Issue 31. – P. 5823-5831.

154 Choudhury S.R., Mandal A., Ghosh M., Basu S., Chakravorty D., Goswami A. Investigation of antimicrobial physiology of orthorhombic and monoclinic nanoallotropes of sulfur at the interface of transcriptome and metabolome // Applied Microbiology and Biotechnology. – 2013. – Vol. 97, Issue 13. – P. 5965-5978.

155 Choudhury S.R., Roy S., Goswami A., Basu S. Polyethylene glycol-stabilized sulphur nanoparticles: an effective antimicrobial agent against multidrug-resistant bacteria // Journal of Antimicrobial Chemotherapy. – 2012. – Vol. 67, Issue 5. – P. 1134-1137.

156 Shalabayev Z., Uralbekov B., Urakaev F., Burkitbayev M., Method for producing sulfur nanoparticles from solutions in dimethyl sulfoxide, in: E.p. organization (Ed.) Russia, 2019, p. 5.

157 The website of US Research Nanomaterials, Inc: https://www.us-nano.com/inc/sdetail/6779.).

158 The website of Skyspring Nanomaterials, Inc: https://www.ssnano.com/inc/sdetail/sulfur_nanoparticles.).

159 The website of US Research Nanomaterials, Inc: https://www.us-nano.com/inc/sdetail/19209.).